博士学位論文

Study on Nanoscale Electronic Properties of Molecule/SWNT Junction

（分子／SWNT 接合における ナノスケール電子物性の研究）

Liu Hong

2012

Department of Chemistry, Graduate School of Science

Osaka University

Study on Nanoscale Electronic Properties of Molecule/SWNT Junction

（分子／SWNT 接合における ナノスケール電子物性の研究）

Liu Hong

2012

Department of Chemistry, Graduate School of Science

Osaka University

Contents

Chapter 1

General Introduction

Abstract: Due to its unique electronic states, single-walled carbon nanotubes (SWNTs) have excellent electrical properties. Molecular adsorption to SWNT can enhance the electrical performances of molecule/SWNT complex and bring novel functionalities to nanotube-based device. The main objective of this thesis is to achieve controlling of the current rectification by the molecular adsorption to SWNT. A brief introduction of a novel nanoscale current-voltage (*I*-*V*) measurement used in this study is stated as well.

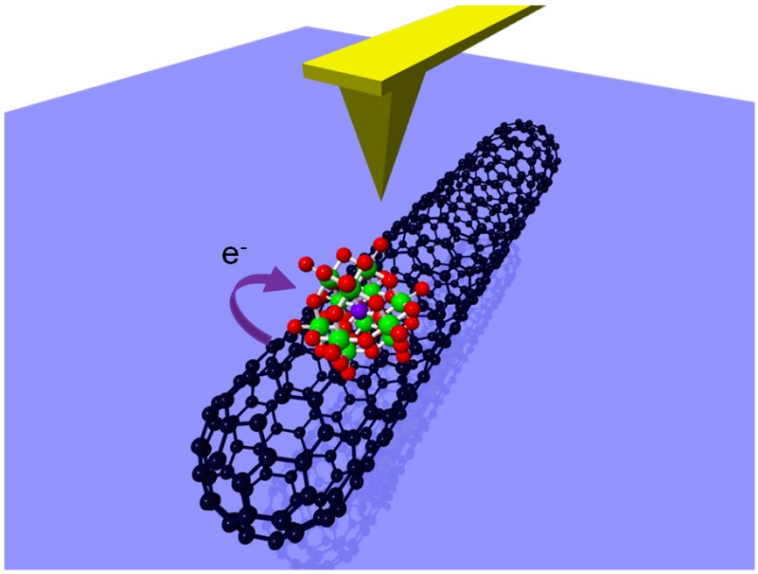

1.1 Electronic states of single-walled carbon nanotube (SWNT)

As one cylindrical nanoscale material consisted of carbon atoms, single-walled carbon nanotube (SWNT) was discovered by S. Iijima and D. Bethune in 1993.[1, 2] A SWNT can be described as a single layer of graphite (graphene), whose chemical bonding is entirely composed of sp^2 bonds,[3] rolled up into a seamless cylinder with a certain "chiral" angle (Φ in **Figure 1**a) with respect to a plane perpendicular to its long axis.[4] Thus, SWNT can be distinguished by its diameter and chiral angle. For convenience, the chiral angle can be represented by a pair of indices (n,m), which is derived from the chiral vector C_h,[5]

$$C_h = n\mathbf{a_1} + m\mathbf{a_2} \quad (1)$$

in which $n\mathbf{a_1}$ and $m\mathbf{a_2}$ denote the number of the unit vectors along the two directions in honeycomb lattice of graphene (Figure 1a). Electronic states of SWNT are strongly affected by its geometric structure specified by (n,m) indices.[6, 7] For a given (n,m) SWNT, if $n = m$, it is metallic; if $n - m = 3j$, where j is a nonzero integer, it is semiconductor with a tiny band gap; otherwise it is semiconductor with moderate band gap, though exceptions exist due to the curvature effects in small diameter SWNTs.[8] Specifically, SWNTs with $n = m$ (chiral angle is 30°) is called as "armchair" (Figure 1b), while "zigzag" (Figure 1c) when $m = 0$ (chiral angel is 0°).

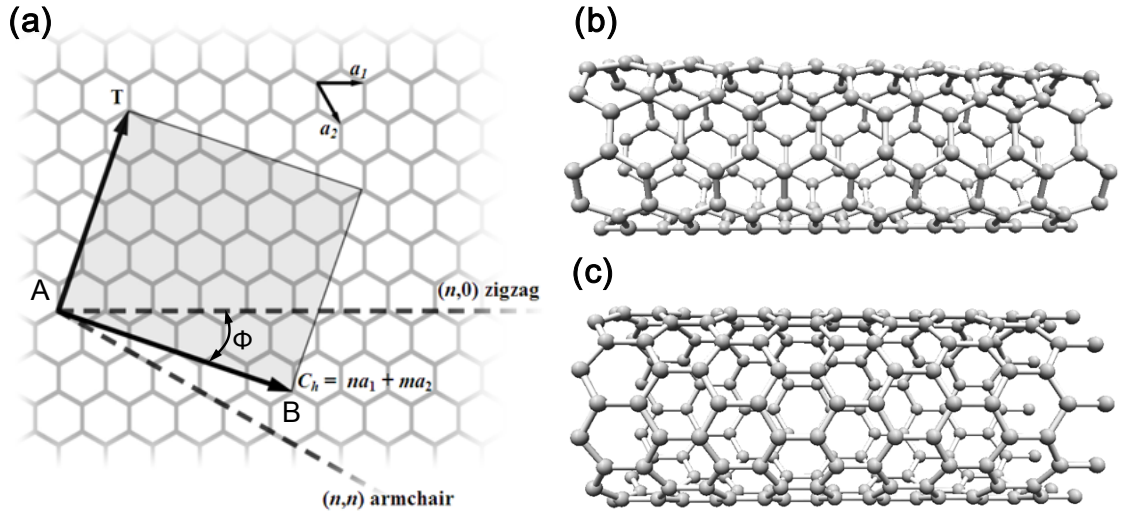

Figure 1. (a) Construction of a SWNT from a single graphene sheet.[3, 9] By rolling up the sheet along the chiral vector C_h, as the arrow starting from point A (0,0) to B shows, a SWNT indicated by indices (n,m) is formed. Chiral vectors along the dashed lines lead to zigzag or armchair SWNT. **T** denotes the tube axis, while $\mathbf{a_1}$ and $\mathbf{a_2}$ are the unit vectors along two directions of graphene honeycomb lattice. The angle Φ between unit vector $\mathbf{a_1}$ and C_h is the chiral angle. Molecular structure of (b) is a (5,5) SWNT (armchair), and (c) is a (10,0) SWNT (zigzag).

The electronic states of SWNTs can be depicted schematically with density of states (DOS) image, which describes the number of states per interval of energy at each energy level that are available to be occupied by electrons (**Figure 2**). In SWNT, each band of graphene splits into a number of 1D sub bands. Highest occupied molecular orbital (HOMO) and lowest unoccupied molecular orbital (LUMO) correspond to the first spike of van Hove singularity in the valence and conduction band, respectively.[10] In the case of metallic SWNT, sub bands cross at Fermi level E_F, and HOMO-LUMO gap is zero. When tube is semiconducting, sub bands do not cross at E_F and a band gap exists.

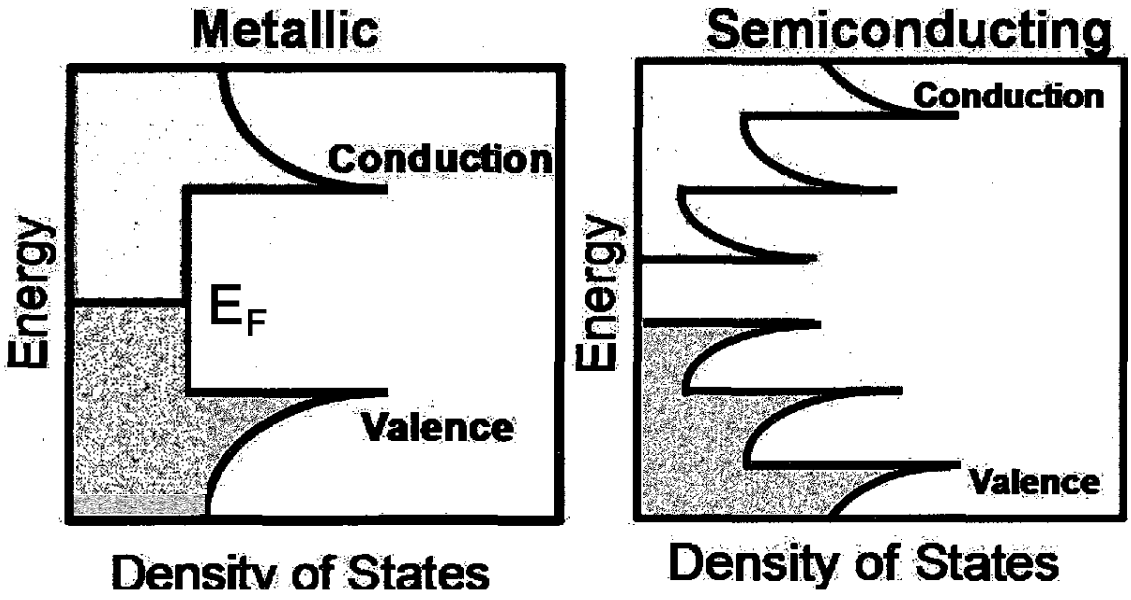

Figure 2. Schematic depiction of the DOS of metallic and semiconducting SWNTs.[11]

The theoretical prediction about the electronic states of SWNT was proved by the scanning tunneling microscopy (STM) and spectroscopy (STS) measurement successfully.[5, 12] The atomically resolved STM image determined the chiral angle of SWNT unambiguously (**Figure 3**), so that chiral tubes could be distinguished from armchair and zigzag ones. In the STS measurement, the differential conductance (dI/dV) of the measured current-voltage (I-V) curves fit well with the DOS of the SWNT sample (**Figure 4**).[13] Combined results of STM and STS further confirmed that the electronic states of SWNT were dependent on the chiral angle and tube diameter.[5]

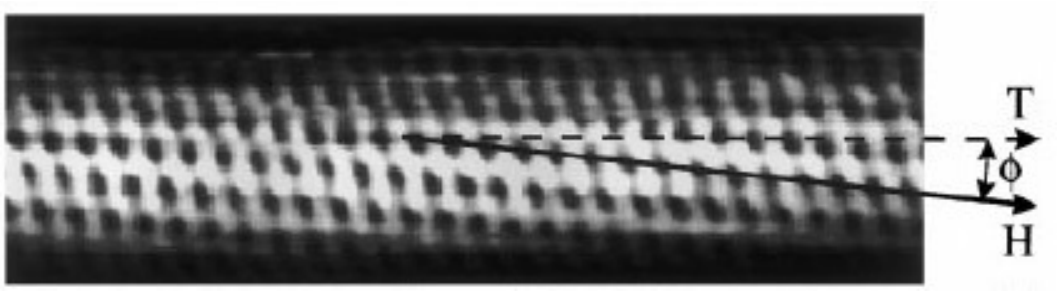

Figure 3. Atomically resolved STM images of an individual chiral SWNT.[5] Dashed arrow is the tube axis **T** and the solid arrow indicates the direction of nearest-neighbour hexagon rows **H**. Chiral angle is denoted with Φ.

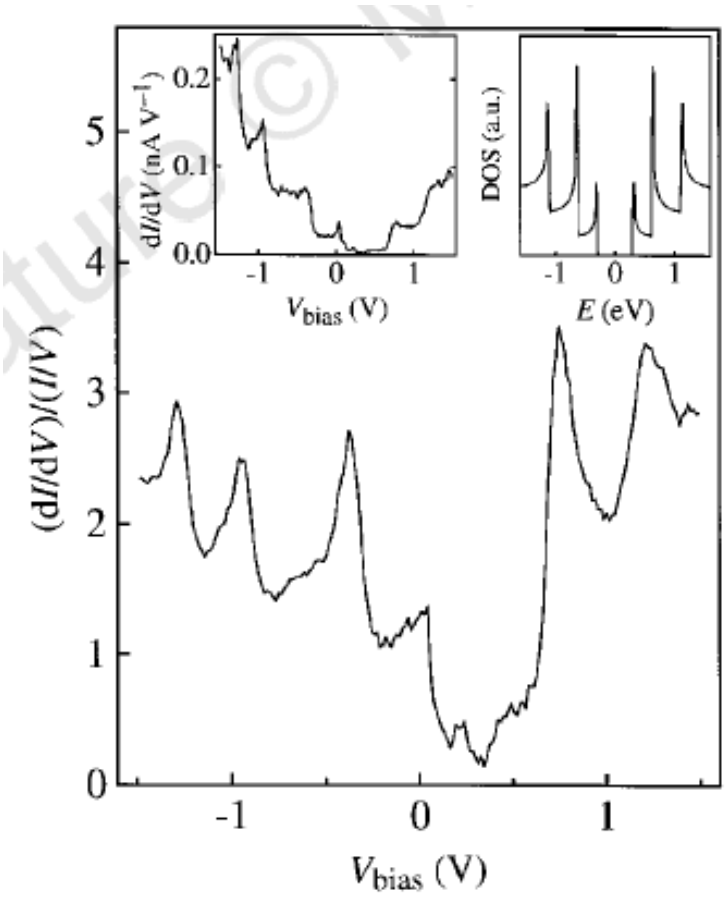

Figure 4. (dI/dV)/(I/V) as a measure of the density of states versus V for a semiconducting SWNT.[5] The asymmetric peaks correspond to van Hove singularities at the onsets of 1D energy bands of the carbon nanotube. The left inset displays the raw dI/dV data. The right inset is the calculated DOS for a (16,0) SWNT, which displays a typical example of the peak-like DOS for a semiconducting tube.

Due to its unique electronic structure, SWNT is considered as a new class of material with excellent electrical properties. Metallic SWNT owns a theoretical current density much larger than traditional metal materials,[14] which provides SWNT the potential as a flexible electronic unit. Z. K. Tang et al. found that SWNT could reveal superconductivity below 20K.[15] High carrier mobility of individual SWNT makes it attractive for the applications of solar cell, field-effect transistor (FET) and memory.[16-18] SWNT has been believed as a good candidate for the nanoscale electronic device in the near future.

1.2 Electrical characteristics of SWNTs modified by molecular adsorption

Due to the excellent electrical properties of SWNTs, lots of efforts have been focused in the molecular functionalization of them. Many approaches have been used for the molecular modification of SWNT, which include substitutional doping, fluorination, covalent functionalization, and so on (**Figure 5**).[19] Via molecular modification, the electrical performances of SWNT-based device were largely improved.[20-22] However, some disadvantages still exist. The chemical stability of carbon nanotubes imposes a hurdle for the selective and controlled functionalization of SWNT, and some electrical characteristics of SWNT may not be well kept due to a chemical bonding of the nanotube to certain molecules.[23]

Recently, more and more attention has been paid on the electrical properties of SWNTs modified by molecular adsorption. It has been indicated that various molecules can be physically adsorbed onto the sidewall of SWNT by van der Waals force,[24] π-π stacking,[25, 26] and wrapping effect,[27] etc. Compared with other molecular modification approaches, physical adsorption can retain the excellent properties of nanotube without damaging its original π-networks.

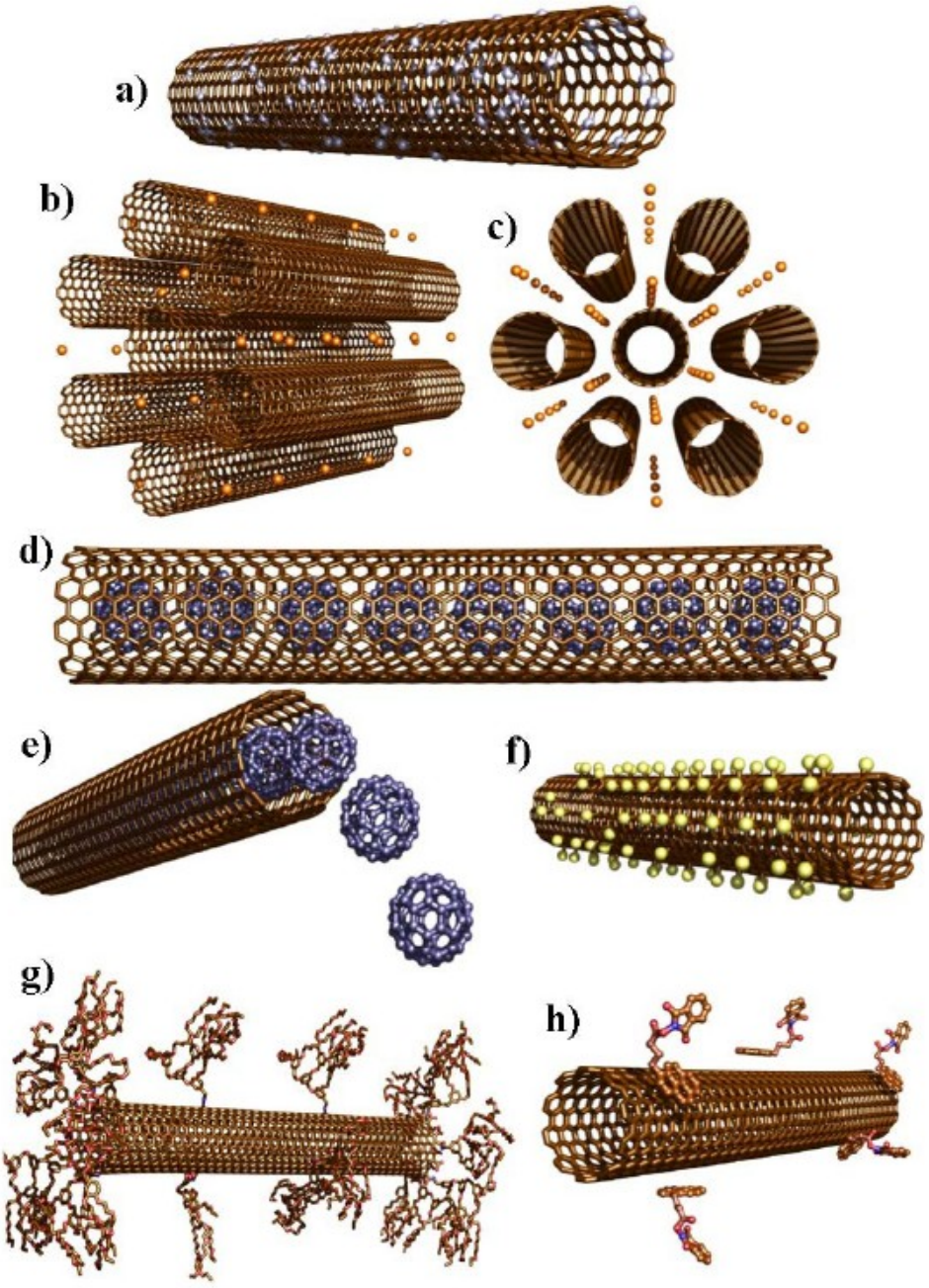

Figure 5. Different approaches of molecular modification to SWNTs.[19] (a) substitutional doping: (b, c) SWNT bundles intercalated with atoms or ions; (d, e) peapod molecules filling; (f) fluorination; (g) covalently functionalization; (h) π-stacking functionalization.

A number of electrical functionalities can be achieved by the molecular adsorption to SWNT. Firstly, electrical characteristics of SWNT can be

controlled by the adsorbed molecules. Research of C. W. Lee et al. showed that the work function of SWNTs FET was tuned successfully by the adsorption of thiolated molecules,[28] while J. Oh et al. observed the conductivity change of SWNTs adsorbed by strong charge transfer molecules (**Figure 6**).[29] Second, novel electrical properties may appear after the molecular adsorption to SWNT. W. Kim et al. demonstrated that the adsorption of water molecule on SWNT could induce hysteresis in the FET device,[30] while H. Tanaka reported that the chirality distribution of the SWNTs adsorbed by naphthalenediimide (NDI) derivatives depended on the alkyl side chain length of NDI (**Figure 7**).[31] Moreover, electronic states of SWNT can be changed by the adsorption of certain molecules. M. Shim et al. discovered a *n*-doping of carbon nanotube by submerging an original *p*-type SWNT into a solution of polyethylene imine (PEI, **Figure 8**),[32] while the DOS of (10,0) SWNT was dramatically changed by the adsorption of various gas molecules according to the research of J. Zhao et al.[33]

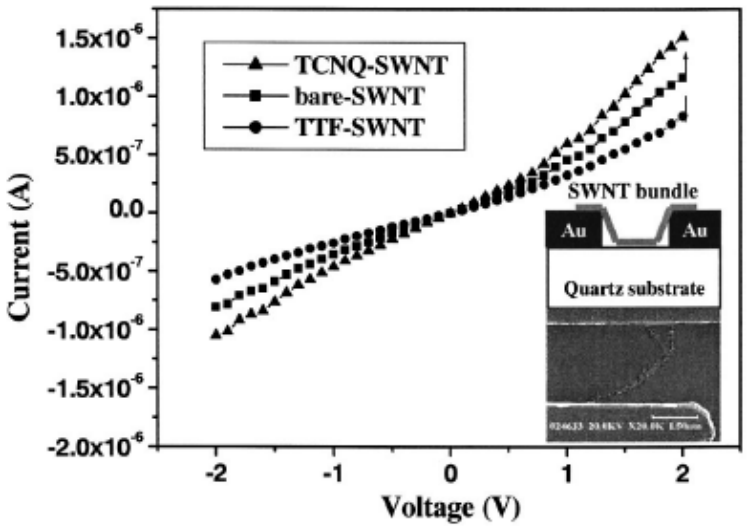

Figure 6. *I–V* curve change of tetracyanoquinodimethane (TCNQ)-adsorbed, bared, and tetrathiafulvalene (TTF)-adsorbed SWNT bundle.[29] Inset represents schematic cross section of a SWNT device, which consists of a bundle SWNT bridging two gold electrode and SEM image of the sample.

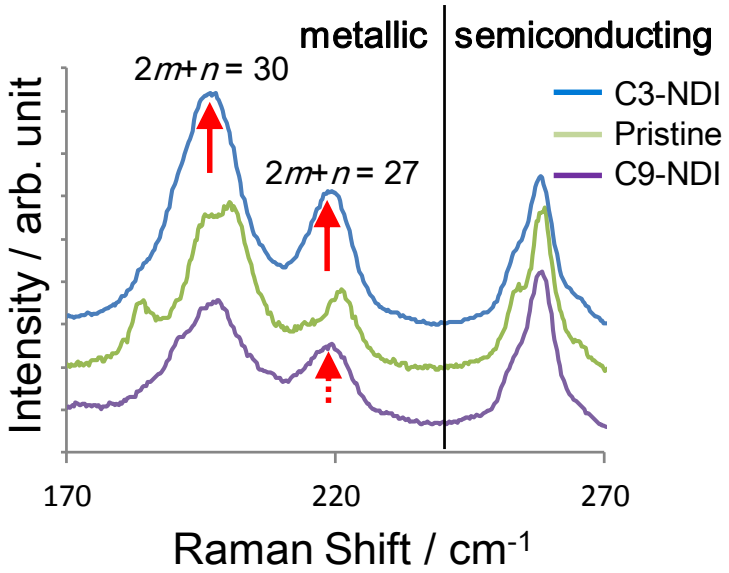

Figure 7. Raman spectra of pristine SWNT, SWNT adsorbed by C3-NDI (NDI derivative with isopropyl side chains) and C9-NDI (NDI derivative with nonyl side chains) taken with a 633 nm laser.[31] Background level of C3-NDI/SWNT is shifted upward and that of C9-NDI/SWNT downward with equal interval for a clear view. Red arrows indicate the peaks of concentrated chirality. Intensity of the metallic chirality ascribed to $2m + n = 27$ and 30 families clearly increased in the case of C3-NDI (solid arrows), while did not change much for C9-NDI/SWNT (dotted arrow).

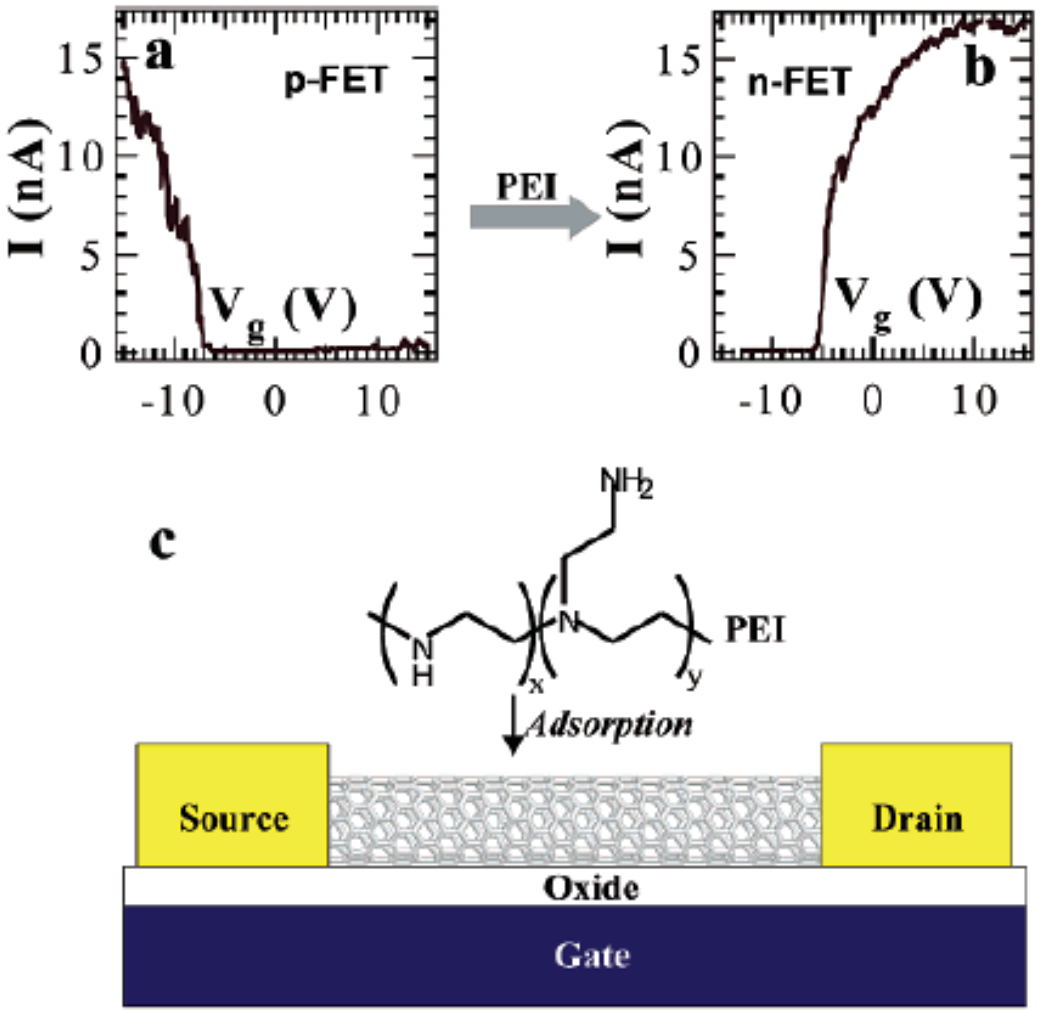

Figure 8. Polymer functionalization for air-stable *n*-type nanotube FET.[34] (a) Current (*I*) vs. gate characteristics of an as-made semiconducting SWNT showing *p*-type FET behavior. (b) The nanotube evolves into an *n*-type FET after adsorption of PEI, schematically shown in (c).

Taking advantage of the electrical characteristics of SWNT modified by molecular adsorption, the application range of the nanotube-based device has been much more widened. SWNTs FET coated by various molecules like polymer and starch could work as a electrochemical sensor in detecting specific protein (**Figure 9**),[35] glucose,[36] and DNA,[37] etc. Molecular

switch tunnel junction was reported fabricated by transferring the Langmuir-Blodgett (LB) monolayer film of amphiphilic dimyristoyl -phosphatidyl anions to the sidewall of a semiconducting SWNT in FET.[38] By submerging SWNTs FET into a solution of triethyloxonium hexachloroantimonate, self-align carbon nanotube transistor was realized.[39] The study in the electrical characteristics of SWNTs adsorbed by different molecules is still ongoing, and will be a very promising research topic in both the academic and industrial fields.

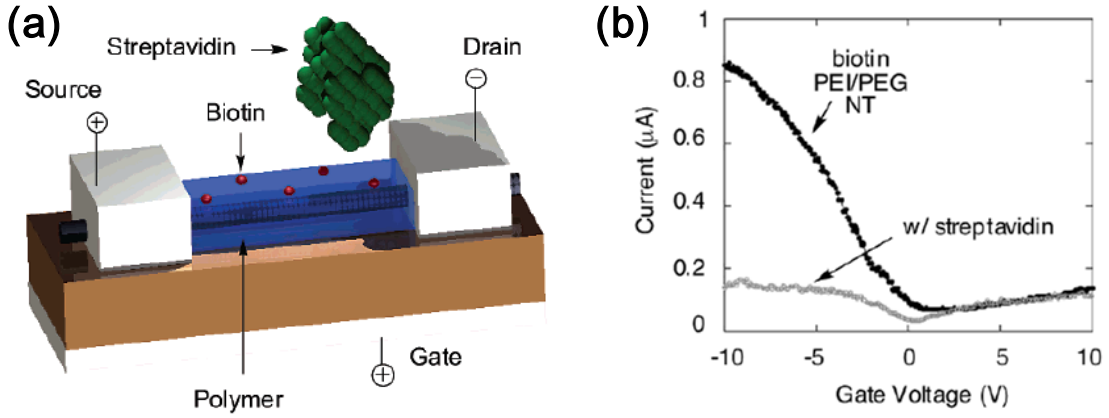

Figure 9. (a) Schematic of SWNTs FET.[35] A polymeric functional layer, which coats the nanotube, is functionalized with a molecular receptor, biotin, a protein that recognizes a biomolecule, streptavidin. (b) Different gate voltage dependence I_{sd} of the biotinylated, polymer-coated SWNTs FET in the absence and in the presence of streptavidin.

1.3 Objective of this thesis: controlling of current rectification of SWNTs complex by molecular adsorption

Current rectification is a process that the current flows in only one direction in the electric circuit, which demonstrates an asymmetry of conductivity between the negative and positive biases in *I-V* curve.[40] As an important feature in the application of commercial electronics units like diode and convertor, rectification has been predicted in the junction of SWNTs by theoretical calculations,[41, 42] and confirmed by a series of experiments.[43-45]

For the purpose in modulating the rectifying behavior more efficiently, some attention was paid to the rectifying role of molecular adsorption to SWNT recently. J. Kong and H. Dai reported that rectifying behavior appeared after the adsorption of amine molecules to semiconducting SWNT FET (**Figure 10**).[46] The research of A. Guo et al. indicated a gate-controlled rectifying behavior in fullerene/SWNTs networks.[47] E. Kymakis and G. Amaratunga indicated a current rectification in the *I-V* curve of poly(3-octylthiophene) (P3OT)/SWNT composite in photovoltaic device.[48] H. Tanaka et al. demonstrated a large current rectification in the case of a porphyrin aggregate of 2-3 nm size adsorbed on SWNT wiring (**Figure 11**).[49]

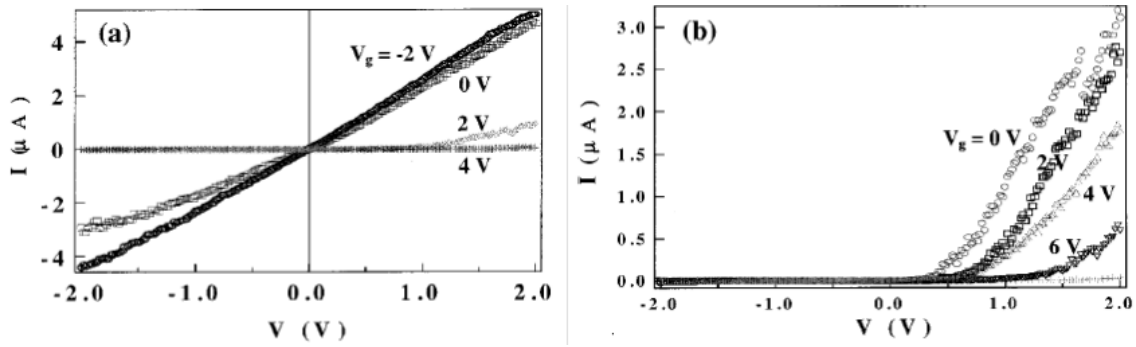

Figure 10. (a) *I-V* characteristic of a SWNT partially covered with poly(methyl methacrylate) (PMMA) before exposure to 3'-(aminopropyl)triethoxysilane (APTES) vapor under various gate voltages. (b) Highly rectifying *I-V* curves recorded after APTES adsorption.[46]

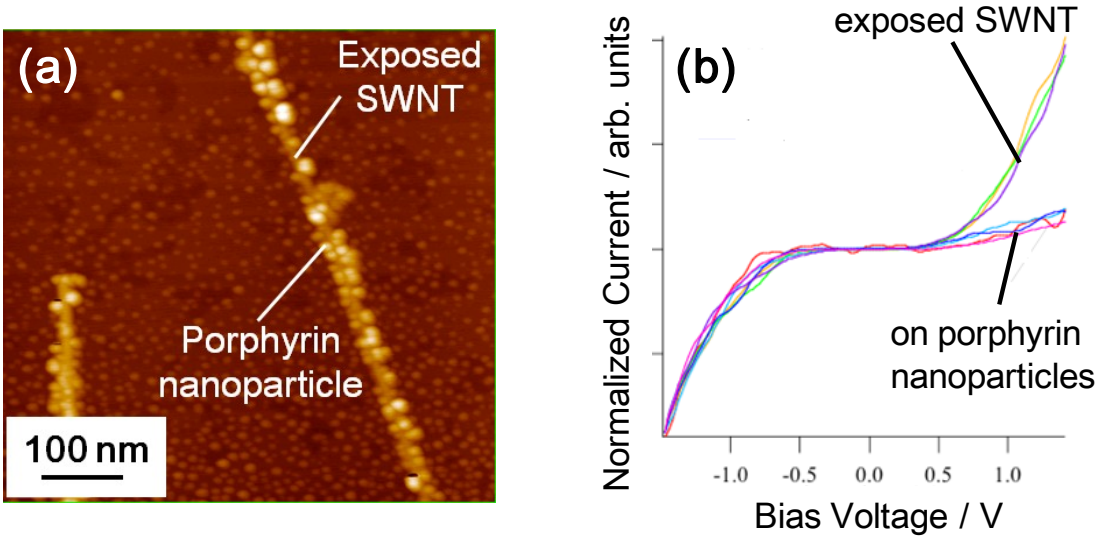

Figure 11. (a) AFM image of porphyrin molecules on a SWNT wiring.[49] (b) *I–V* curves normalized to –1.5 V. All the curves are coincident below 0 V. *I–V* curves are classified into two types above 0 V. One group of curves is symmetric around the origin where no porphyrin molecules are adsorbed, and the second group is asymmetric, corresponding to the adsorption of porphyrin molecules.

Though a number of researches have focused on the current rectification induced by the molecular adsorption to SWNT, it is necessary to research on the influence factors of rectification properties of molecule/SWNT

complex systematically. These rectification properties include rectification ratio (RR), plateau width (PW) in *I-V* curve and rectification direction. With the adsorption of certain molecules to SWNT, tunable RR, PW and rectification direction are expected. Therefore, the main objective of this thesis is to achieve a controlling of current rectification by the molecular adsorption to SWNT. Besides, rectification mechanism of molecular adsorption to SWNT needs to be clarified. The experimental results of this thesis are expected to be important for a better optimization of molecular electronics in future.

1.4 PCI-AFM: a novel electrical characterization method used in this thesis

Electrical properties of the molecule/SWNT complex in this study were mainly measured by a novel nanoscale *I-V* measurement as called point-contact current imaging atomic force microscopy (PCI-AFM), which has been developed by Prof. T. Matsumoto and his colleagues in 2002.[50] With the combination of tapping mode used for topography and point-contact mode used for electrical properties measurement, PCI-AFM can provide high-resolution topographic image and *I-V* characteristic at every pixel of topography simultaneously. By using PCI-AFM, large damage of the sample brought by the heavy loading force applied to cantilever tip can be avoid,[50, 51] and a precise positioning of the tip during the scanning process can be achieved as well.

The PCI-AFM measurement is conducted by a scanning probe microscope equipped with two function generators. Platinum-coated cantilever is used for current detection. Before measurement, a gold electrode is deposited on half of the surface of insulator substrate to form electrical contacts with nano-materials like SWNTs or DNA nanowires. During the measurement, a bias voltage is applied on the gold electrode while the cantilever is grounded. Each signal is stored into a storage oscilloscope.

A schematic depiction of PCI-AFM procedure is shown as **Figure 12**. Topography of sample is measured using tapping mode AFM, while *I-V* curve at the same pixel is measured by point-contact mode AFM during the interruption of tapping mode scan. A current image of a certain bias

voltage can be obtained based on the spatially resolved *I*-*V* measurements. With all the optimized parameter set up, the resolution of current image can be high enough to distinguish each SWNT in a bundle of carbon nanotube, as shown in **Figure 13**.

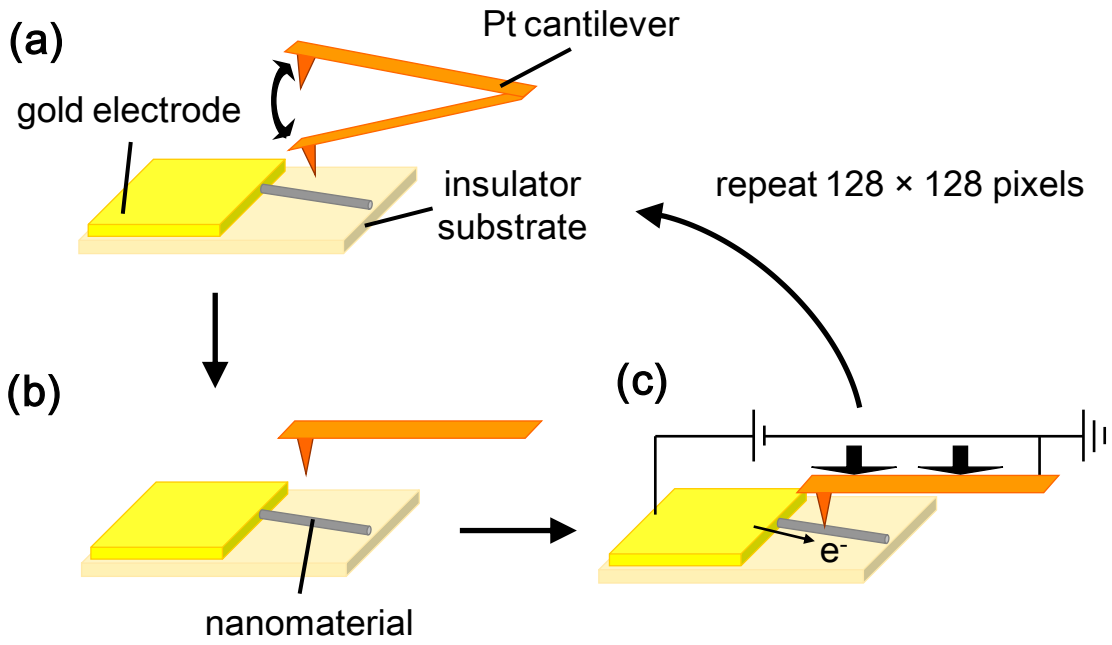

Figure 12. Schematic depiction of PCI-AFM procedure.[52] (a) A topographic image is obtained by tapping-mode AFM. (b) Cantilever vibration is stopped for *I*–*V* measurement. (c) Pt cantilever is forced pressed to the sample to make electrical contact, and *I*–*V* curve is then measured with cantilever stops. Steps (a) – (c) are repeated at each of the 128 × 128 pixels of the AFM image.

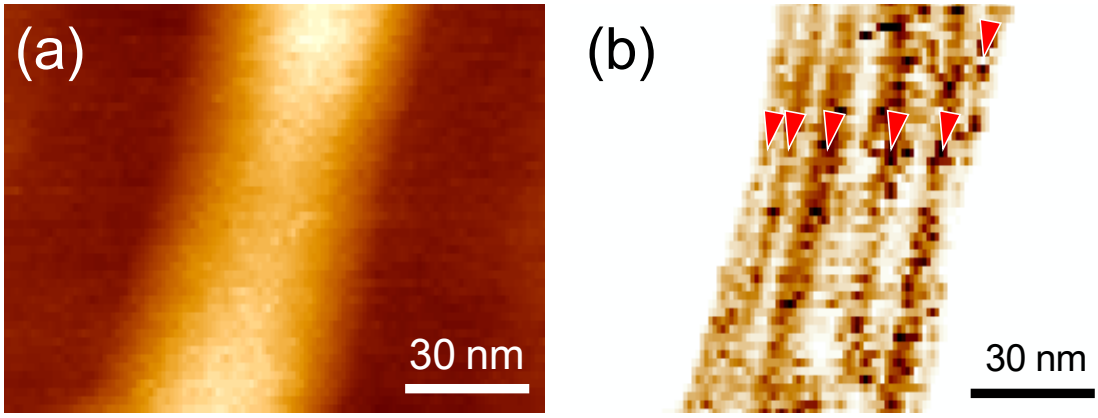

Figure 13. (a) Topography and (b) current image of bundled SWNTs measured by PCI-AFM.[52] Red triangles indicate six dark stripes observed in the current image of SWNTs bundle, and the stripe can be distinguished by each other as individual SWNT.

PCI-AFM has been proved useful in measuring electrical properties of various nanoscale materials with different shapes. Electrical conductivity of fibrous molecules like tetrathiafulvalenes (TTF) and 2,3,5,6-tetrafluoro-7,7',8,8'-tetracyanop-quinodimethane (F_4TCNQ) has been successfully obtained by PCI-AFM.[53] Incorporating with carbon nanotube, *I-V* characteristics of various particles including porphyrin,[49, 54] naphthalenediimide,[31] and noble metal,[55] were measured. Recent researches further illustrated that PCI-AFM was feasible in current detecting of organic thin film on metal electrode.[56, 57] Therefore, PCI-AFM can be an ideal means for the nanoscale *I-V* measurement in this study.

1.5 Contents of this thesis

In this thesis, the author studies the electrical properties of SWNT adsorbed by two different molecules, naphthalenediimide (NDI) and phosphododecamolybdic acid (PMo_{12}) mainly by PCI-AFM. Research on PMo_{12}/graphene nanoribbon (GNR) complex is also included.

Chapter 2 concerns the electrical properties of SWNT adsorbed by NDI derivatives using PCI-AFM. By changing the alkyl side chain lengths of NDI derivatives, separation of metallic SWNTs from semiconducting SWNTs was succeeded. Molecular size of NDI was found as an influencing factor to the magnitude of RR and PW, which was further theoretically explained. Besides, large current rectification was observed in a SWNTs junction, and the rectification mechanism was discussed in detail.

Chapter 3 concerns the electrical properties of SWNT adsorbed by PMo_{12} molecules. In PCI-AFM measurement, rectification direction was inversed as the height of PMo_{12} nanoparticle varied, and the inversion tendency of rectification direction against PMo_{12} nanoparticle size differed between metallic and semiconducting SWNTs. Opposite surface potentials shift of PMo_{12} were found between metallic and semiconducting SWNTs cases according to Kelvin probe force microscopy (KPFM) results. Two possible mechanisms were discussed for the reason to the reversible rectification direction. Additionally, negative differential resistance (NDR) properties were observed in the PMo_{12}/SWNT complex.

Chapter 4 concerns the rectification properties of graphene nanoribbon (GNR) adsorbed by PMo_{12}. The preliminary results indicated tunable RR and PW controllable by GNR width and molecular size of PMo_{12} adsorbed on GNR, respectively.

Chapter 5 gives the conclusion and future work.

References

1. Iijima, S.; Ichihashi, T. *Nature* **1993,** 363, (6430), 603-605.
2. Bethune, D. S.; Kiang, C. H.; Devries, M. S.; Gorman, G.; Savoy, R.; Vazquez, J.; Beyers, R. *Nature* **1993,** 363, (6430), 605-607.
3. Dresselhaus, M. S.; Dresselhaus, G.; Saito, R. *Carbon* **1995,** 33, (7), 883-891.
4. Yu, D.; Liu, F. *Nano Lett.* **2007,** 7, (10), 3046-3050.
5. Wildoer, J. W. G.; Venema, L. C.; Rinzler, A. G.; Smalley, R. E.; Dekker, C. *Nature* **1998,** 391, (6662), 59-62.
6. Saito, R.; Fujita, M.; Dresselhaus, G.; Dresselhaus, M. S. *Appl. Phys. Lett.* **1992,** 60, (18), 2204-2206.
7. Hamada, N.; Sawada, S.; Oshiyama, A. *Phys. Rev. Lett.* **1992,** 68, (10), 1579-1581.
8. Gulseren, O.; Yildirim, T.; Ciraci, S. *Phys. Rev. B* **2002,** 65, (15), 153405.
9. Sinnott, S. B.; Andrews, R. *Crit. Rev. Solid State Mater. Sci.* **2001,** 26, (3), 145-249.
10. Joselevich, E. *ChemPhysChem* **2004,** 5, (5), 619-624.
11. Duque, J. G. Electrochemistry and Self-Assembly of Complex Single-Walled Carbon Nanotube (SWNT) Nanostructures. Rice University, Houston, United States, 2009.
12. Odom, T. W.; Huang, J. L.; Kim, P.; Lieber, C. M. *Nature* **1998,** 391, (6662), 62-64.
13. Dekker, C. *Phys. Today* **1999,** 52, (5), 22-28.
14. Hong, S.; Myung, S. *Nat. Nanotechnol.* **2007,** 2, (4), 207-208.
15. Tang, Z. K.; Zhang, L. Y.; Wang, N.; Zhang, X. X.; Wen, G. H.; Li, G. D.; Wang, J. N.; Chan, C. T.; Sheng, P. *Science* **2001,** 292, (5526), 2462-2465.
16. Ren, S.; Bernardi, M.; Lunt, R. R.; Bulovic, V.; Grossman, J. C.; Gradecak, S. *Nano Lett.* **2011,** 11, (12), 5316-5321.
17. Javey, A.; Guo, J.; Wang, Q.; Lundstrom, M.; Dai, H. J. *Nature* **2003,** 424, (6949), 654-657.
18. Fuhrer, M. S.; Kim, B. M.; Durkop, T.; Brintlinger, T. *Nano Lett.* **2002,** 2, (7), 755-759.
19. Glerup, M.; Kristic, V.; Ewels, C.; Holzinger, M.; van Lier, G.,

Doping of Carbon Nanotubes. In *Doped Nanomaterials and Nanodevices*, Wei, C., Ed. American Scientific Publisher: California, United States, 2010.
20. Latil, S.; Roche, S.; Mayou, D.; Charlier, J.-C. *Phys. Rev. Lett.* **2004,** 92, (25), 256805.
21. Dettlaff-Weglikowska, U.; Skakalova, V.; Meyer, J.; Cech, J.; Mueller, B. G.; Roth, S. *Curr. Appl. Phys.* **2007,** 7, (1), 42-46.
22. Zhao, J. J.; Park, H. K.; Han, J.; Lu, J. P. *J. Phys. Chem. B* **2004,** 108, (14), 4227-4230.
23. Balasubramanian, K.; Burghard, M. *Small* **2005,** 1, (2), 180-192.
24. Star, A.; Steuerman, D. W.; Heath, J. R.; Stoddart, J. F. *Angew. Chem. Int. Ed.* **2002,** 41, (14), 2508-2512.
25. Star, A.; Stoddart, J. F.; Steuerman, D.; Diehl, M.; Boukai, A.; Wong, E. W.; Yang, X.; Chung, S. W.; Choi, H.; Heath, J. R. *Angew. Chem. Int. Ed.* **2001,** 40, (9), 1721-1725.
26. Nakashima, N.; Tomonari, Y.; Murakami, H. *Chem. Lett.* **2002**, (6), 638-639.
27. Liu, Y.; Chipot, C.; Shao, X.; Cai, W. *Nanoscale* **2012,** 4, (8), 2584-2589.
28. Lee, C. W.; Zhang, K.; Tantang, H.; Lohani, A.; Mhaisalkar, S. G.; Li, L.-J.; Nagahiro, T.; Tamada, K.; Chen, Y. *Appl. Phys. Lett.* **2007,** 91, (10), 103515.
29. Oh, J.; Roh, S.; Yi, W.; Lee, H.; Yoo, J. *J. Vac. Sci. Technol. B* **2004,** 22, (3), 1416.
30. Kim, W.; Javey, A.; Vermesh, O.; Wang, O.; Li, Y. M.; Dai, H. J. *Nano Lett.* **2003,** 3, (2), 193-198.
31. Tanaka, H.; Hong, L.; Fukumori, M.; Negishi, R.; Kobayashi, Y.; Tanaka, D.; Ogawa, T. *Nanotechnology* **2012,** 23, (21), 215701.
32. Shim, M.; Javey, A.; Kam, N. W. S.; Dai, H. J. *J. Am. Chem. Soc.* **2001,** 123, (46), 11512-11513.
33. Zhao, J. J.; Buldum, A.; Han, J.; Lu, J. P. *Nanotechnology* **2002,** 13, (2), 195-200.
34. Dai, H. J. *Acc. Chem. Res.* **2002,** 35, (12), 1035-1044.
35. Star, A.; Gabriel, J. C. P.; Bradley, K.; Gruner, G. *Nano Lett.* **2003,** 3, (4), 459-463.
36. Star, A.; Joshi, V.; Han, T. R.; Altoe, M. V. P.; Gruner, G.; Stoddart, J. F. *Org. Lett.* **2004,** 6, (13), 2089-2092.

37. Tang, X. W.; Bansaruntip, S.; Nakayama, N.; Yenilmez, E.; Chang, Y. L.; Wang, Q. *Nano Lett.* **2006,** 6, (8), 1632-1636.
38. Diehl, M. R.; Steuerman, D. W.; Tseng, H. R.; Vignon, S. A.; Star, A.; Celestre, P. C.; Stoddart, J. F.; Heath, J. R. *ChemPhysChem* **2003,** 4, (12), 1335-1339.
39. Chen, J.; Klinke, C.; Afzali, A.; Avouris, P. *Appl. Phys. Lett.* **2005,** 86, (12), 123108.
40. Metzger, R. M.; Chen, B.; Hopfner, U.; Lakshmikantham, M. V.; Vuillaume, D.; Kawai, T.; Wu, X. L.; Tachibana, H.; Hughes, T. V.; Sakurai, H.; Baldwin, J. W.; Hosch, C.; Cava, M. P.; Brehmer, L.; Ashwell, G. J. *J. Am. Chem. Soc.* **1997,** 119, (43), 10455-10466.
41. Treboux, G.; Lapstun, P.; Silverbrook, K. *J. Phys. Chem. B* **1999,** 103, (11), 1871-1875.
42. Srivastava, D.; Menon, M.; Ajayan, P. M. *J. Nanoparticle Res.* **2003,** 5, (3-4), 395-400.
43. Collins, P. G.; Zettel, A.; Bando, H.; Thess, A.; Smalley, R. E. *Science* **1997,** 278, (5335), 100-102.
44. Zhou, C.; Kong, J.; Yenilmez, E.; Dai, H. *Science* **2000,** 290, (5496), 1552-1555.
45. Lee, J. U.; Gipp, P. P.; Heller, C. M. *Appl. Phys. Lett.* **2004,** 85, (1), 145.
46. Kong, J.; Dai, H. J. *J. Phys. Chem. B* **2001,** 105, (15), 2890-2893.
47. Guo, A.; Fu, Y. Y.; Liu, J.; Guan, L. H.; Shi, Z. J.; Gu, Z. N.; Huang, R.; Zhang, X. *J. Phys. Chem. B* **2006,** 110, (20), 9923-9926.
48. Kymakis, E.; Amaratunga, G. A. J. *Appl. Phys. Lett.* **2002,** 80, (1), 112.
49. Tanaka, H.; Yajima, T.; Matsumoto, T.; Otsuka, Y.; Ogawa, T. *Adv. Mater.* **2006,** 18, (11), 1411-1415.
50. Otsuka, Y.; Naitoh, Y.; Matsumoto, T.; Kawai, T. *Jap. J. Appl. Phys.* **2002,** 41, (Part 2, No. 7A), L742-L744.
51. de Pablo, P. J.; Martinez, M. T.; Colchero, J.; Gomez-Herrero, J.; Maser, W. K.; Benito, A. M.; Munoz, E.; Baro, A. M. *Adv. Mater.* **2000,** 12, (8), 573-576.
52. Yajima, T.; Tanaka, H.; Matsumoto, T.; Otsuka, Y.; Sugawara, Y.; Ogawa, T. *Nanotechnology* **2007,** 18, (9), 095501.
53. Tatewaki, Y.; Hatanaka, T.; Tsunashima, R.; Nakamura, T.; Kimura,

M.; Shirai, H. *Chem. Asian J.* **2009,** 4, (9), 1474-9.
54. Tanaka, H.; Yajima, T.; Kawao, M.; Ogawa, T. *J. Nanosci. Nanotechnol.* **2006,** 6, (6), 1644-1648.
55. Subramaniam, C.; Sreeprasad, T.; Pradeep, T.; Pavan Kumar, G.; Narayana, C.; Yajima, T.; Sugawara, Y.; Tanaka, H.; Ogawa, T.; Chakrabarti, J. *Phys. Rev. Lett.* **2007,** 99, (16), 167404.
56. Kondo, M.; Iida, K.; Dewa, T.; Tanaka, H.; Ogawa, T.; Nagashima, S.; Nagashima, K. V.; Shimada, K.; Hashimoto, H.; Gardiner, A. T.; Cogdell, R. J.; Nango, M. *Biomacromolecules* **2012,** 13, (2), 432-438.
57. Tabuchi, S.; Otsuka, Y.; Kanai, M.; Tabata, H.; Matsumoto, T.; Kawai, T. *Org. Electron.* **2010,** 11, (5), 916-924.

Chapter 2

Electrical Characteristics of Naphthalenediimide / Single-Walled Carbon Nanotube Complexes and Influence by the Nanoparticle Size

Abstract: When nanoparticles of N,N'-bis(n-alkyl)tetracarbonate-naphthalenediimide (NDI) were adsorbed on single-walled carbon nanotube (SWNT) wires dispersed on a SiO_2 substrate, physical properties of the SWNT could be modified significantly. The first observation was that by the adsorption of NDI with different alkyl chain length, chirality distribution of dispersed SWNTs largely differed from the pristine ones. The second finding is that rectification occurred at the interface of NDI particles with SWNTs, and the plateau width of *I–V* curve decreased as the particle size increased, while the rectification ratio increased. The conduction mechanism changed from tunneling conduction to Schottky-like conduction when the particles size was more than ca. 3 nm. By a combination of SWNTs junction and NDI/SWNT interface, large rectification ratios were observed.

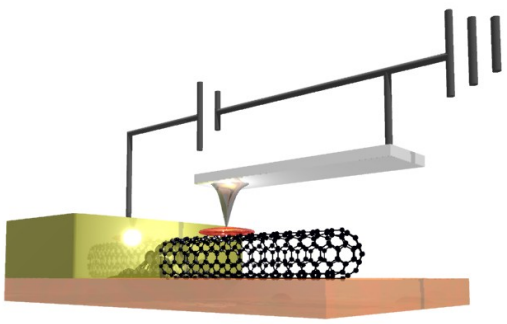

2.1 Introduction

Hybridization of single-walled carbon nanotube (SWNT) and organic molecules has been of particular interest in the recent development of bottom-up nanotechnology.[1] Previous research indicates that current rectification appeared at the interface between SWNT and porphyrin, a typical organic planar electron-donating molecule.[2] This finding proves the feasibility of molecular rectification device on carbon nanotube. Since the porphyrins are relatively good donor molecules, it is important to understand how electron-accepting molecules like imides behave on individual SWNT wires. It will be quite interesting if the rectification properties can be controlled by the properties of the molecules on SWNT.

Naphthalenediimides (NDIs) are chosen as the good electron-acceptor molecules which have been utilized in various applications as organic electronic materials.[3-5]

NDI derivatives of different alkyl chain lengths were physically adsorbed on the side-wall of SWNT, and electrical properties of the complex were measured by PCI-AFM. By changing the alkyl side chain length of NDI derivatives, obvious change in the chirality distribution of SWNTs adsorbed by NDI molecules was observed. Different rectification characteristics like rectification ratio (RR) and plateau width (PW) were found correlated with particle size of NDI. Additionally, extremely large rectification on SWNTs junction was also discussed.

2.2 Experimental

N,N'-bis(n-alkyl) tetra -carbonatenaphthalenediimide (Cx-NDI, where x is the number of methylene units in the alkyl side chains) was used as the molecule adsorbed on SWNTs. Cx-NDIs (with x = 3, 9), whose molecular structure was shown as **Figure 1**, were prepared using a modified version of a reported procedure.[6] As-prepared SWNTs (Carbon Nanotechnologies, Inc. Houston, TX) were purified by washing with hydrochloric acid (1 M) and rinsed with deionized water. Purified SWNTs (0.5 mg) were added to a DMF solution of Cx-NDI (0.1 mM, 5 ml), which was then sonicated for 30 min. The supernatant was collected after centrifuging the solution at 2000 G for 4 h. A Cx-NDI/SWNT complex was obtained on filter paper (polytetrafluoroethylene membrane 0.5 μm, Millipore) by filtering the supernatant. Excess Cx-NDI was washed from the filter using chloroform (100 ml). Solid Cx-NDI/SWNT from the filter paper was added to DMF (2 ml) and sonicated for 30 min. The solution was then drop-cast onto a cleaved SiO_2 substrate. Topographic observation was performed using tapping-mode AFM. After that 30-nm-thick gold was thermally evaporated onto half of the substrate as an electrode, and then a PCI-AFM measurement was performed to measure the electrical properties of the complex in nanoscale as introduced in

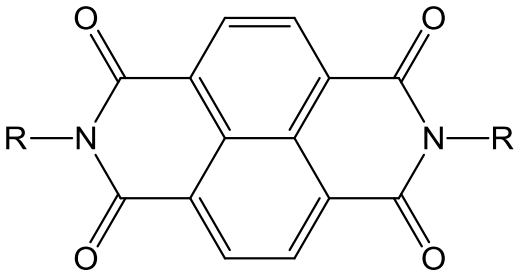

Figure 1. Molecular structure of Cx-NDI: x is number of methylene units in the alkyl side chain (R = $(CH_2)_{x-1}CH_3$).

In the case of C3-NDI, wires of the complex were observed to be 2.5–4.5 nm high, as shown in **Figure 2**a. Due to the diameter of the SWNTs was 1.1–1.5 nm, the height of the C3-NDI molecules could be calculated as 1.4–3.0 nm. This corresponds to approximately 4–8 NDI molecules for the π-π stacking distance between two adjacent similar NDI molecular planes is approximately 0.36 nm.[7] In the C9-NDI/SWNT complex, whose alkyl side chain was different to that of C3-NDI, the density of nanoparticles adsorbed onto the SWNTs was slightly lower than that for C3-NDI, as shown in Figure 2b.

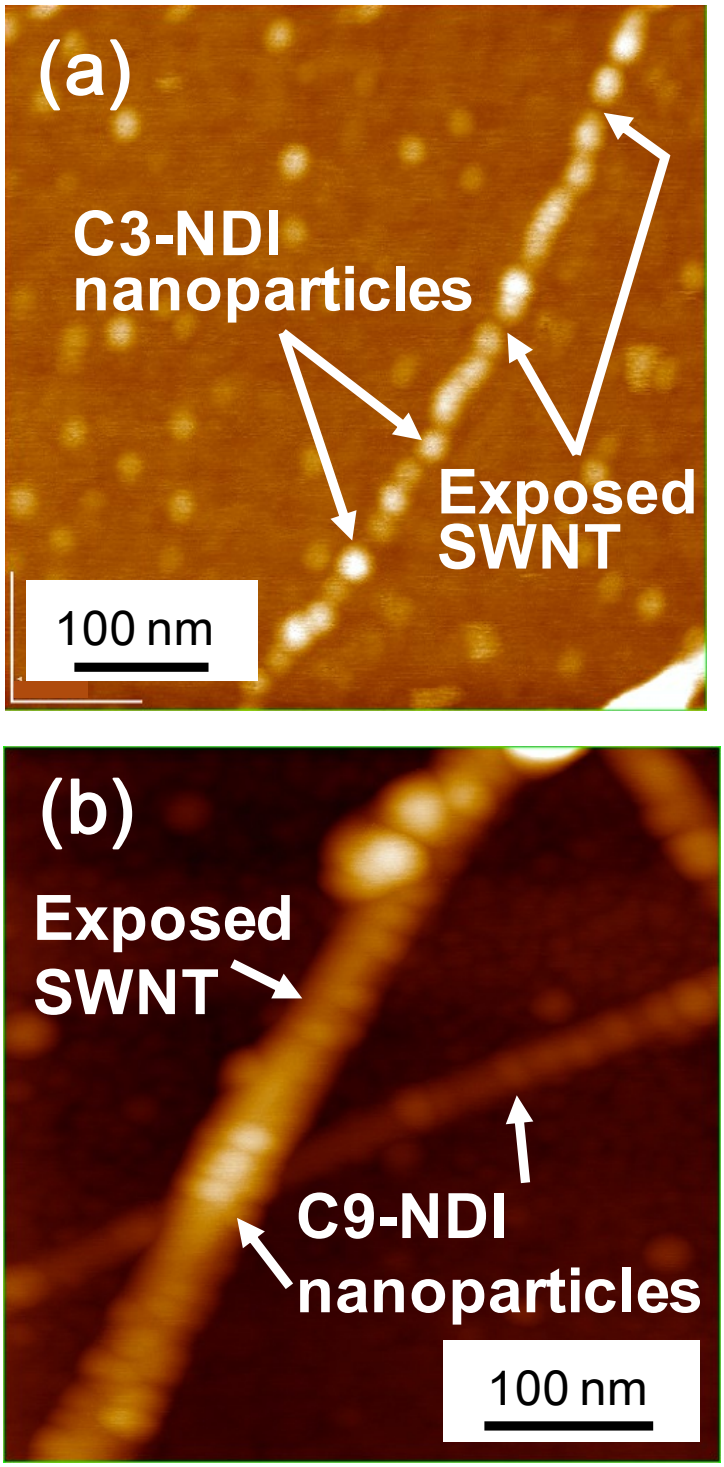

Figure 2. AFM image of (a) C3-NDI and (b) C9-NDI nanoparticles adsorbed on the side-wall of SWNTs.

2.3 Chirality distribution of SWNTs adsorbed by Cx-NDIs with different alkyl side chains

As described in Chapter 1, 1/3 of the pristine SWNTs should have metallic electronic structures and 2/3 of them are semiconducting statistically.[8, 9] The electronic structures can be confirmed by measuring *I-V* curves of the SWNT by PCI-AFM, because by the small contact measurement d*I*/d*V*-*V* curves are known to be proportional to the density of states (DOS). If the materials are metallic d*I*/d*V* shows positive finite values at zero bias, whereas for semiconducting materials d*I*/d*V* exhibit zero at zero bias voltage.

Measured on exposed carbon nanotube, typical *I-V* curves of SWNT extracted using C3-NDI are shown in **Figure 3**a, indicating they are metallic. In contrast, typical *I-V* curves for SWNTs extracted by C9-NDI could be ascribed as semiconducting due to the presence of plateau region around zero bias (Figure 3b). According to the *I-V* analysis of ca. 40 Cx-NDI/SWNT wires, majority of SWNT was metallic (69%) if C3-NDI was adsorbed, while semiconducting (59%) in the case of C9-NDI. The results clearly indicate that C3-NDI have selective adsorption toward metallic SWNT while C9-NDI did not. The selective adsorption of Cx-NDIs to SWNTs has been confirmed by the Raman spectra (Figure 7 in Chapter 1).

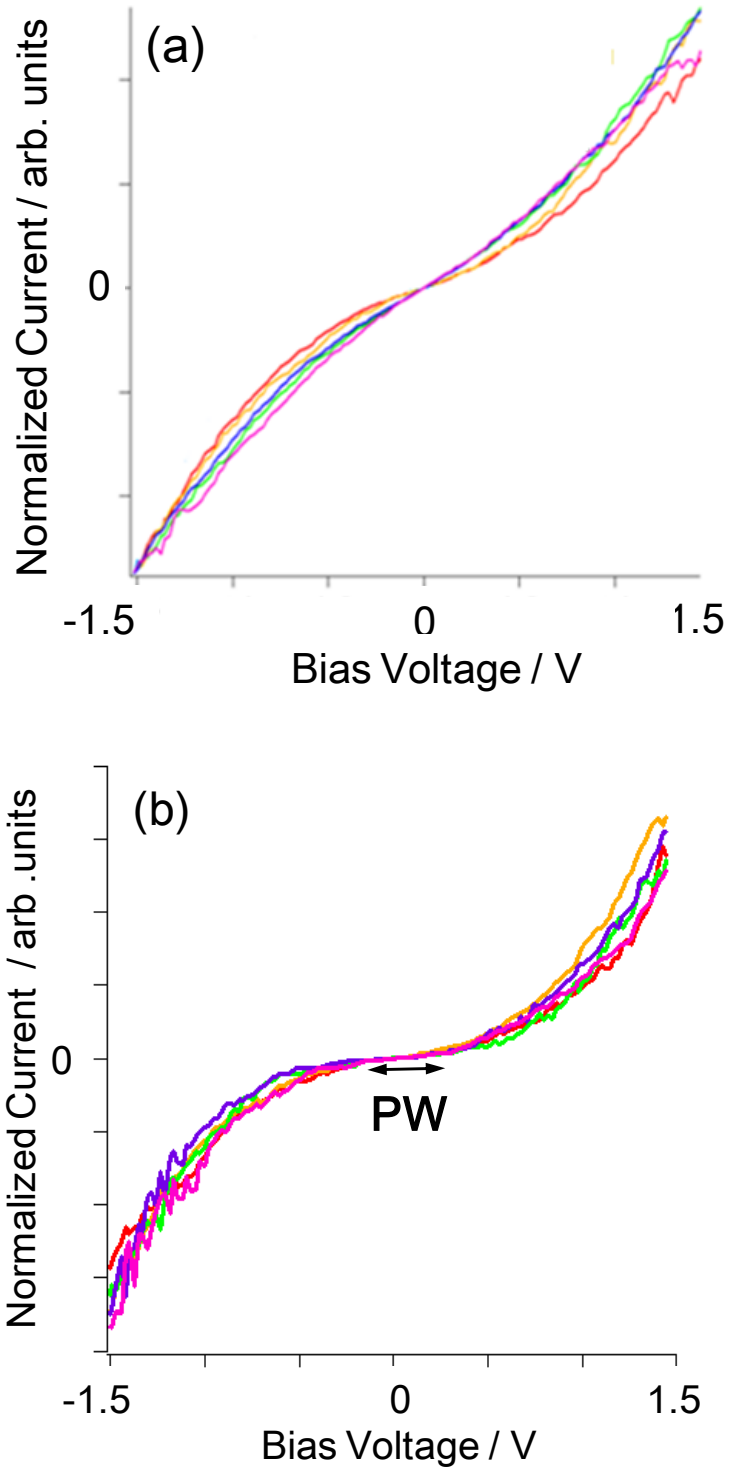

Figure 3. Normalized *I-V* curves measured on exposed carbon nanotube in the case of SWNTs adsorbed by (a) C3-NDI and (b) C9-NDI. All the *I-V* curves were normalized at -1.5 V. PW indicate the plateau width as defined by the bias difference of zero current region.

2.4 Rectification characteristics of Cx-NDI/SWNT controlled by the nanoparticle size

I-V curves measured at C3-NDI molecules adsorbed on metallic SWNTs were shown in **Figure 4**a. Similar to the case of porphyrin,[2] current rectification appeared and all the currents were suppressed at the positive bias. However, the normalized *I-V* curves at the negative bias were not coincident with each other, which was different to those in porphyrin/SWNT. Rectification ratio (RR) was defined as the absolute value of current at -2.5 V divided by current at 2.5 V (|a / b| in Figure 4a), so that degree of electrical rectification could be compared in quantity. Relationships of PW and RR against the height of C3-NDI particle were plotted respectively in Figure 4b. As the particle height increased, PW decreased, while RR was almost constant as the particle size was below 3 nm and gradually increased with a further increase of particle height. The experimental results indicated that PW and RR could be controlled by the particle size of C3-NDI.

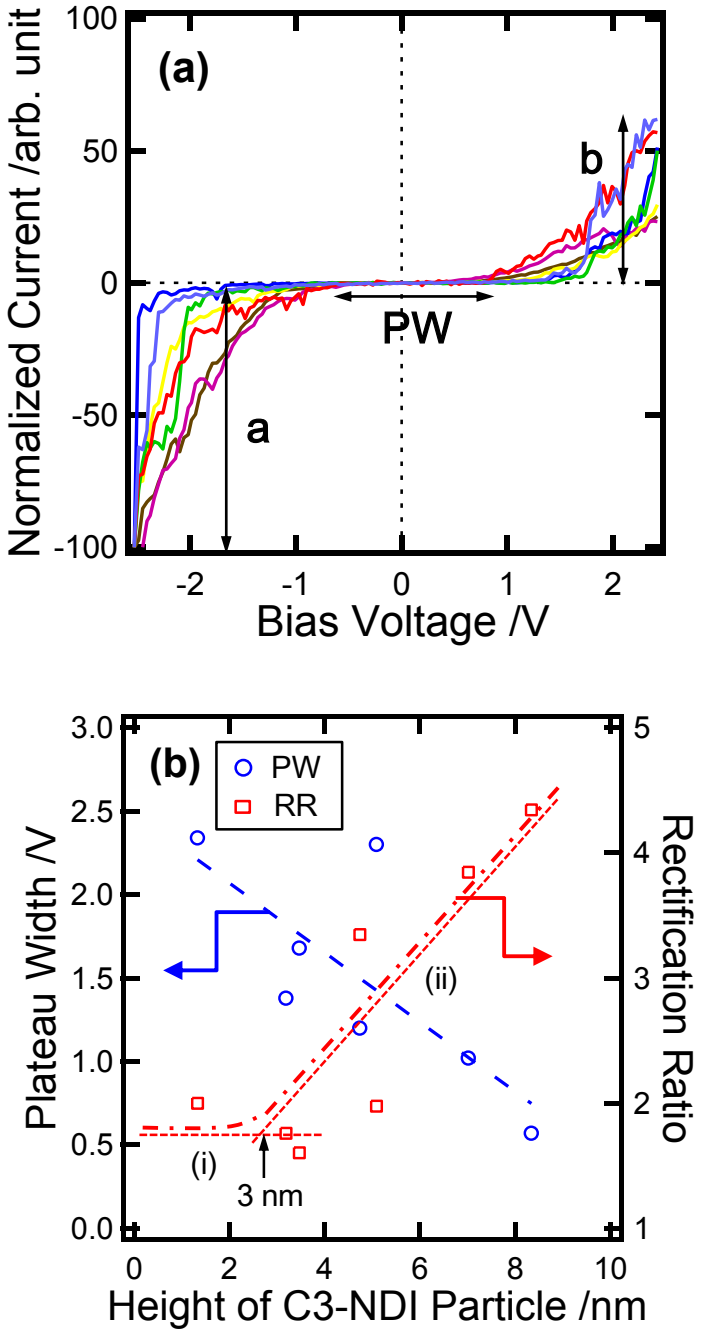

Figure 4. (a) Normalized *I–V* curves measured at C3-NDI particles on metallic SWNTs. PW was marked around zero bias while RR was defined as |a / b|. (b) RR and PW plotted against height of C3-NDI nanoparticles on SWNT. All data were obtained from *I-V* curves of the same SWNTs wiring. As C3-NDI particle height increased, RR initially kept constant as indicated by (i), and gradually increased which was shown as (ii). Dotted lines were added as a guide for eyes, and black color arrow indicated the (i)-(ii) boundary size of C3-NDI particle, which was around 3 nm.

Figure 5 showed *I–V* curves obtained from C9-NDI/semiconducting SWNT. Compared to the pristine SWNTs with a narrow PW (0.2 V) shown in Figure 3b, C9-NDI nanoparticles showed a wider PW (0.5 V). As the height of particles increased from 1.8 to 5.3 nm, currents at positive bias decreased obviously. Since all the *I-V* curves were normalized at -1.5 V, RR increased with an increase of particle size. This tendency was similar to that in the case of C3-NDI, although no sudden increase of RR was observed. This indicated that conduction of Cx-NDI on SWNT was determined by its main body regardless of alkyl side chain. A summary of the electrical properties of Cx-NDI/SWNT was listed as **Table 1**.

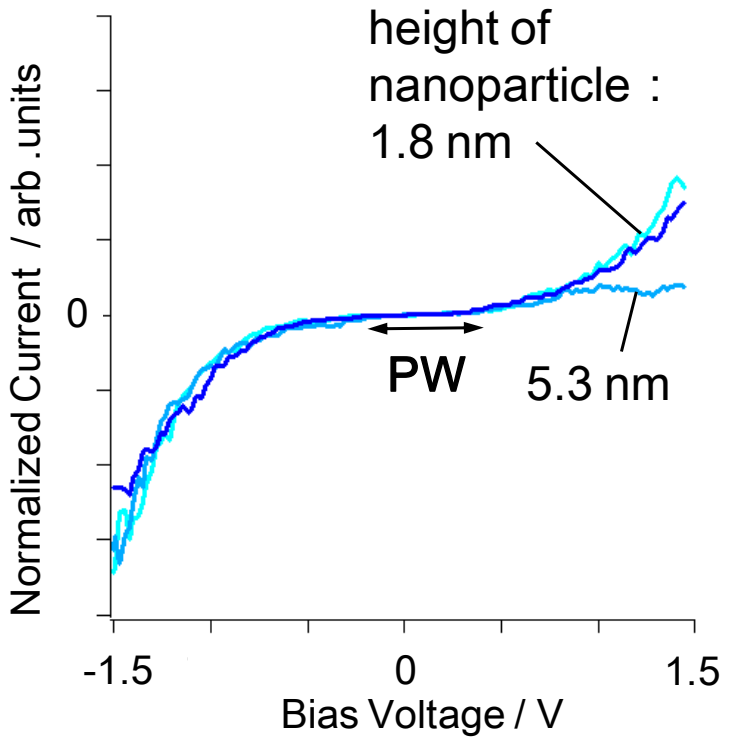

Figure 5. Normalized *I-V* curves measured at C9-NDI of different particle height adsorbed on SWNTs with a larger PW. As the height of particle increased from 1.8 to 5.3 nm, RR increased obviously.

Table 1. Summary of the electrical characteristics of Cx-NDI/SWNT

	C3-NDI	C9-NDI
***I-V* change after molecular adsorption**	Metallic state turned to semiconducting.	Rectification appeared.
plateau width (PW)	PW decreased when nanoparticle size became larger.	PW slightly increased compared with pristine SWNTs
rectification ratio (RR)	RR kept constant as nanoparticle height was below 3 nm, while increased with a further increase of particle size.	RR increased with an increase in nanoparticle height.

Curve-fitting of *I-V* data was proceeded by using several equations of different conduction mechanisms including Schottky emission, Frankel-Poole conduction, Fowler-Nordheim tunneling,[10] and Coulomb blockade.[11] The best fit was obtained using Frankel-Poole conduction and Schottky emission, as shown in **Figure 6**.

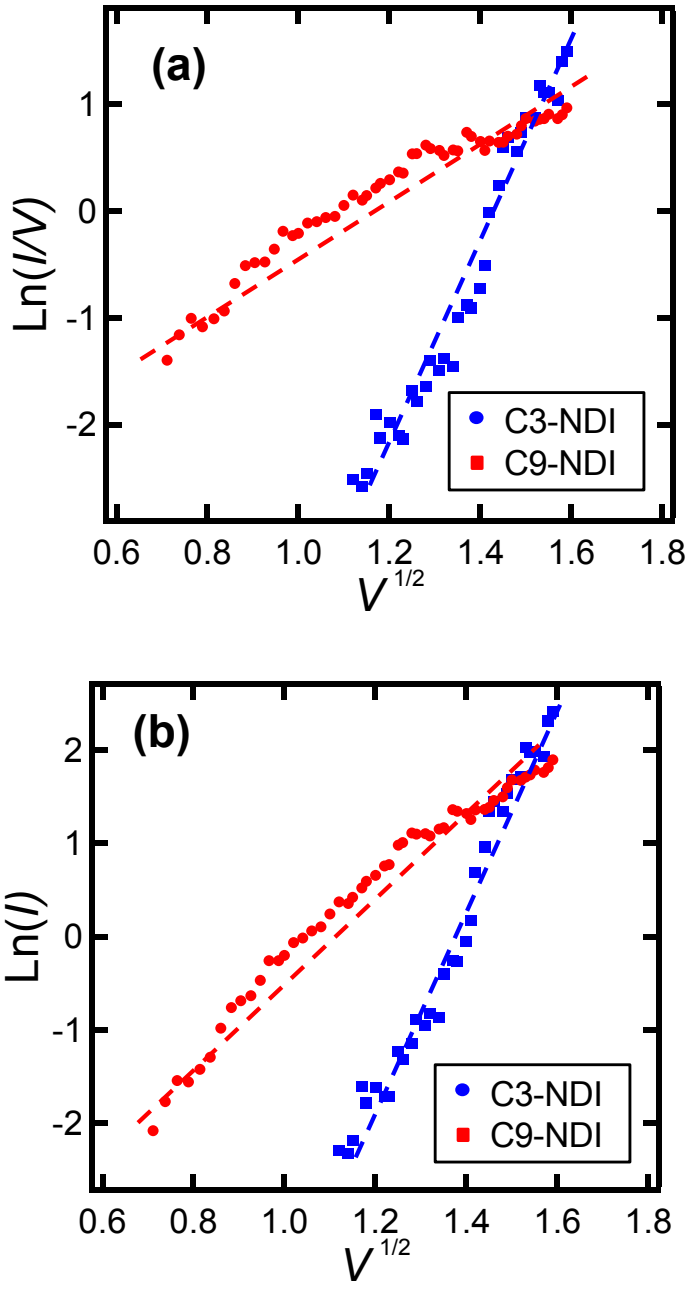

Figure 6. Curve-fitting of *I-V* data for C3-NDI/SWNT and C9-NDI/SWNT based on the voltage dependence equations of (a) Frankel-Poole conduction and (b) Schottky emission. Only the data between -2.5 V and -0.5 V were used in the fitting to avoid the invisible current around the zero bias.

The change of PW is considered as the result of a shift in the vacuum level at the interface of nanoparticles/SWNT, which is induced by a charge

transfer between particles and carbon nanotube. Such a vacuum level shift can be as large as 1.0 eV, and decreases with a reduction of molecular layer number.[12] Within a small thickness range (< 10 nm), work function of nanoparticle can be changed by the magnitude of dipole at the interface, which may be another reason to the change of PW. The observed change of PW (< 1.5 eV) as plotted in Figure 4b is reasonable compared with the reported results.

As for the change of RR, the height of nanoparticle on SWNTs is an important factor. C3-NDI is taken as an example for Cx-NDIs. At room temperature, equations of Schottky emission and Frankel-Poole conduction are too similar to be distinguished with each other as shown in Figure 6. Only Schottky emission will be discussed hereafter, because C3-NDI nanoparticle on SWNT is too thin to form a large crystal which is required to have a band structure for Frankel-Poole conduction.[10] As shown in **Figure 7**a, in the case of thin particle (< approximately 3 nm), electrons tunnel through a molecular potential barrier induced by a mirror charge. Thus RR keeps constant to particle height of C3-NDI as indicated by the dashed line (i) in Figure 6b. However, when the particle becomes thicker, electrons cannot tunnel through but pass over the whole potential barrier, as shown in Figure 7b. Due to a charge transfer from Pt to C3-NDI, the energy level is lifted up at the interface. As the particle height of C3-NDI continues increasing, energy level at the interface is further lifted up to make a larger barrier, and would be saturated around 10 nm as described above. Therefore, RR gradually increases as the particle size of C3-NDI

increase in the range of 3-10 nm, as indicated by the dashed line (ii) in Figure 4b. Unfortunately, due to a steric hindrance on SWNT wire, height of C3-NDI nanoparticle cannot reach to 10 nm. Thus it becomes impossible to prove the proposed saturation of RR. The dashed lines (i) and (ii) cross at around 3 nm in Figure 4b, which is considered as the boundary size between tunneling conduction and Schottky-like emission.

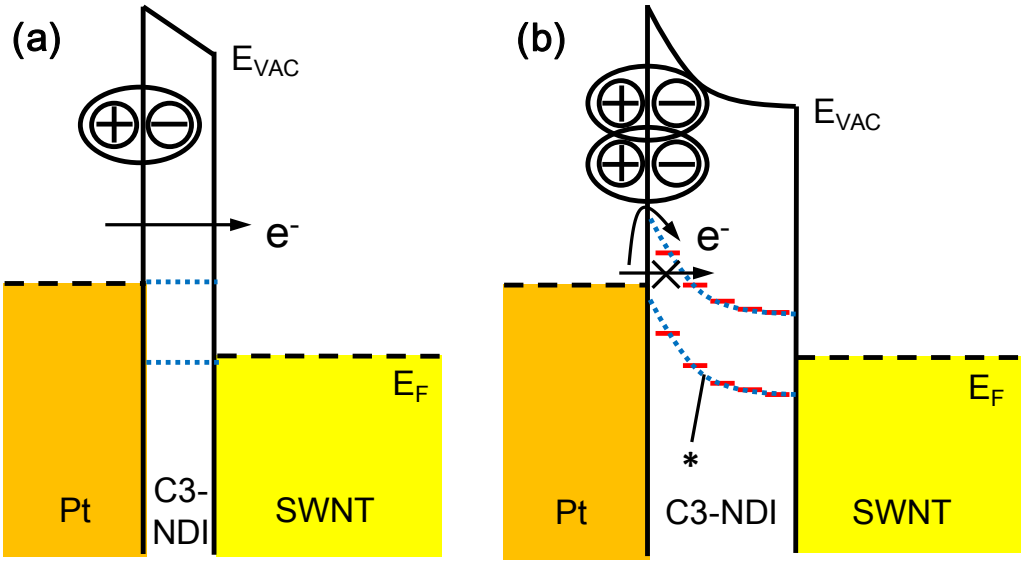

Figure 7. Schematic depiction of band structure at the interface of SWNT/C3-NDI/Pt in the case of (a) thin and (b) thick nanoparticles of C3-NDI. A positive bias is applied to SWNT in both cases. Electrons tunnel through the potential barrier when C3-NDI particle is thin, therefore RR is constant with the height of nanoparticles. As nanoparticle becomes thicker, electrons have to pass over the whole potential. Energy level of C3-NDI is lifted up at the interface due to the electrical field induced by charge transfer from Pt to C3-NDI, which is marked as *. Thus, RR increases with a further increase of C3-NDI particle size, since the potential barrier becomes larger when layer number of C3-NDI molecules increases. E_{VAC}: vacuum level; E_F: Fermi level.

It should be noticed that the so-called Schottky-like emission is a totally different mechanism from general Schottky barrier appearing at semiconductor–metal interface. Generally speaking, in the case of

junction between *p*-type semiconductor and metal, electrons come from metal to the semiconductor interface and become neutral as depleted layer at the Schottky junction. In the present case of neutral acceptor molecule and metal, electron from metal comes to interface to be electron rich status. That is why the energy level of NDI at the interface increased to be Schottky-like barrier. Comparing from the porphyrin (electron-donor molecule) case,[2] it is similar that electron energy level bending is occurred at the interface between Pt and NDI, but difference between the present Schottky-like conduction and Fowler–Nordheim conduction in porphyrin case is considered to be occurred by a difference of their Fermi levels. In other words, this is caused by the difference between electron-donor and -acceptor molecules.

2.5 Large rectification effect achieved by a combination of SWNTs junction and C3-NDI/SWNT interface

Recently, configuration and electronic transport of SWNTs junction have been intensively researched from both theoretical and experimental perspectives, and rectifying barrier was reported formed at the junction.[13-18] A rectification effect much larger than common semiconducting-metal diode can be possible, if such SWNTs junction is combined with certain rectifying interface between nanoparticle and SWNTs. C3-NDI can be a good candidate of such particle as described in this chapter.

Figure 8a showed a typical AFM image of a SWNTs junction formed by two SWNT wires, one of which was bared (nanotube I of 2.3 nm high) and linked to the gold electrode while the other (nanotube II of 2.1 nm high) was adsorbed by C3-NDI molecules, as shown in the insets. Different from SWNTs junctions reported previously,[13, 18, 19] only nanotube I directly connected to the gold electrode, as shown schematically in Figure 8b. In other words, all electrons from (to) nanotube II must pass through the junction.

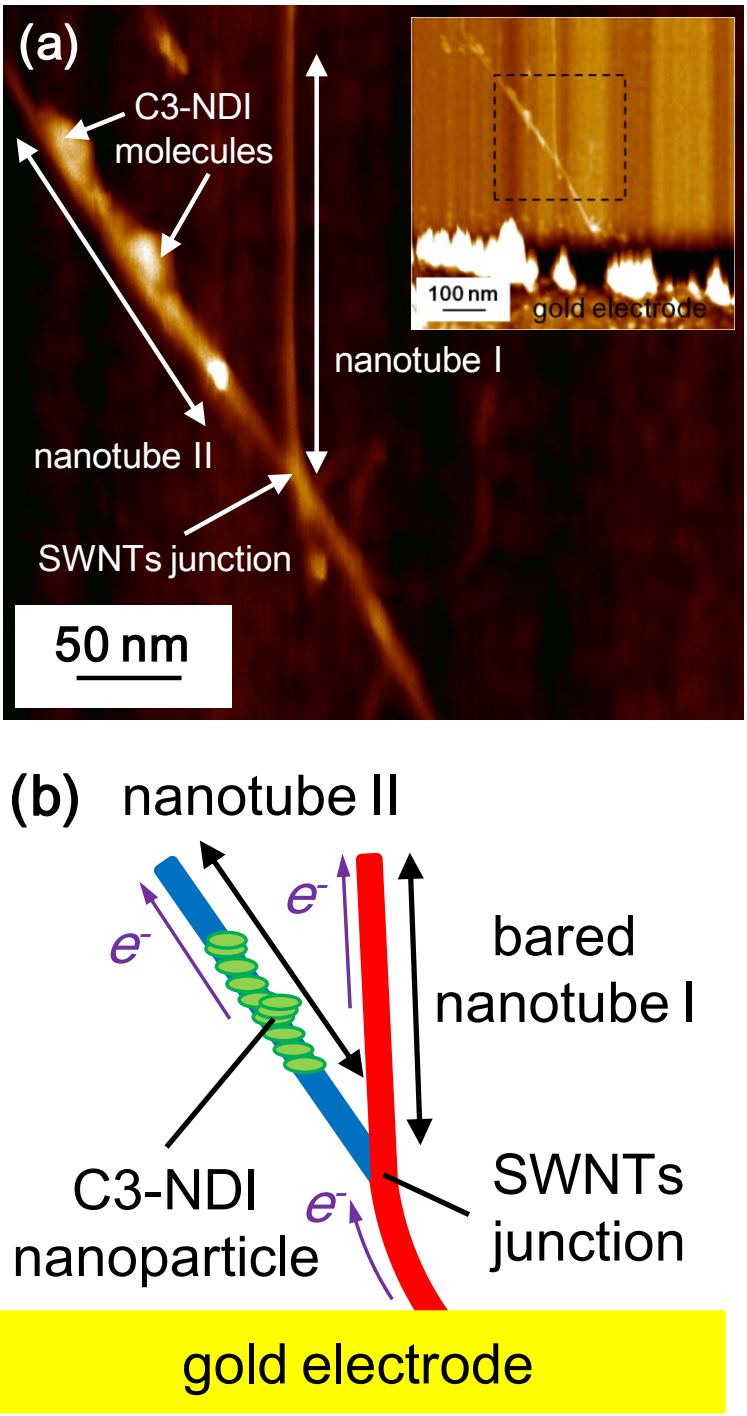

Figure 8. (a) AFM image of a SWNTs junction formed by two SWNT wires indicated as nanotube I and II, respectively. Inset: AFM image containing nanotube I, II and gold electrode, and the dashed box indicated magnified area. (b) Schematic depiction of the SWNTs junction.

I-V curves were measured at several positions in Figure 8a. Large

conductivity was detected in nanotube I, which indicated a metallic state as demonstrated in **Figure 9**a. However, rectification appeared on the bared part of nanotube II according to Figure 9b. In Figure 9c, larger degree of rectification was detected through C3-NDI nanoparticles (2 ~ 3.2 nm high) adsorbed on nanotube II. According to the insets in Figure 9b and c, the average RR of bared nanotube II was calculated as 11.4, while C3-NDI molecules on nanotube II as 38.2.

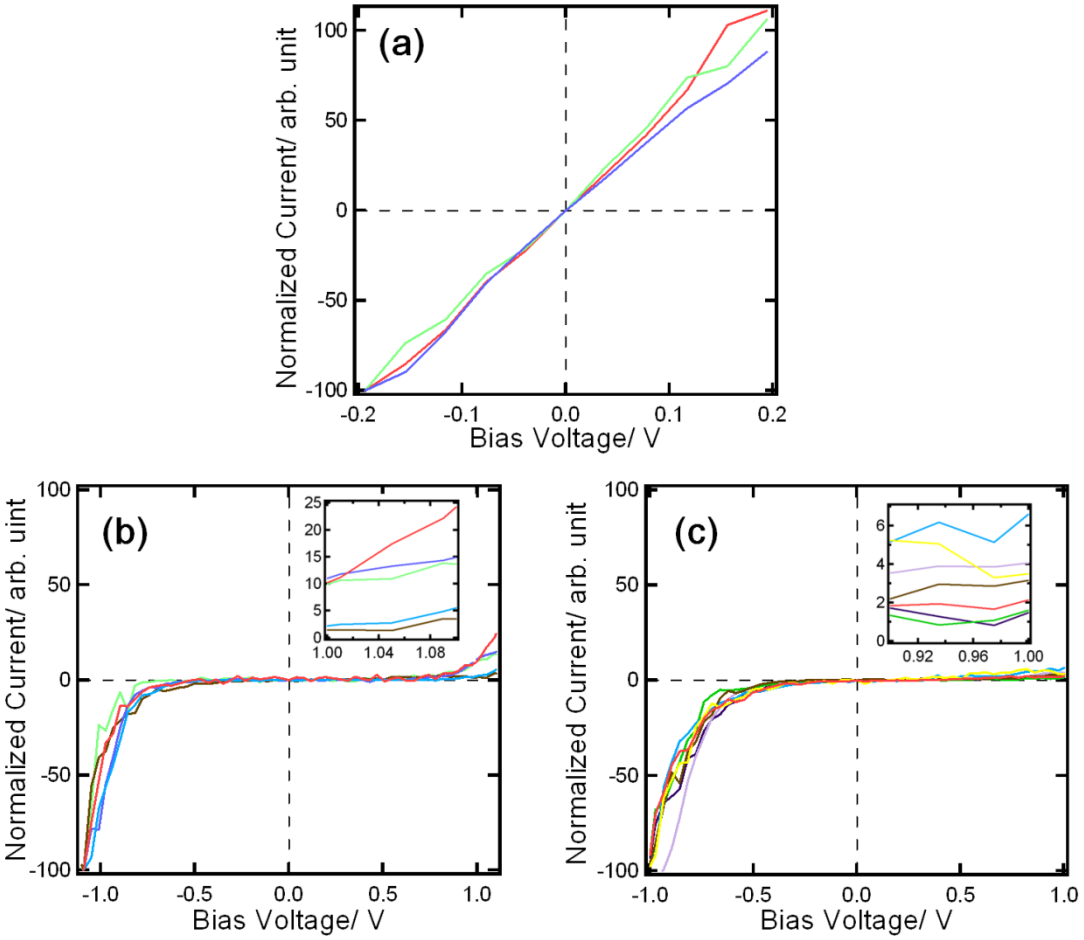

Figure 9. Normalized *I-V* curves measured at (a) nanotube I, (b) nanotube II and (c) C3-NDI nanoparticle on nanotube II. *I-V* curves of (a) and (b) were normalized at -1 V, and the suppressed currents at positive bias were demonstrated in the insets so that average RR could be calculated. Axis labels of the insets were omitted for simplicity.

Figure 10 showed that current images made up by *I-V* curve normalized at -1.0 V, by which shapes of nanotubes I and II are confirmed. The magnitude of current at each pixel is proportional to its grayscale, where large conductivity is indicated by white color and gray color indicates no conductivity. When bias was almost 0 V (Figure 10a), there was no conductivity except metallic nanotube I connected to the gold electrode directly. As bias was increased to 1.0 V (Figure 10b), conductivity appeared at nanotube II, while current of C3-NDI parts was lower than that of bared nanotube II. This result confirmed a larger current rectification at C3-NDI nanoparticles compared with that of bared nanotube II, as described before.

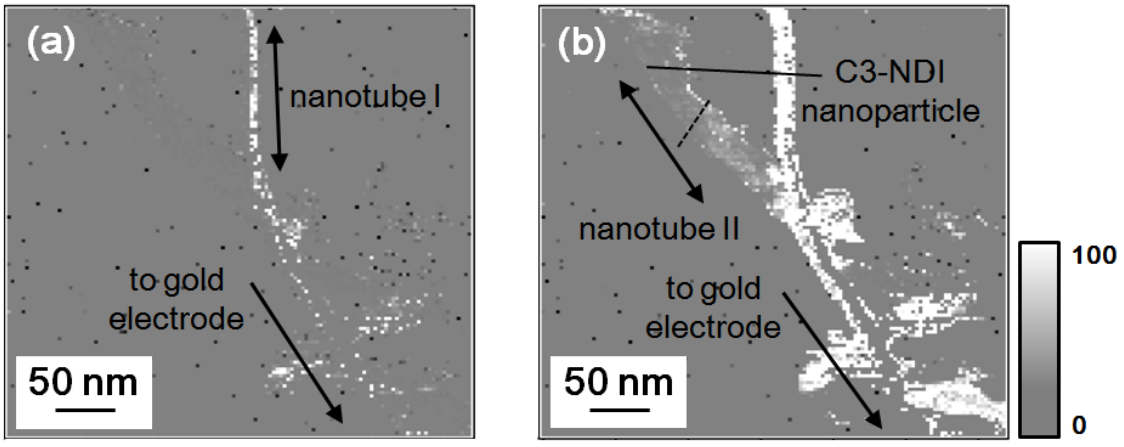

Figure 10. Normalized current image of SWNTs junction under bias is (a) 0.1 V and (b) 1.0 V. Both current images were made by Igor Pro and normalized at -1.0 V. The magnitude of current at each pixel is proportional to its grayscale, where large conductivity is indicated by white color and gray color indicates no conductivity.

Because of the doping effect of oxygen in the atmosphere,[20-22] nanotube II is considered as a *p*-type semiconductor, which forms the junction in

Figure 8a with metallic nanotube I. Due to the appearance of rectification at exposed part of nanotube II, certain rectifying barrier must exist at the junction. Average conductance of bared nanotube II under -1 V is calculated as 9.24 nS based on dI/dV data derived from I-V curves in Figure 9b, which is also equal to $1.19 \times 10^{-4} G_0$ ($G_0 = 2e^2/h$, where e is electric charge and h is Planck constant). The contact resistance between Pt cantilever and nanotube at -1 V is less than 10 MΩ as reported,[23] which is much fewer than the resistance of SWNTs junction itself here. Transmission probability is calculated as 6×10^{-5} according to reported results,[13, 24] which is similar compared with the magnitude of total transmission probability of the Schottky barrier.[13] This indicates that the rectification barrier at SWNTs junction in this study should be the Schottky barrier. In the case of forward bias (negative bias applied on metallic SWNT), which is shown as **Figure 11**b, Fermi level of metallic SWNT is lifted up and Schottky barrier height (SBH) is reduced, thus hole can transfer from top of valence band of semiconducting SWNT to Fermi level of metallic SWNT. On the contrary, reverse bias (positive bias applied on metallic SWNT) increases Schottky barrier height, as seen in Figure 11c, that hole transfer is not favored.

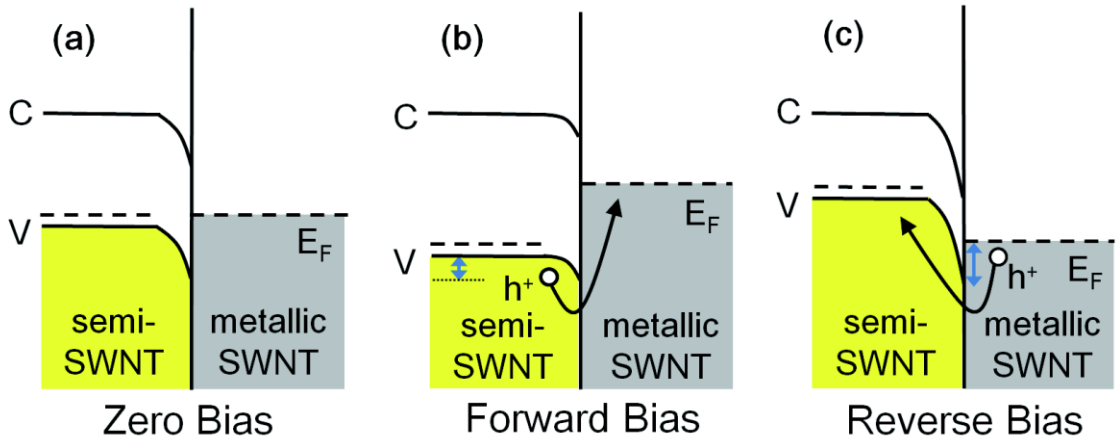

Figure 11. Schematic energy level diagram of Schottky barrier formed by metallic and *p*-type semiconducting SWNTs, in the case of (a) zero bias, (b) forward (negative) bias and (c) reverse (positive) bias. Bias is applied to the metallic SWNT. Conduction band, valence band, and Fermi level are respectively represented as *C*, *V*, E_F, while Schottky barrier height is indicated by the blue arrow.

As discussed in the previous section, polarization induced by charge transfer is considered between C3-NDI and Pt. In the case of forward (negative) bias, energy level of C3-NDI bends in consistent to the up-lifting Fermi level of semiconducting SWNT while pins at the interface formed with grounded Pt. Thus, electrons pass over the potential barrier. When reverse (positive) bias is applied, energy level of C3-NDI is lifted down and electrons from Pt to C3-NDI are suppressed to pass over.

It is already known that SWNTs junction is indispensible for electron transfer from gold electrode to nanotube II. Therefore, the large rectification effect of C3-NDI molecules on nanotube II is considered as a combination of Schottky barrier at SWNTs junction and rectification induced by polarization between Pt cantilever and C3-NDI. It is speculated that total rectification ratio of C3-NDI molecule on nanotube II

$RR_{total} = RR_{NDI} \times RR_{junction}$, where RR_{NDI} is the degree of rectification induced by polarization between Pt and C3-NDI, and $RR_{junction}$ is ascribed to the rectification of Schottky barrier at the junction. Thus RR_{NDI} can be calculated as 3.4 based on the average RR as discussed above. This magnitude fits well with the plot of RR against C3-NDI molecular height as shown in Figure 4b.

2.6 Summary

In this chapter, Cx-NDIs with different alkyl side chains were physically adsorbed on SWNTs, and electrical properties of the complexes were measured by PCI-AFM. *I-V* analysis indicated that the majority of SWNTs adsorbed by C3-NDI was metallic while semiconducting in the case of C9-NDI. Current rectification appeared at the Cx-NDI nanoparticles on SWNTs, and the currents were suppressed at the positive bias. With an increasing of C3-NDI nanoparticle size, plateau width (PW) in *I-V* curve decreased while rectification ratio (RR) kept constant initially and gradually increased when nanoparticle height further increased. Polarization induced by the charge transfer between Pt and C3-NDI, which can be largely influenced by particle size, has been considered as the reason for the changes in PW and RR. Besides, a large rectification effect was achieved by a combination of the rectifications induced by SWNTs junction and C3-NDI/SWNT interface.

References

1. Ajayan, P. M.; Tour, J. M. *Nature* **2007,** 447, (7148), 1066-1068.
2. Tanaka, H.; Yajima, T.; Matsumoto, T.; Otsuka, Y.; Ogawa, T. *Adv. Mater.* **2006,** 18, (11), 1411-1415.
3. Guo, X. F.; Gan, Z. H.; Luo, H. X.; Araki, Y.; Zhang, D. Q.; Zhu, D. B.; Ito, O. *J. Phys. Chem. A* **2003,** 107, (46), 9747-9753.
4. Ahmed, E.; Ren, G.; Kim, F. S.; Hollenbeck, E. C.; Jenekhe, S. A. *Chem. Mater.* **2011,** 23, (20), 4563-4577.
5. Erten, S.; Alp, S.; Icli, S. *J. Photochem. Photobiol. Chem.* **2005,** 175, (2-3), 214-220.
6. Katz, H. E.; Johnson, J.; Lovinger, A. J.; Li, W. J. *J. Am. Chem. Soc.* **2000,** 122, (32), 7787-7792.
7. Ji, H. F.; Majithia, R.; Yang, X.; Xu, X. H.; More, K. *J. Am. Chem. Soc.* **2008,** 130, (31), 10056-10057.
8. Bandaru, P. R. *J. Nanosci. Nanotechnol.* **2007,** 7, (4-5), 1239-1267.
9. Ajayan, P. M. *Chem. Rev.* **1999,** 99, (7), 1787-1799.
10. Barsanti, L.; Evangelista, V.; Gualtieri, P.; Passarelli, V.; Vestri, S., *Molecular Electronics: Bio-sensers and Bio-computers (NATO Science Series II: Mathematics, Physics and Chemistry)*. Springer: 2003.
11. Aleshin, A. N.; Lee, H. J.; Jhang, S. H.; Kim, H. S.; Akagi, K.; Park, Y. W. *Phys. Rev. B* **2005,** 72, (15), 153202.
12. Ishii, H.; Sugiyama, K.; Ito, E.; Seki, K. *Adv. Mater.* **1999,** 11, (8), 605-625.
13. Fuhrer, M. S.; Nygard, J.; Shih, L.; Forero, M.; Yoon, Y.-G.; Mazzoni, M. S. C.; Choi, H. J.; Ihm, J.; louie, S. G.; Zettl, A.; McEuen, P. L. *Science* **2000,** 288, (5465), 494-497.
14. Fuhrer, M. S.; Lim, A. K. L.; Shih, L.; Varadarajan, U.; Zettl, A.; McEuen, P. L. *Physica E* **2000,** 6, (1-4), 868-871.
15. Fujiwara, A.; Iijima, R.; Suematsu, H.; Kataura, H.; Maniwa, Y.; Suzuki, S.; Achiba, Y. *Physica B* **2002,** 323, (1-4), 227-229.
16. Terrones, M.; Banhart, F.; Grobert, N.; Charlier, J. C.; Terrones, H.; Ajayan, P. *Phys. Rev. Lett.* **2002,** 89, (7), 075505.
17. Son, Y.-W.; Lee, S.; Lee, C.-K.; Ihm, J. *Phys. Rev. B* **2005,** 71, (20), 205422.
18. Kim, D. H.; Huang, J.; Rao, B. K.; Choi, W. B. *IEEE T.*

Nanotechnol. **2006,** 5, (6), 731-736.
19. Liu, L.; Fang, J.; Lu, L.; Zhou, F.; Yang, H.; Jin, A.; Gu, C. *Phys. Rev. B* **2005,** 71, (15), 155424.
20. Xian, X.; Yan, K.; Zhou, W.; Jiao, L.; Wu, Z.; Liu, Z. *Nanotechnology* **2009,** 20, (50), 505204.
21. Collins, P. G.; Bradley, K.; Ishigami, M.; Zettl, A. *Science* **2000,** 287, (5459), 1801-1804.
22. Derycke, V.; Martel, R.; Appenzeller, J.; Avouris, P. *App. Phys. Lett.* **2002,** 80, (15), 2773.
23. Otsuka, Y.; Naitoh, Y.; Matsumoto, T.; Kawai, T. *Appl. Phys. Lett.* **2003,** 82, (12), 1944.
24. Landauer, R. *Phys. Scripta* **1992,** T42, 110-114.

Chapter 3

Electrical Properties of Phosphododecamolybdic Acid Adsorbed on Single-Walled Carbon Nanotube

Abstract: Electrical properties of phosphododecamolybdic acid (PMo_{12}) nanoparticle/SWNTs complexes were measured by PCI-AFM. Rectification direction was reversed as PMo_{12} particle size varied, and the relation between rectification direction inversion and particle size was found opposite between semiconducting and metallic SWNTs. Kelvin probe force microscopy (KPFM) results indicated an opposite charge distribution of PMo_{12} on semiconducting SWNT to that of metallic SWNT, which was due to the different charging efficiencies between SWNTs and PMo_{12}. Two mechanisms including usual *p*-*n* junction and *I*-*V* curve drift induced by dipole moment at the PMo_{12}/SWNT interface, have been proposed for the inversion of rectification direction. Negative differential resistance (NDR) properties were observed in the *I*-*V* curves of PMo_{12} complex as well.

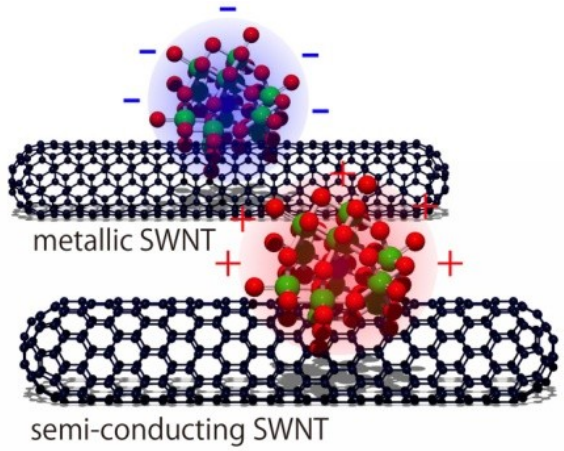

3.1 Introduction

By hybridizing single-walled carbon nanotube (SWNT) with molecules, new functionalities can emerge,[1-3] which combines the functionalities of the molecules and the high carrier mobility of SWNT,[4, 5] to afford important electronic parts in molecular scale electronics.[6-8] Rectification functionality emerged when planar electron-donating organic molecules like porphyrin,[9] as well as electron-accepting molecules like naphthalenediimide adsorbed on SWNT, which have been described in previous chapters. In the both molecular systems the rectification were observed just one direction, that is when the positive bias were applied to the carbon nanotube side (and negative bias to the molecules) the current was suppressed. Since such nanoscale junctions can be possibly the smallest diodes, it can be an interesting topic in controlling the diode behavior of the system. The most important challenge can be inversion of the rectification direction.

Although the mechanism of the emergence of the rectification functionality by the combination of SWNT and molecules is not clear perfectly yet, it is a reasonable prediction that the molecular orbital (MO) energy levels of the molecules might be responsible for determining the rectification direction. Polyoxometalates (POMs) can be a good candidate for the trials because they have unique redox property and electronic versatility.[10-13] Phosphododecamolybdic acid ($H_3PMo_{12}O_{40}$, PMo_{12}, **Figure 1**) is one compound of the family of POMs, which shows reversible multi-electron redox property,[14, 15] and can work as a good cathode for

lithium ion battery when hybridized with SWNT.[16] Such a multi-electron redox material having low redox potential would show quite different electronic properties compared to ordinal organic molecules like porphyrins or naphthalenediimides when hybridized with SWNT. By using PMo_{12} with highly electron deficient property, reversed rectification might be observed at the interface with SWNT.

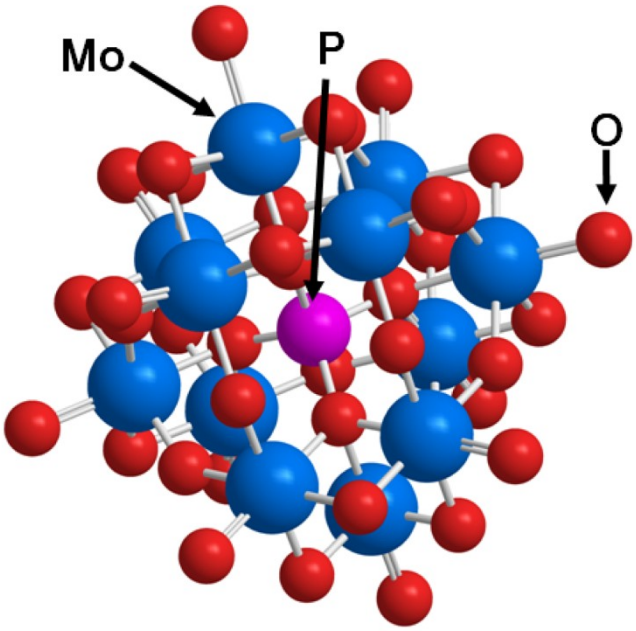

Figure 1. Molecular structure of PMo_{12}. Reproduced from the reported X-ray crystallographic structure.[17]

In this chapter, the electrical properties of PMo_{12}/SWNT complex were measured by PCI-AFM, and an inversion of rectification direction was observed with a change of particle size or "chirality" of SWNT. Kelvin probe force microscopy (KPFM) was used to measure the surface potential of the PMo_{12} nanoparticles adsorbed onto SWNTs, which was proved

opposite between semiconducting and metallic SWNTs. Two possible mechanisms have been established to explain the observed results. Additionally, negative differential resistance (NDR) property was also found in the PMo_{12}/SWNT nanoscale junction.

3.2 Experimental

Purified SWNTs and PMo_{12} hydrate (1 mg, Wako Pure Chemical Industries, Ltd., Japan) were mixed in ethanol (10 mL) and sonicated for 2 h. The suspension was then cast onto a SiO_2 substrate using a syringe and then dried in air. The topography observations were performed using tapping-mode AFM (JEOL JSPM 4210). Subsequently, a 30-nm-thick layer of gold was thermally evaporated onto half of the substrate to form an electrode. The electrical properties of the complex were measured at the nanoscale using PCI-AFM with a bias sweep from +2.5 to −2.5 V. During this measurement, bias was applied to the gold electrode and the Pt cantilever was grounded.

For the KPFM measurement, a PMo_{12}/SWNT complex suspension prepared by the same procedure was cast onto freshly cleaved highly oriented pyrolytic graphite (HOPG) using a syringe and then dried in air. The KPFM measurements were performed using an AFM modified by a lock-in amplifier (JEOL, TM-26031), which allowed simultaneous topography and contact potential difference (CPD) image measurements. For both the *I-V* and KPFM measurements, a commercially available Pt-coated AFM cantilever was used.

Figure 2 showed the AFM image of a typical PMo_{12}/SWNT complex wire cast onto a SiO_2/Si substrate, and the height of the complex wire ranged from 2.3 to 7.4 nm. As the diameter of the SWNT could be estimated to be 1.3 nm from the exposed part of the complex, the heights of the PMo_{12} nanoparticles were ~1.0 – 6.1 nm, which corresponded to ~1 – 6

PMo_{12} molecules given that the molecular size of PMo_{12} was 1.1 nm.[18]

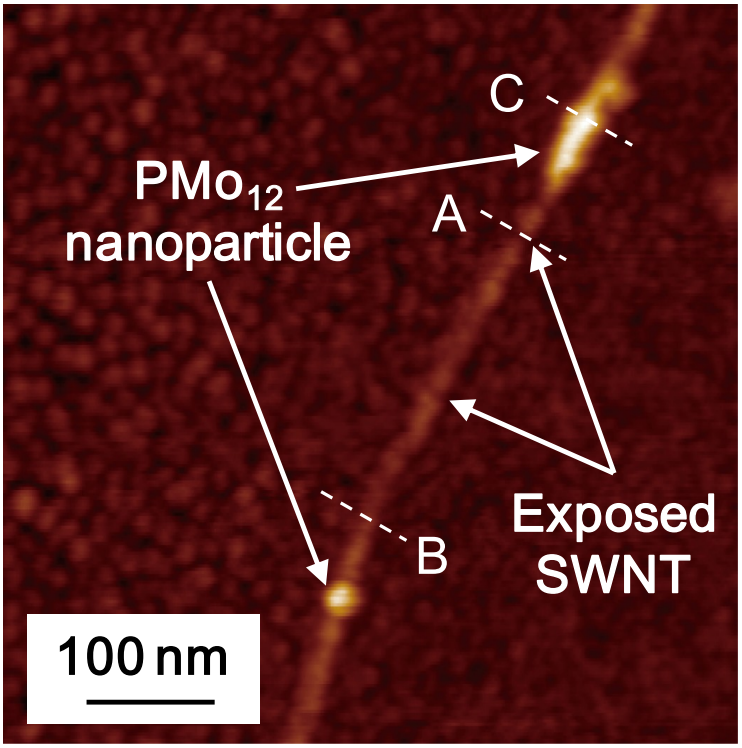

Figure 2. AFM image of the PMo_{12}/SWNT complex. Lines A, B, and C indicated the exposed part of the nanotube (the observed height was 1.3 nm), and the middle (2.3 nm) and highest (7.4 nm) parts of the PMo_{12}/SWNT complex, respectively.

3.3 Rectification direction inversion in PMo_{12}/SWNT complex

As described above, the rectification direction in organic planar molecule/SWNT complexes is always the same, i.e., the current is suppressed at a positive bias. However, in the present study, both rectification directions were observed depending on the samples and the position of the measurement.

The rectification directions were dependent on the position of the measurement even on the same wire, as shown in **Figure 3**. In the position which was assigned as an exposed nanotube based on the apparent AFM height (Zone I, Figure 3b), symmetrical *I-V* curves with plateau widths of approximately zero bias were observed indicating that the carbon nanotube is semiconducting. In the area which comprised the medium topological heights (Zone II, Figure 3c), currents were suppressed at a positive bias. In contrast, in the case of the highest topological heights (Zone III, Figure 3d), the opposite rectification direction was observed and the currents were suppressed at a negative bias.

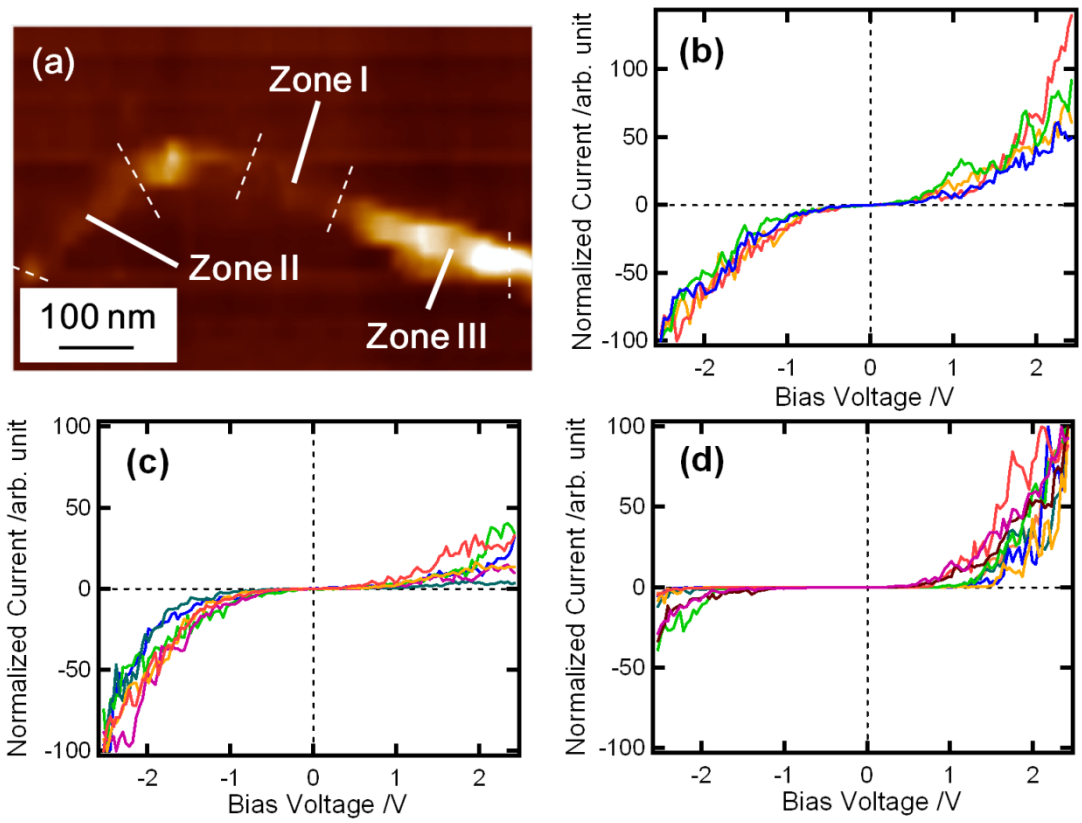

Figure 3. (a) AFM image of PMo_{12}/semiconducting SWNT, which can be classified into three zones: Zone I (exposed nanotube), II (low complex height) and III (high complex height). Normalized *I-V* curves obtained in (b) Zone I, (c) Zone II and (d) Zone III.

When metallic SWNTs were used, different results were shown in **Figure 4**. The exposed parts of the nanotube were confirmed to be metallic via the *I-V* curves (Figure 4b). The relationship between the rectification direction and complex height was completely opposite to that of the semiconducting SWNTs discussed above. When measured at a relatively low complex height (Zone II, Figure 4c), the currents were suppressed at a negative bias; in contrast, at a high complex height (Zone III, Figure 4d), the currents were suppressed at a positive bias.

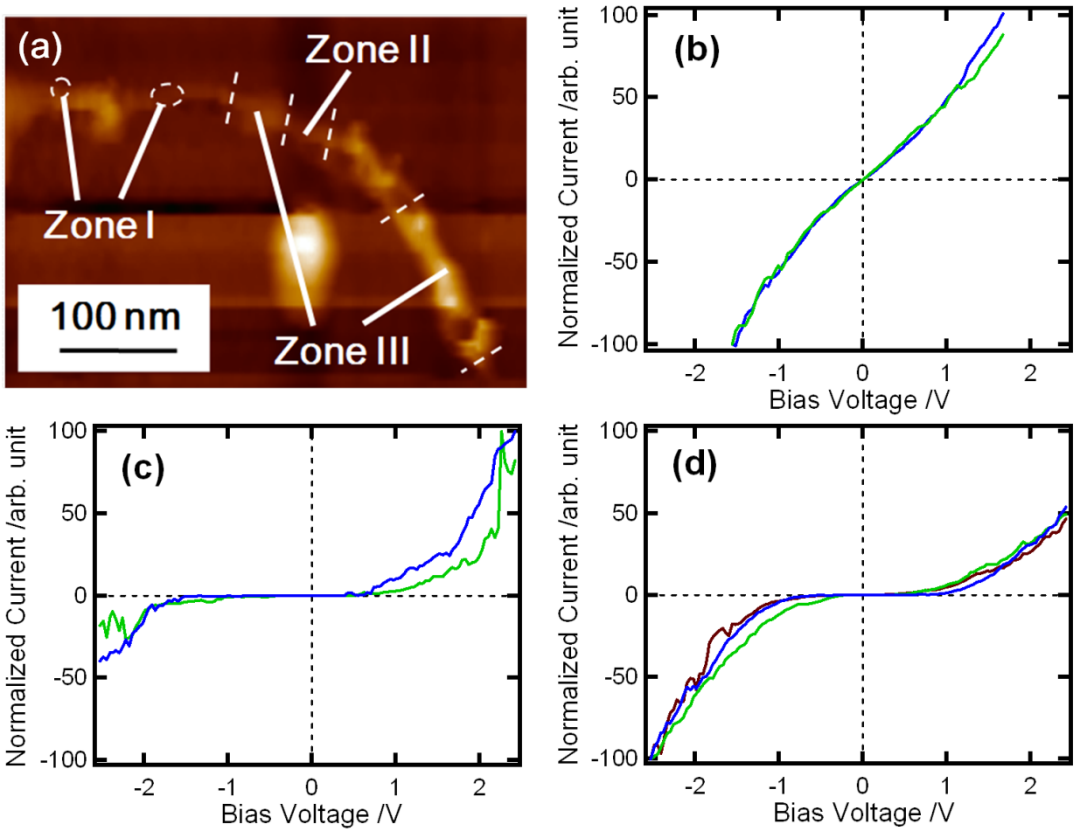

Figure 4. (a) AFM image of PMo_{12}/metallic SWNT, which can be classified into three zones: Zone I (exposed nanotube), II (low complex height) and III (high complex height). Normalized *I-V* curves obtained in (b) Zone I, (c) Zone II and (d) Zone III.

Representative results for the semiconducting and metallic SWNTs are summarized in **Figure 5**, which features the natural logarithm of the rectification ratio (RR) plotted against the height of the nanoparticles. Accordingly, when *I-V* curves are symmetric RR is equal to 1 and the $\log_e$(RR) is 0 (**Figure 6**). When current is suppressed at positive bias, RR is larger than 1 to give positive $\log_e$(RR), while the opposite rectification is observed $\log_e$(RR) is negative. If the diameter of SWNT was assumed homogenous anywhere in the same complex wire, height of PMo_{12} nanoparticles adsorbed on SWNT could be estimated from the complex

height observed by AFM. A prominent finding was that $\log_e$(RR) decreased from positive to negative value as the PMo_{12} nanoparticle height increased for semiconducting SWNTs. In contrast, negative $\log_e$(RR) increased to positive value as the PMo_{12} nanoparticle height increased for metallic SWNTs. In other words, as the PMo_{12} nanoparticle size increased, rectification direction of PMo_{12}/SWNT complex was inversed. The relation of rectification direction inversion with particle size was further found opposite between semiconducting and metallic SWNTs.

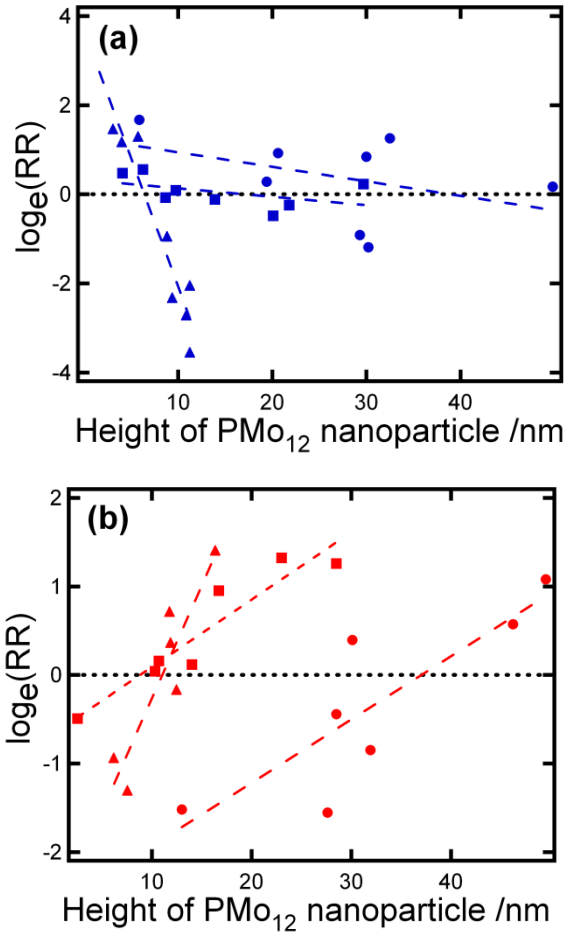

Figure 5. Plots of $\log_e$(RR) vs. PMo_{12} nanoparticle height for (a) PMo_{12} /semiconducting SWNT complex and (b) PMo_{12}/metallic SWNT complex. Each graph was obtained from *I-V* data of three individual PMo_{12}/ SWNT complexes.

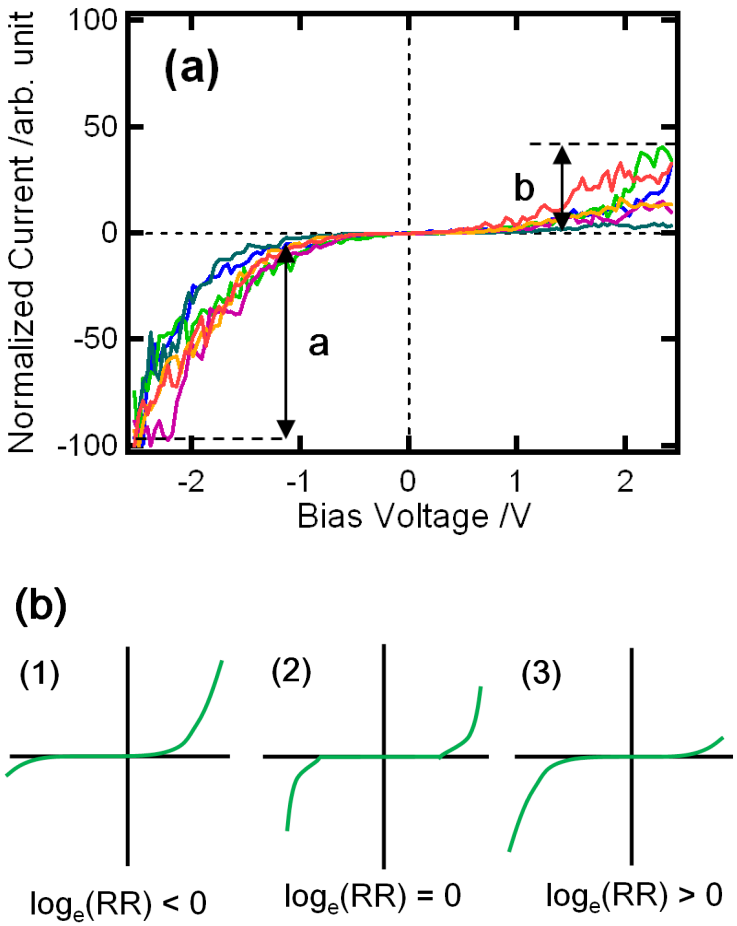

Figure 6. (a) Typical *I-V* curves of PMo_{12}/SWNT complex measured using PCI-AFM. Rectification ratio is defined as |a / b|. (b) Explanation about $\log_e$(RR). When current is suppressed at negative bias as shown in the *I-V* curve (1), |a / b| < 1 and $\log_e$(RR) < 0. If there is no rectification observed like in the *I-V* curve (2), |a / b| = 1 and $\log_e$(RR) = 0. When current is suppressed at positive bias shown as curve (3), RR > 1 and $\log_e$(RR) > 0.

3.4 Surface potential of PMo_{12} nanoparticle on SWNTs

The charge distribution on the PMo_{12}/SWNT complexes was studied by using Kelvin probe force microscopy (KPFM). In the case of semiconducting SWNTs, the contact potential difference (CPD) values for the PMo_{12} nanoparticles were lower than those of the semiconducting SWNTs (**Figure 7**), while the CPD values decreased as the thickness of the PMo_{12} nanoparticles increased (**Figure 8**). For metallic SWNTs, the CPD values of the PMo_{12} nanoparticles were larger than those of the metallic SWNTs (**Figure 9**) and the CPD values increased as the height of PMo_{12} nanoparticles increased (**Figure 10**).

Based on the working principle of KPFM, CPD of sample is defined as the difference between vacuum level of cantilever and the samples, as shown in **Figure 11**. In this sense, if the Fermi levels of the Pt cantilever, SWNTs, and PMo_{12} were aligned, the vacuum level of PMo_{12} was lower than that of semiconducting SWNTs and higher than that of metallic SWNTs. As the work function (Φ) is the potential difference between vacuum level and Fermi level in the electronic band perspective, the results shown above indicated that the work function of PMo_{12} (Φ_{PMo12}) was lower than that of semiconducting SWNTs ($\Phi_{semi\text{-}SWNT}$) but higher than that of metallic SWNTs ($\Phi_{metallic\ SWNT}$). Accordingly, PMo_{12} were positively charged relative to the semiconducting SWNTs, while negatively charged relative to the metallic SWNTs. This inversion of charge was potentially the source of the inversion of rectification direction.

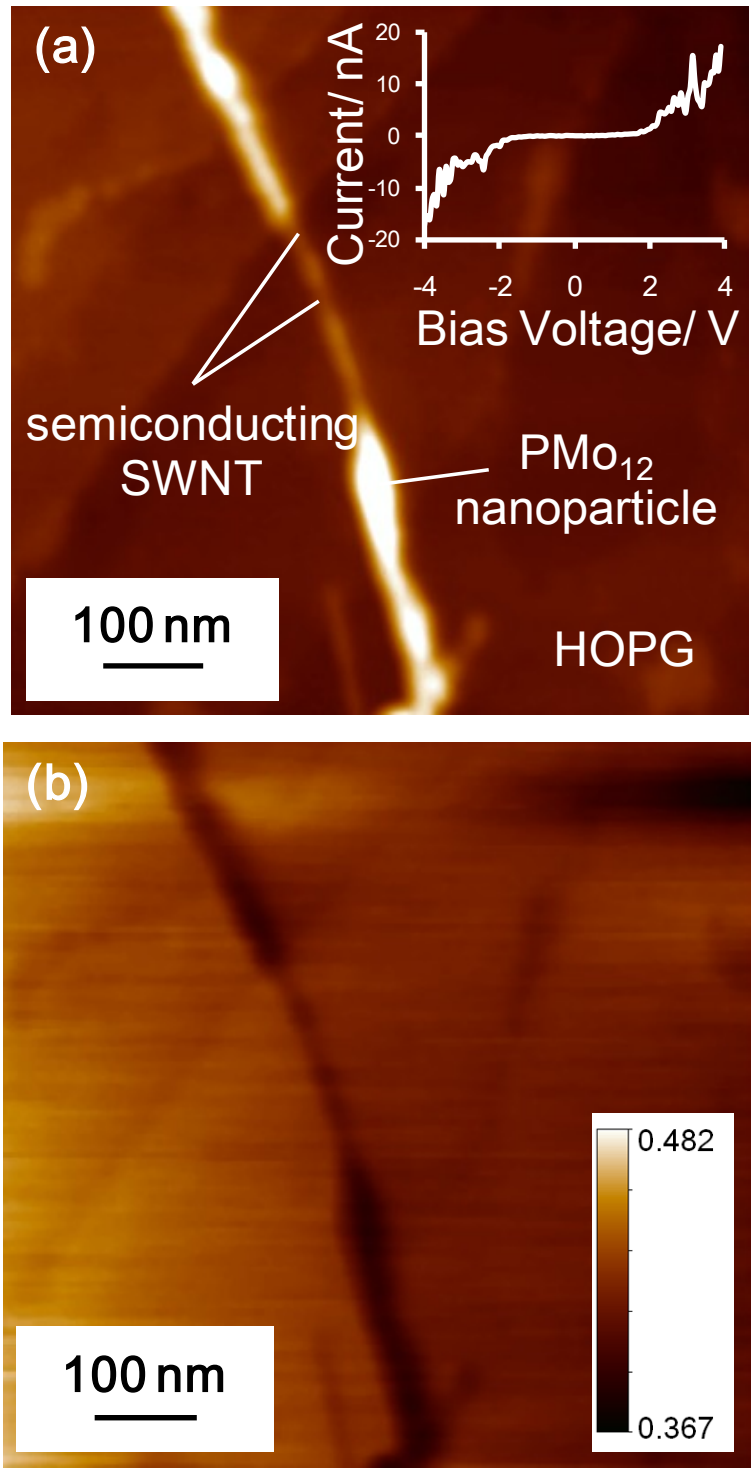

Figure 7. (a) AFM topography and (b) CPD image of PMo_{12}/semiconducting SWNT complex. Inset in (a): *I-V* curve of exposed nanotube obtained by PCI-AFM. The darker contrast of PMo_{12} nanoparticle in CPD image indicated that CPD value of PMo_{12} was lower than those of semiconducting SWNT.

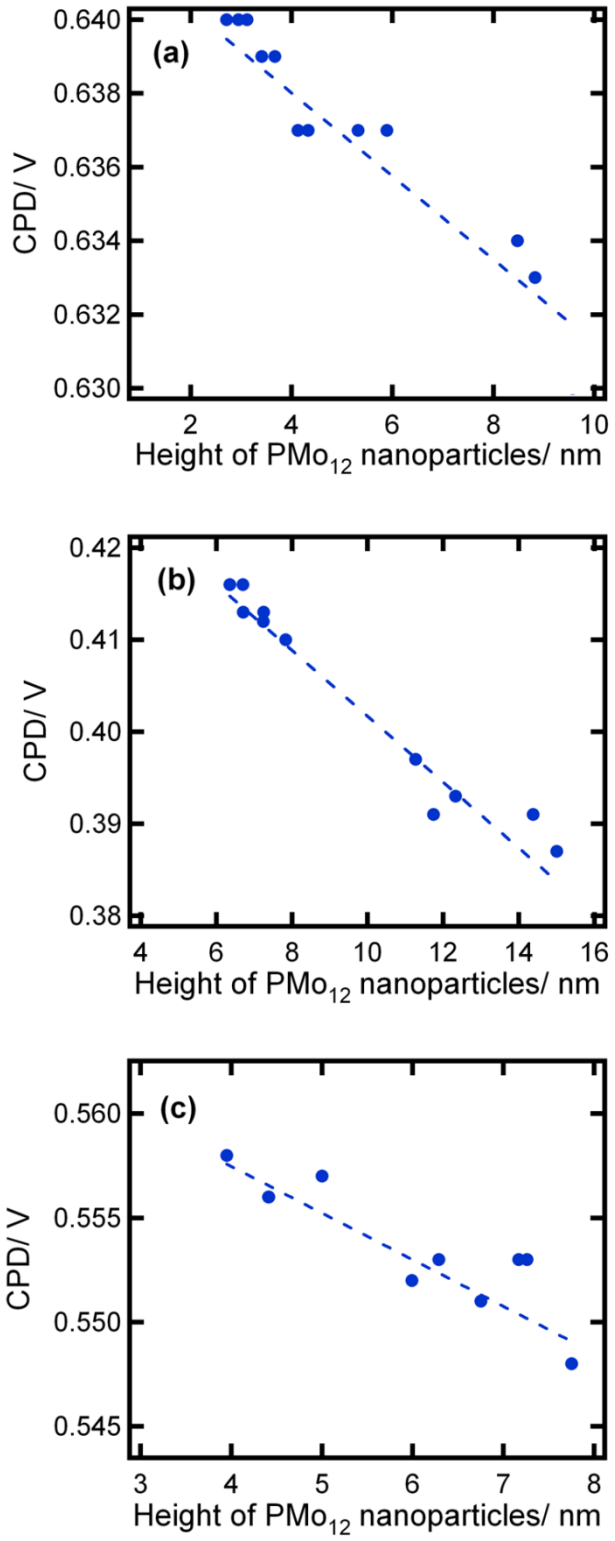

Figure 8. Plots of CPD value against complex height of PMo_{12}/semiconducting SWNT for three individual complexes. In all the three plots, CPD value decreased as complex height increased.

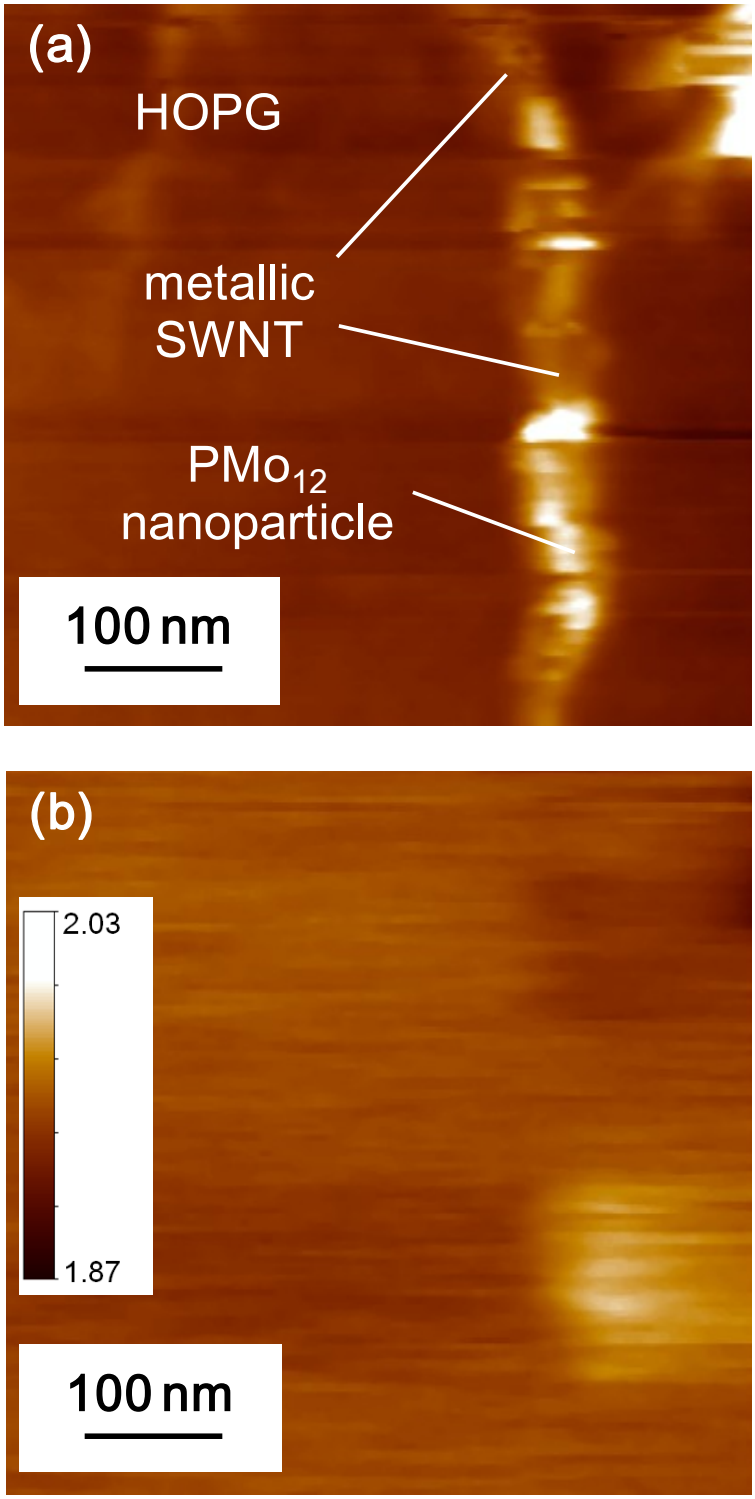

Figure 9. (a) AFM topography and (b) CPD image of PMo_{12}/metallic SWNT complex. The brighter contrast of PMo_{12} nanoparticle in CPD image indicated that CPD value of PMo_{12} was larger than those of metallic SWNT.

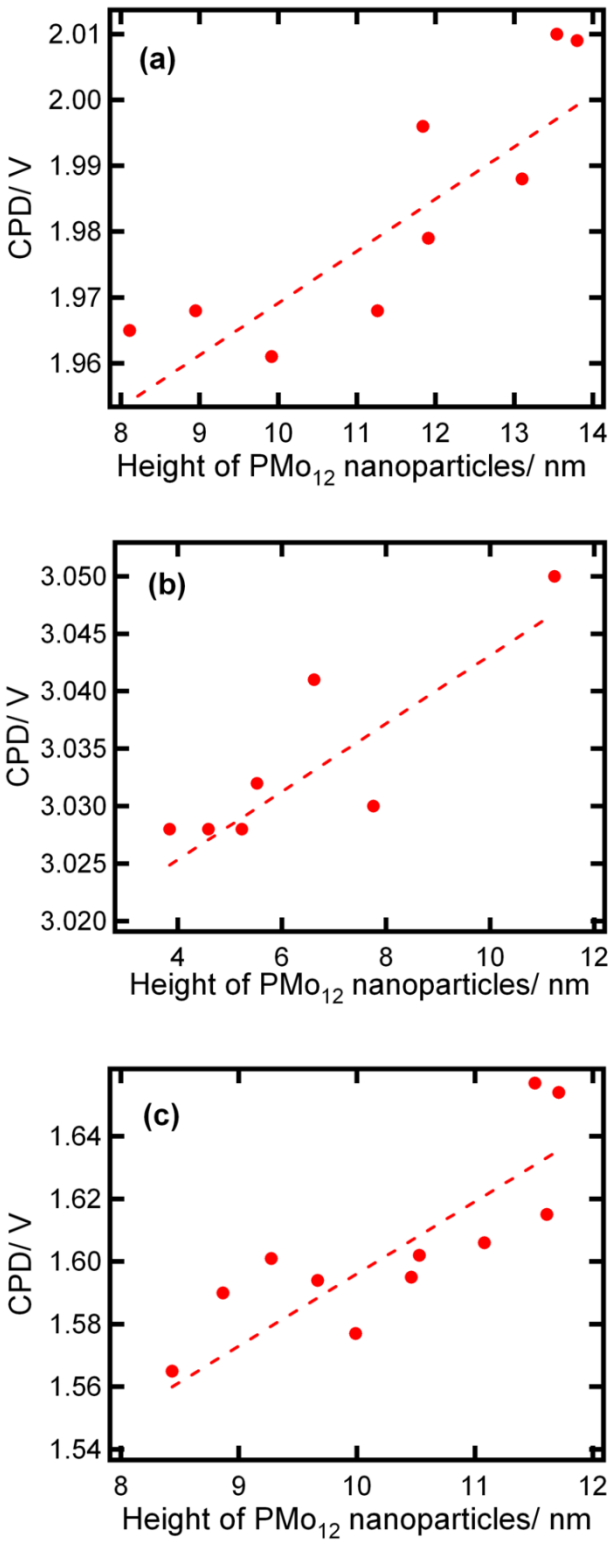

Figure 10. Plots of CPD value against complex height of PMo_{12}/metallic SWNT in three individual complexes. In all the three plots, CPD value increased as complex height increased.

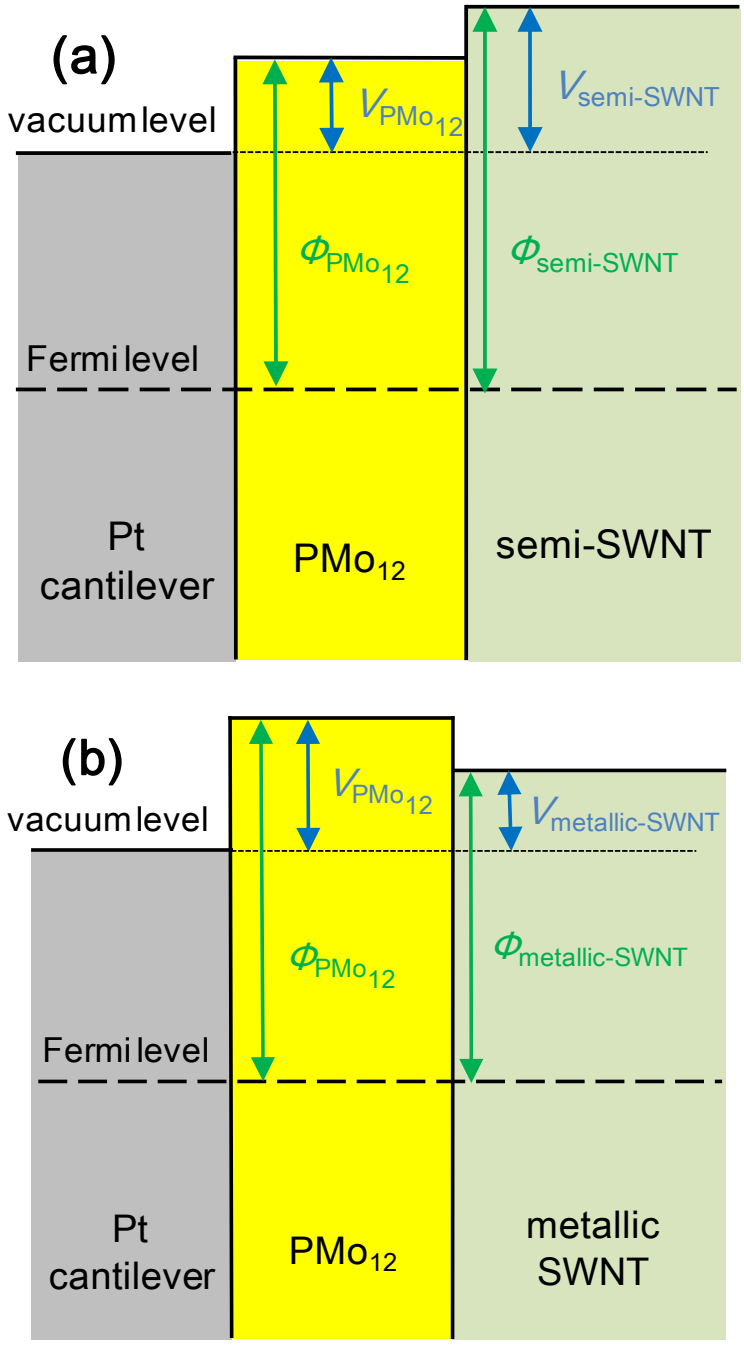

Figure 11. Schematic band structure diagram of Pt cantilever (gray color), PMo_{12} (yellow color) and SWNT (light green color) in KPFM measurement of (a) PMo_{12}/semiconducting and (b) PMo_{12}/metallic SWNT. Contact potential difference (CPD, V) and work function (Φ) were shown as blue color and green color respectively. In the case of semiconducting SWNT, Φ_{PMo12} was lower than $\Phi_{semi\text{-}SWNT}$ since V_{PMo12} was lower than $V_{semi\text{-}SWNT}$. V_{PMo12} was larger than $V_{metallic\ SWNT}$ if SWNT was metallic, thus Φ_{PMo12} was larger than $\Phi_{metallic\ SWNT}$.

A summary of the rectification direction inversion and surface potential of PMo_{12}/SWNT complex, which were measured by PCI-AFM and KPFM respectively, is given in **Table 1**.

Table 1. Summary of experimental results obtained by PCI-AFM and KPFM

	PCI-AFM: rectification direction inversion	KPFM: surface potential
PMo_{12}/semiconducting SWNT	$\log_e$(RR) decreased as PMo_{12} particle height increased	$V_{PMo12} < V_{semi\text{-}SWNT}$ $\Phi_{PMo12} < \Phi_{semi\text{-}SWNT}$
PMo_{12}/metallic SWNT	$\log_e$(RR) increased as PMo_{12} particle height increased	$V_{PMo12} > V_{metallic\ SWNT}$ $\Phi_{PMo12} > \Phi_{metallic\ SWNT}$

3.5 Mechanisms discussion on the rectification direction inversion

The PMo_{12} molecules are most likely partially protonated by carboxylic acids formed on the surface or edge of the SWNTs and atmospheric moisture, as has been reported for similar POM compounds.[19, 20] The effect of moisture was confirmed by comparing *I-V* measurements in air, vacuum and oxygen, which was shown in **Figure 12**. Current could flow through PMo_{12}/SWNT in the open air according to Figure 12b, while no conductivity was shown in the case of vacuum or pure oxygen atmosphere. This indicated that water vapor in the air was indispensible in the *I-V* measurement of PMo_{12}/SWNT complex. In other words, protonation of PMo_{12} was a necessity to the conductivity of PMo_{12}/SWNT complex in this study. The positive charge incurred by the protonation of PMo_{12} can be partially neutralized by negative charge transfer from the semiconducting SWNTs. However, the efficiency of charge neutralization is not very high because the electrons on the semiconducting SWNTs are not fully delocalized.[21] Consequently, PMo_{12} nanoparticles remain positively charged. In contrast, the electrons on the metallic SWNTs are sufficiently delocalized and the contact of the carbon nanotube with the HOPG surface can be considered to be Ohmic. As a result, negative charge transfer from the metallic SWNTs and HOPG to the PMo_{12} nanoparticles is more efficient and the intrinsically electron-deficient protonated PMo_{12} accepts electrons until the nanoparticles are relatively negatively charged. As the PMo_{12} particle size increases, the amount of charge accumulated on the particle also increases, which can be proved by Figure 8 and 10.

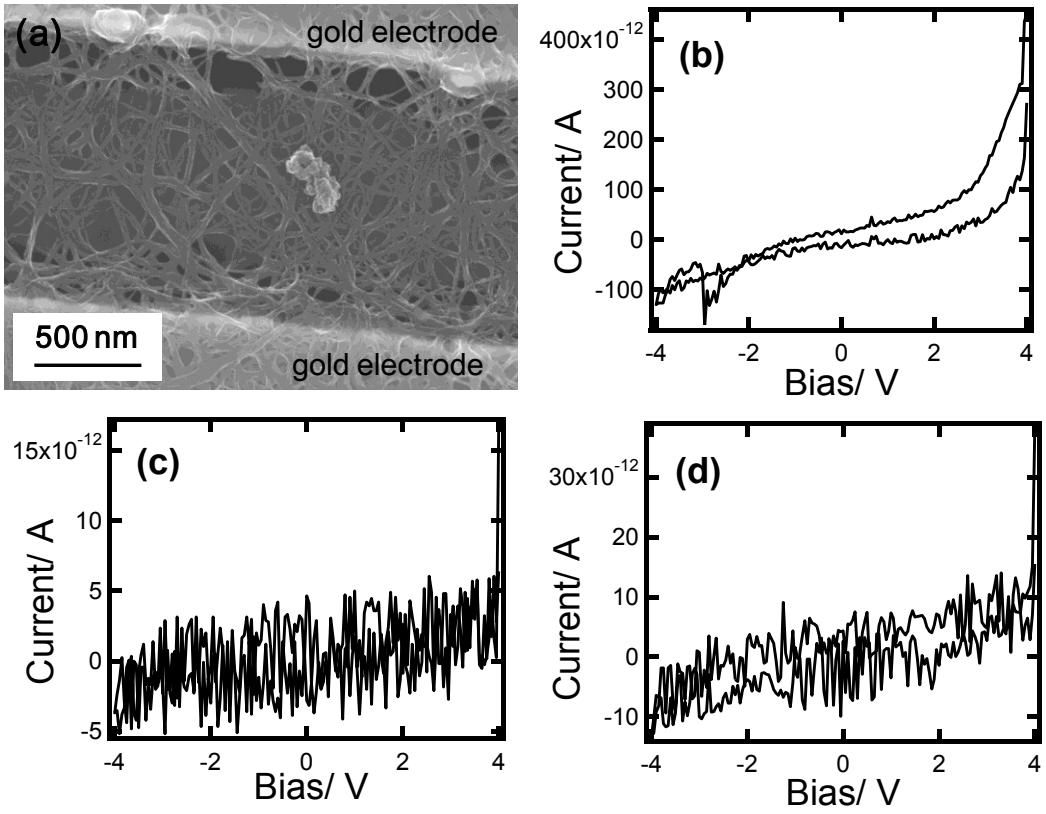

Figure 12. (a) SEM image of PMo_{12}/SWNT wires at micro-sized gap between two electrodes. *I-V* curves of PMo_{12}/SWNT complex measured in (b) the air, (c) vacuum and (d) pure oxygen atmosphere using four-point probe. All the measurements were performed at room temperature.

Modifications of the molecular orbital energies of PMo_{12} due to protonation and negative charge transfer were confirmed by density functional theory (DFT) calculations, as seen in **Figure 13** and **Table 2**. By using the Gaussian09 program, the calculations were performed using the DFT method with LANL2DZ and 6-311G basis sets for Mo and other lighter elements, respectively. The neutral PMo_{12} molecule (i.e., $H_3PMo_{12}O_{40}$) has higher HOMO and LUMO energies (−2.17 and −1.45 eV, respectively) than those of typical zigzag (13,0) SWNTs (−4.26 and −3.07 eV, respectively). However, protonation decreases the energies of both

frontier orbitals (−6.25 and −5.38 eV for the HOMO and LUMO, respectively) to be lower than those of the SWNTs, which indicates that electron transfer from the SWNTs to protonated PMo_{12} is feasible. After accepting one electron, the HOMO and LUMO energies of the protonated PMo_{12} rise to −3.14 and −2.12 eV, respectively, while two electrons raise the energies to −0.40 and 0.53 eV, respectively, which is much higher than those of the SWNTs. These calculations indicate that the transfer of less than one electron from the SWNTs to the $H_4PMo_{12}O_{40}^{+}$ molecule imparts an electronic equilibrium.

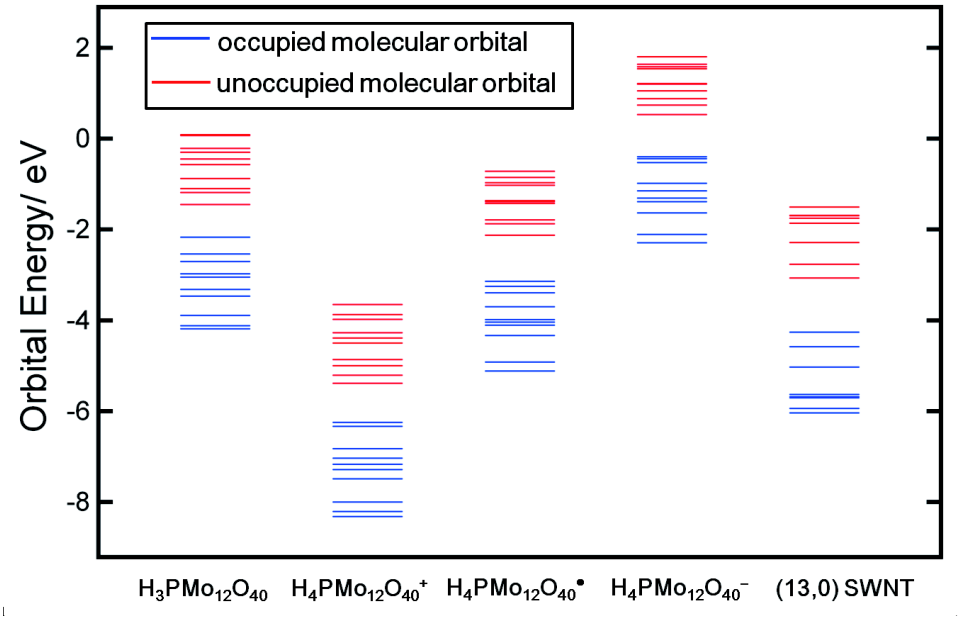

Figure 13. DFT calculations for PMo_{12} and SWNT. The structure of PMo_{12} was fixed at the reported X-ray crystallographic structure,[17] while that of zigzag (13,0) SWNT was fully optimized with hydrogen atoms at the terminal carbons. Blue lines indicate the energies of the top 10 HOMOs, and the red lines indicate those of the 10 LUMOs. The neutral PMo_{12} molecule is denoted as $H_3PMo_{12}O_{40}$, $H_4PMo_{12}O_{40}^{+}$ denotes the protonated form, $H_4PMo_{12}O_{40}^{\bullet}$ is the protonated form reduced by one electron (i.e., a neutral radical), and $H_4PMo_{12}O_{40}^{-}$ represents the protonated form reduced by two electrons (i.e., an anion).

Table 2. Calculated molecular orbital energies (eV) for PMo_{12} and SWNT

	$H_3PMo_{12}O_{40}$	$H_4PMo_{12}O_{40}^{+}$	$H_4PMo_{12}O_{40}^{\bullet}$	$H_4PMo_{12}O_{40}^{-}$	(13,0) SWNT
LUMO-9	0.0887098	-3.65152	-0.719475	1.80222	-1.50399
LUMO-8	0.0693896	-3.8733	-0.854716	1.63977	-1.68848
LUMO-7	-0.214972	-3.97779	-0.968189	1.58426	-1.68875
LUMO-6	-0.2996	-4.27277	-1.02397	1.53582	-1.69392
LUMO-5	-0.448175	-4.39005	-1.36357	1.21527	-1.75107
LUMO-4	-0.568178	-4.49781	-1.38698	1.2003	-1.86263
LUMO-3	-0.879479	-4.86217	-1.4248	1.05527	-1.86318
LUMO-2	-1.0988	-4.99959	-1.7859	0.882472	-2.28768
LUMO-1	-1.1886	-5.20694	-1.87352	0.737434	-2.76824
LUMO	-1.4531	-5.38436	-2.12523	0.531987	-3.06511
HOMO	-2.17067	-6.25023	-3.14022	-0.398922	-4.26134
HOMO-1	-2.53721	-6.33323	-3.25396	-0.442461	-4.58325
HOMO-2	-2.70511	-6.82467	-3.39165	-0.525728	-5.03115
HOMO-3	-2.97504	-7.03365	-3.70295	-0.984516	-5.63335
HOMO-4	-3.0496	-7.16944	-3.98514	-1.14833	-5.68042
HOMO-5	-3.32281	-7.28645	-4.03657	-1.30915	-5.68124
HOMO-6	-3.4703	-7.48836	-4.10977	-1.39024	-5.70546
HOMO-7	-3.89316	-8.00157	-4.3359	-1.6327	-5.94138
HOMO-8	-4.12256	-8.21246	-4.91659	-2.10645	-5.94192
HOMO-9	-4.18732	-8.32022	-5.11605	-2.29231	-6.03961
HOMO-LUMO gap	0.71757	0.86587	1.01499	0.930909	1.19623
HOMO-LUMO average energy	-1.811885	-5.817295	-2.632725	0.0665325	-3.663225

Mechanism for the inversion of the rectification direction has been considered based on the assumption and calculation results shown above. One possible explanation is similar to that for usual semiconductor *p*-*n* junctions. As shown in **Figure 14**, in the case of the semiconducting SWNTs, the positively charged PMo_{12} can be considered to be a "*p*-type" semiconductor, while the negatively charged SWNT is an "*n*-type"

semiconductor. When a negative (i.e., forward) bias is applied to the SWNT (Figure 14a), hole is injected into "*p*-type" side while electron is injected into "*n*-type" side, thus carriers in both the "*p*-" and "*n*-type" semiconductors are pushed toward the junction. As the bias voltage increases, the depletion region near the junction becomes thin enough to enable electron flow from the anode (i.e., the SWNT) to the cathode (i.e., PMo_{12}). In contrast, if a positive (i.e., reverse) bias is applied (Figure 14b), hole is injected into "*n*-type" side while electron is injected into "*p*-type" side. Carriers are pulled from the junction thereby widening the depletion region and preventing electron flow through the junction. For metallic SWNTs, the SWNTs can be doped to form a "*p*-type" semiconductor. Schottky junction is not considered here for its rectification direction goes against the experimental result.

Another possible rectification mechanism is the drift of the effective potential due to the dipole moment generated at the SWNT/PMo_{12} interface.[22] When negatively or positively charged PMo_{12} particles form junctions with SWNTs, an interfacial electric field can be induced; this causes the original symmetric *I-V* to drift in either a negative or positive direction. The intensity of the drift depends on the degree of charge, which is dependent on the PMo_{12} particle size, while the direction of the drift is determined by whether PMo_{12} is negatively or positively charged relative to the SWNTs. Since the bias sweep range does not change during the *I-V* measurements, the intrinsically symmetrical *I-V* curves might indicate a rectification, as shown in **Figure 15**. If this is occurring,

the rising voltages should shift in a similar manner at both positive and negative biases. However, the results indicate that the rising voltages at positive bias shift in the opposite direction to those at a negative bias (**Figure 16**). Therefore, the mechanism behind the rectification is a combination of the *p*-*n* junction and bias shift mechanisms.

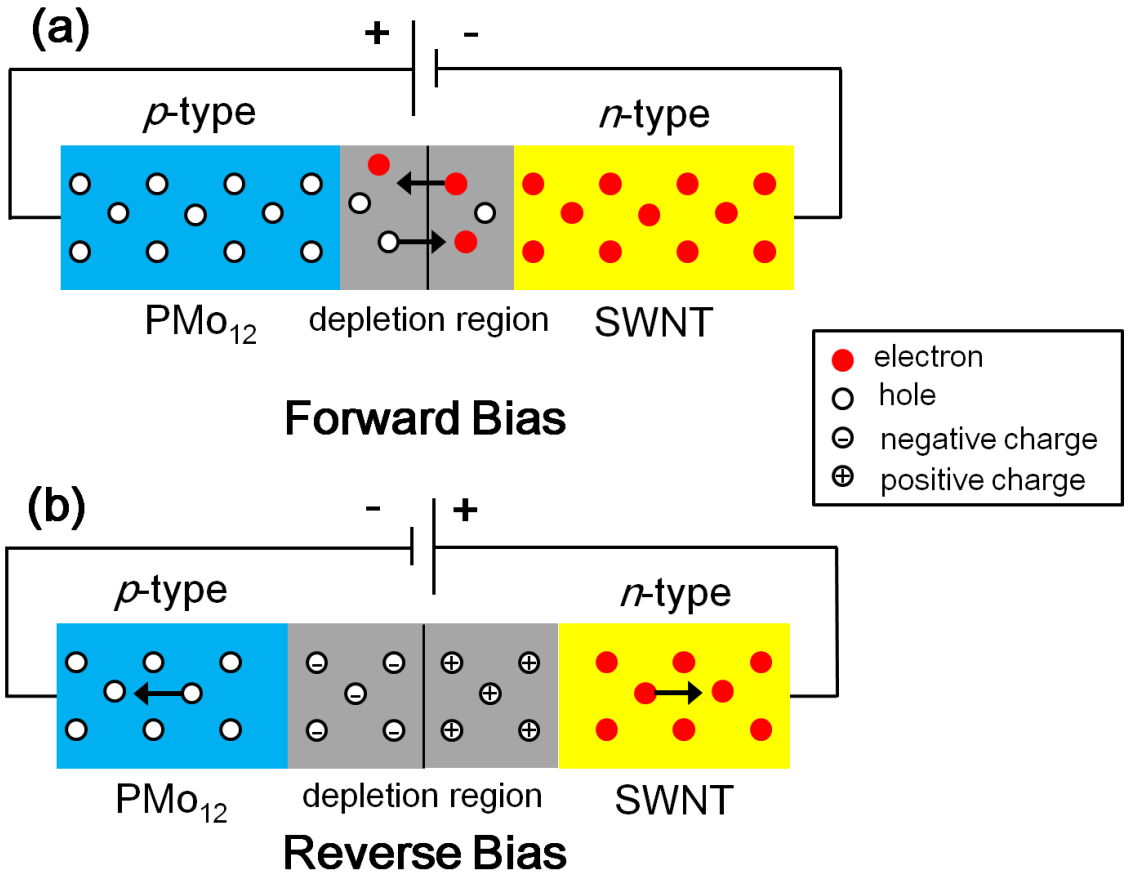

Figure 14. Schematic depiction of *p*-*n* junction consisted of "*p*-type" PMo_{12} and "*n*-type" SWNT in the case of positive charged PMo_{12} nanoparticle adsorbed on semiconducting SWNT wire. (a) forward bias; (b) reverse bias.

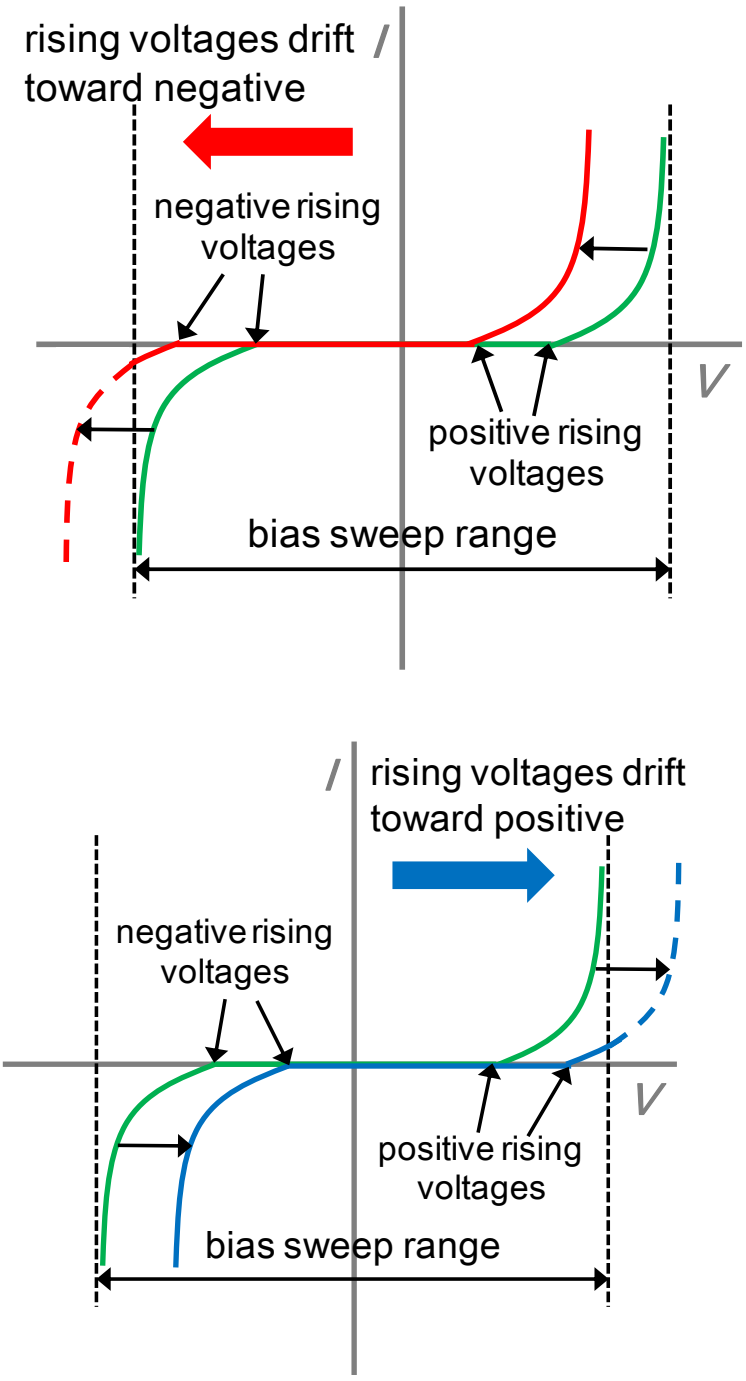

Figure 15. Schematic depiction of *I-V* drift. Drift direction is determined by the surface charge of PMo_{12} on SWNT, i.e., negatively or positively charged.

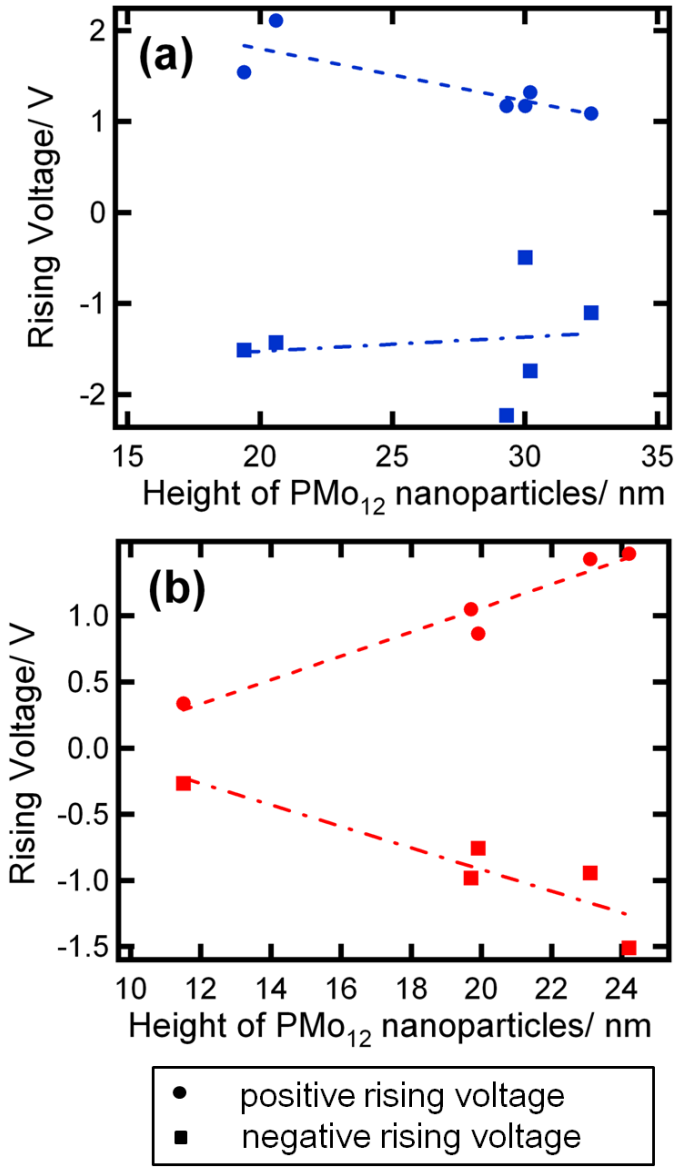

Figure 16. Plots of rising voltage against complex height in the case of (a) PMo_{12}/semiconducting SWNT and (b) PMo_{12}/metallic SWNT.

3.6 Negative differential resistance property of PMo_{12} complex

Negative differential resistance (NDR) behavior, a property that an increase of current results in decreasing of voltage has been observed in nanoscale *I-V* measurements.[23-28] NDR has been an essential characteristic in various applications like Esaki tunneling diode,[29] memory,[30] and light-emitting diode (LED).[31] By using scanning tunneling microscopy (STM) and tunneling spectra (TS), NDR properties of several POMs on HOPG have been observed.[32-38] In this sense, NDR property of PMo_{12} complex is worthy to be researched by PCI-AFM.

In the first step, ethanol solution of PMo_{12} was cast on HOPG and thin film of PMo_{12} could be formed, as seen in **Figure 17**a. *I-V* curves of PMo_{12} cast on HOPG surface were then measured by PCI-AFM. As shown in Figure 17b, two major NDR peaks which were at around -1.9 and -2.3 V were observed at the negative bias. This result was different to the case of similar POMs, which had only one NDR peak at negative bias of *I-V* curves measured by STM.[32-38]

I-V characteristics were further researched in the case of PMo_{12}/SWNT, as shown in **Figure 18**. Similar to the previous results, two NDR peaks were found at -1.8 and -2.3 V, respectively. The NDR peaks in Figure 18 became wider compared with those in Figure 17b, which was due to the inhomogeneous adsorption of PMo_{12} particles to SWNT wiring. Nevertheless, multiple NDR peaks of PMo_{12} complex could be confirmed by the *I-V* results of PMo_{12} in different measurements.

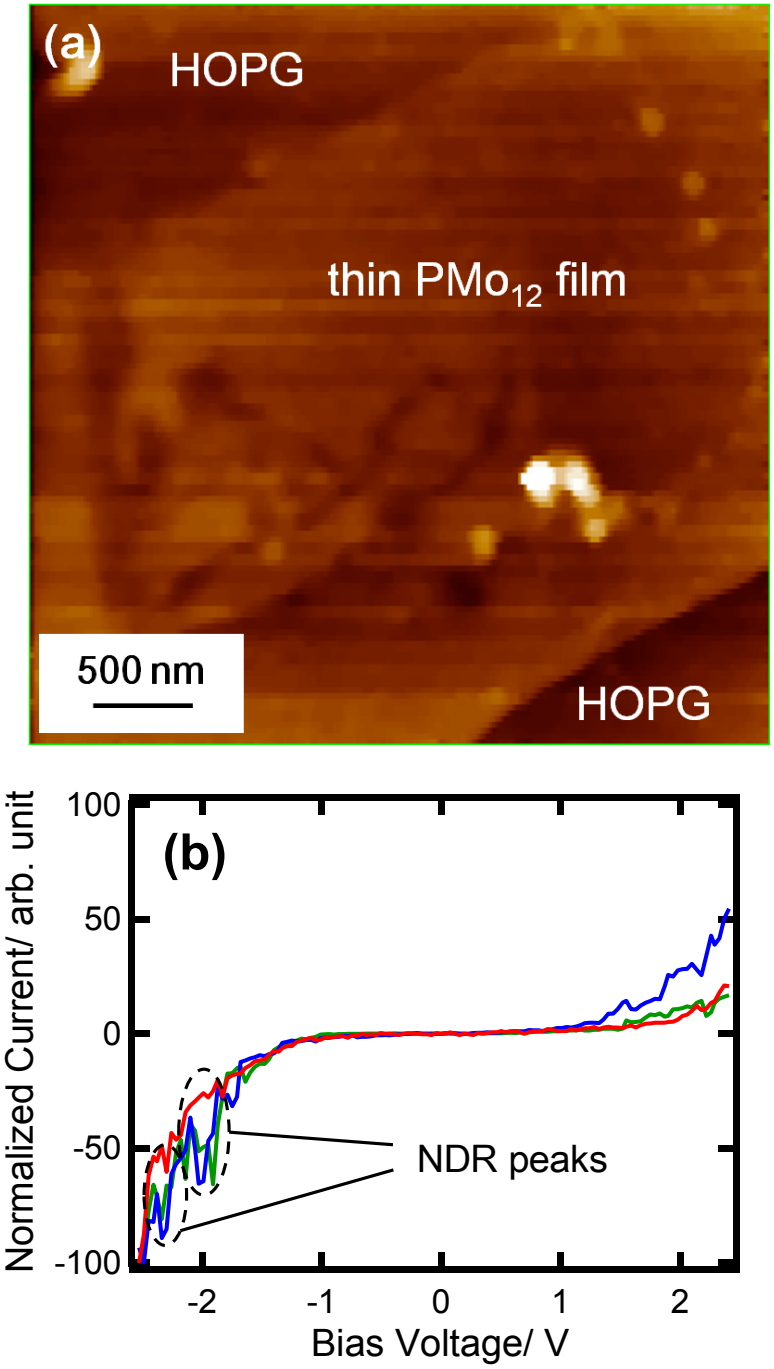

Figure 17. (a) AFM image of PMo_{12} thin film on HOPG. (b) Normalized *I-V* curves measured at the PMo_{12} film on HOPG by PCI-AFM, and two major NDR peaks at around -1.9 and -2.3 V were observed.

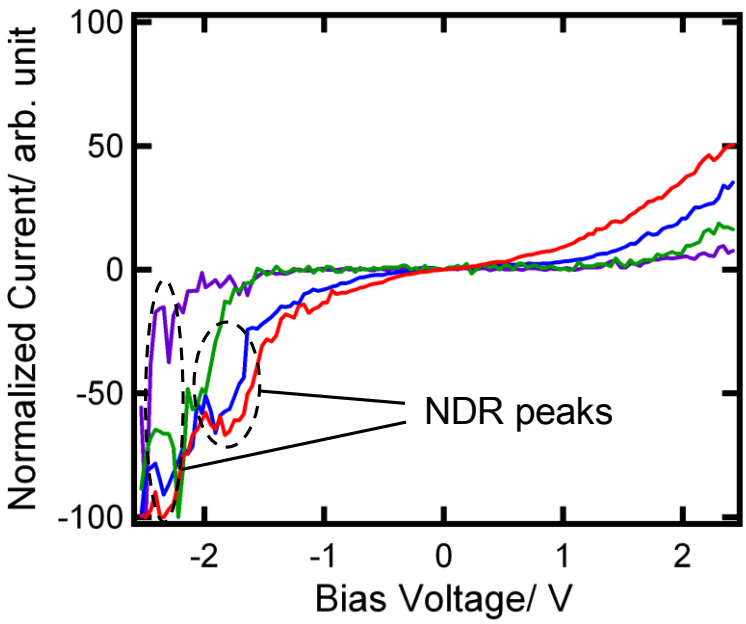

Figure 18. Normalized *I-V* curves of PMo_{12}/SWNT measured by PCI-AFM. Two NDR peaks were found at -1.8 and -2.3 V.

Although the detailed mechanism for NDR characteristic is not clear yet, the redox property of molecule has been considered as an important factor.[33, 38] It is well known that PMo_{12} can undergo a multi-electron stepwise reduction,[10, 39] which can be a possible reason to the observed NDR peaks. As shown in **Figure 19**, when the voltage increases to the reduction potential, PMo_{12} molecule initially accepts one electron, thereby supplying a charge carrier for electron flow through the system ((ii) in Figure 19b). A further increase in voltage causes a second electron reduction with subsequent blocking of the current ((iii) in Figure 19b).[40] As the increasing voltage reaches to the next reduction potential, another NDR peak may form. Such a two-steps reduction may be very fast so that the observed NDR peak is quite sharp.

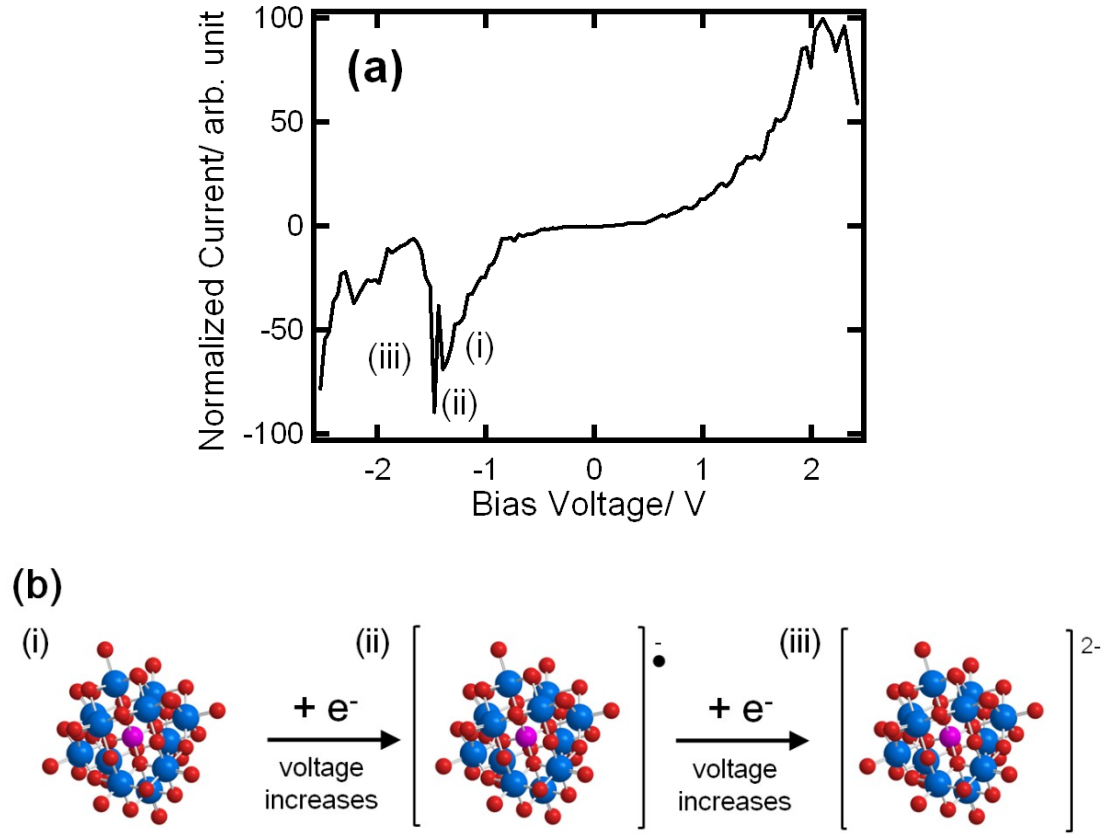

Figure 19. (a) NDR peak in a normalized *I-V* curve. Different stages of the NDR peak were indicated as (i), (ii) and (iii), respectively. (b) Schematic description of the two-steps reduction related to (i)-(iii). Initially one-electron reduction of PMo_{12} supplies one charge carrier (ii) for electron flow, while a second electron reduction (iii) blocks the current.

Several nanodevices are expected to be fabricated utilizing the NDR characteristic of PMo_{12} complex. Such devices include oscillator and organic light-emitting diode (OLED), which have hopeful prospect in future. Relative experimental work is still ongoing.

3.7 Summary

In this chapter, electrical properties of PMo_{12} nanoparticle on SWNTs were researched mainly by PCI-AFM systematically. It has been found that rectification direction was inversed as PMo_{12} particle size increased, and the relation of rectification direction inversion with particle height was further found opposite between semiconducting and metallic SWNTs. KPFM results indicated that the surface potential of PMo_{12} nanoparticle on semiconducting SWNT was opposite to that in the case of metallic SWNT, which was assumed due to the different efficiencies of the electron charging from SWNTs to PMo_{12}. Two mechanisms, which include usual *p*-*n* junction and *I*-*V* curve drift induced by dipole moment at the PMo_{12}/SWNT interface, have been proposed for the inversion of rectification direction. Additionally, multiple negative differential resistance (NDR) peaks were observed in the *I*-*V* curves of PMo_{12} complex, which was thought related to its multi-electron stepwise reduction process.

References

1. Fernando, K. A. S.; Lin, Y.; Wang, W.; Kumar, S.; Zhou, B.; Xie, S. Y.; Cureton, L. T.; Sun, Y. P. *J. Am. Chem. Soc.* **2004,** 126, (33), 10234-10235.
2. Li, Q. W.; Zhang, J.; Yan, H.; He, M. S.; Liu, Z. F. *Carbon* **2004,** 42, (2), 287-291.
3. Zhou, J.; Maeda, Y.; Lu, J.; Tashiro, A.; Hasegawa, T.; Luo, G. F.; Wang, L.; Lai, L.; Akasaka, T.; Nagase, S.; Gao, Z. X.; Qin, R.; Mei, W. N.; Li, G. P.; Yu, D. P. *Small* **2009,** 5, (2), 244-255.
4. Franklin, N. R.; Wang, Q.; Tombler, T. W.; Javey, A.; Shim, M.; Dai, H. *Appl. Phys. Lett.* **2002,** 81, (5), 913.
5. Fuhrer, M. S.; Kim, B. M.; Durkop, T.; Brintlinger, T. *Nano Lett.* **2002,** 2, (7), 755-759.
6. Bo, X. Z.; Tassi, N. G.; Lee, C. Y.; Strano, M. S.; Nuckolls, C.; Blanchet, G. B. *Appl. Phys. Lett.* **2005,** 87, (20), 203510-203510.
7. Takenobu, T.; Takano, T.; Shiraishi, M.; Murakami, Y.; Ata, M.; Kataura, H.; Achiba, Y.; Iwasa, Y. *Nat. Mater.* **2003,** 2, (10), 683-688.
8. Feldman, A. K.; Steigerwald, M. L.; Guo, X. F.; Nuckolls, C. *Acc. Chem. Res.* **2008,** 41, (12), 1731-1741.
9. Tanaka, H.; Yajima, T.; Matsumoto, T.; Otsuka, Y.; Ogawa, T. *Adv. Mater.* **2006,** 18, (11), 1411-1415.
10. Wang, R. Y.; Jia, D. Z.; Zhang, L.; Liu, L.; Guo, Z. P.; Li, B. Q.; Wang, J. X. *Adv. Funct. Mater.* **2006,** 16, (5), 687-692.
11. Pope, M. T.; Muller, A. *Angew. Chem. Int. Ed.* **1991,** 30, (1), 34-48.
12. Velessiotis, D.; Douvas, A. M.; Athanasiou, S.; Nilsson, B.; Petersson, G.; Södervall, U.; Alestig, G.; Argitis, P.; Glezos, N. *Microelectron. Eng.* **2011,** 88, (8), 2775-2777.
13. Guo, X.; Guo, D.-J.; Wang, J.-S.; Qiu, X.-P.; Chen, L.-Q.; Zhu, W.-T. *J. Electroanal. Chem.* **2010,** 638, (1), 167-172.
14. Skunik, M.; Kulesza, P. J. *Anal. Chim. Acta* **2009,** 631, (2), 153-160.
15. Lewera, A.; Chojak, M.; Miecznikowski, K.; Kulesza, P. J. *Electroanalyisis* **2005,** 17, (15-16), 1471-1476.
16. Kawasaki, N.; Wang, H.; Nakanishi, R.; Hamanaka, S.; Kitaura, R.; Shinohara, H.; Yokoyama, T.; Yoshikawa, H.; Awaga, K. *Angew. Chem. Int.*

Ed. **2011,** 50, (15), 3471-3474.
17. Gaunt, A. J.; May, I.; Sarsfield, M. J.; Collison, D.; Helliwell, M.; Denniss, I. S. *Dalton Trans.* **2003**, (13), 2767-2771.
18. Kulesza, P. J.; Chojak, M.; Karnicka, K.; Miecznikowski, K.; Palys, B.; Lewera, A.; Wieckowski, A. *Chem. Mater.* **2004,** 16, (21), 4128-4134.
19. Dey, C.; Kundu, T.; Banerjee, R. *Chem. Commun.* **2012,** 48, (2), 266-268.
20. Han, Z.; Bond, A. M.; Zhao, C. *Sci. China Chem.* **2011,** 54, (12), 1877-1887.
21. Strano, M. S.; Huffman, C. B.; Moore, V. C.; O'Connell, M. J.; Haroz, E. H.; Hubbard, J.; Miller, M.; Rialon, K.; Kittrell, C.; Ramesh, S.; Hauge, R. H.; Smalley, R. E. *J. Phys. Chem. B* **2003,** 107, (29), 6979-6985.
22. Matsumoto, T.; Yamada, F.; Mikamo-Satoh, E.; Takagi, A.; Kawai, T. *J. Surf. Sci. Soc. Jpn.* **2008,** 29, 246-252.
23. Guisinger, N. P.; Basu, R.; Greene, M. E.; Baluch, A. S.; Hersam, M. C. *Nanotechnology* **2004,** 15, (7), S452-S458.
24. Chen, J.; Wang, W.; Reed, M. A.; Rawlett, A. M.; Price, D. W.; Tour, J. M. *Appl. Phys. Lett.* **2000,** 77, (8), 1224-1226.
25. Leonard, F.; Tersoff, J. *Phys. Rev. Lett.* **2000,** 85, (22), 4767-4770.
26. Larade, B.; Taylor, J.; Mehrez, H.; Guo, H. *Phys. Rev. B* **2001,** 64, (7), 075420.
27. Xue, Y. Q.; Datta, S.; Hong, S.; Reifenberger, R.; Henderson, J. I.; Kubiak, C. P. *Phys. Rev. B* **1999,** 59, (12), R7852-R7855.
28. Guo, Y. D.; Yan, X. H.; Xiao, Y. *Appl. Phys. Lett.* **2011,** 98, (16), 163107.
29. Esaki, L. *Physical Review* **1958,** 109, (2), 603-604.
30. Tseng, R. J.; Huang, J. X.; Ouyang, J.; Kaner, R. B.; Yang, Y. *Nano Lett.* **2005,** 5, (6), 1077-1080.
31. Tseng, R. J.; Ouyang, J.; Chu, C.-W.; Huang, J.; Yang, Y. *Appl. Phys. Lett.* **2006,** 88, (12), 123506.
32. Song, I. K.; Kaba, M. S.; Nomiya, K.; Finke, R. G.; Barteau, M. A. *J. Mol. Catal. A: Chem.* **2007,** 262, (1-2), 216-226.
33. Kaba, M. S.; Song, I. K.; Barteau, M. A. *J. Phys. Chem.* **1996,** 100, (50), 19577-19581.
34. Song, I. K.; Kaba, M. S.; Barteau, M. A. *J. Phys. Chem.* **1996,** 100, (44), 17528-17534.

35. Dalidchik, F. I.; Balashov, E. M.; Budanov, B. A.; Gatin, A. K.; Grishin, M. V.; Kirsankin, A. A.; Kovalevskii, S. A.; Kolchenko, N. N.; Slutskii, V. G.; Shub, B. R. *Russ. J. Phys. Chem. B* **2011,** 4, (6), 896-903.
36. Kaba, M. S.; Song, I. K.; Barteau, M. A. *J. Phys. Chem. B* **2002,** 106, (9), 2337-2342.
37. Song, I. K.; Barteau, M. A. *Langmuir* **2004,** 20, (5), 1850-1855.
38. Kinne, M.; Barteau, M. A. *Surf. Sci.* **2000,** 447, (1-3), 105-111.
39. Skunik, M.; Kulesza, P. J. *Anal. Chim. Acta.* **2009,** 631, (2), 153-160.
40. Chen, J. *Science* **1999,** 286, (5444), 1550-1552.

Chapter 4

Research toward the Tuning of Rectification Properties of Phosphododecamolybdic Acid on Graphene Nanoribbon

Abstract: Phosphododecamolybdic acid (PMo_{12}) has been physically adsorbed on graphene nanoribbon (GNR) synthesized by unzipping of carbon nanotubes. The preliminary results indicated that rectification ratio (RR) of PMo_{12}/GNR decreased sharply as the width of GNR increased, and plateau width (PW) decreased as the height of PMo_{12} particle increased.

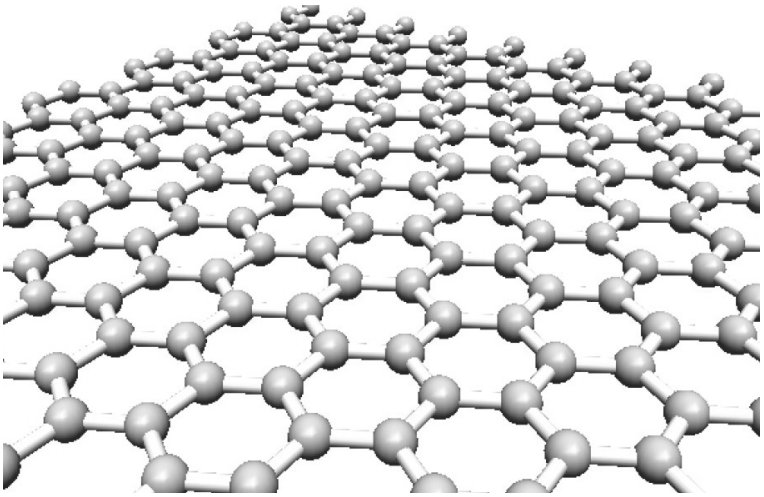

4.1 Introduction

Graphene is a single atomic layer of sp^2-hybridization carbon atoms with 2D honeycomb structure, which has been experimentally separated from graphite in 2004.[1] As a basic building block for graphitic materials of all dimensions,[2] which include 0D fullerene, 1D SWNT and 3D graphite (**Figure 1**), graphene has attracted a lot of research interests due to its excellent electronic,[3, 4] optical,[5, 6] mechanical,[7, 8] thermal,[9, 10] and electrochemical properties.[11, 12] Graphene has been actively used in recent applications such like sensor,[13, 14] energy storage,[15, 16] transistor,[17, 18] electrode,[19, 20] and solar cell.[21, 22]

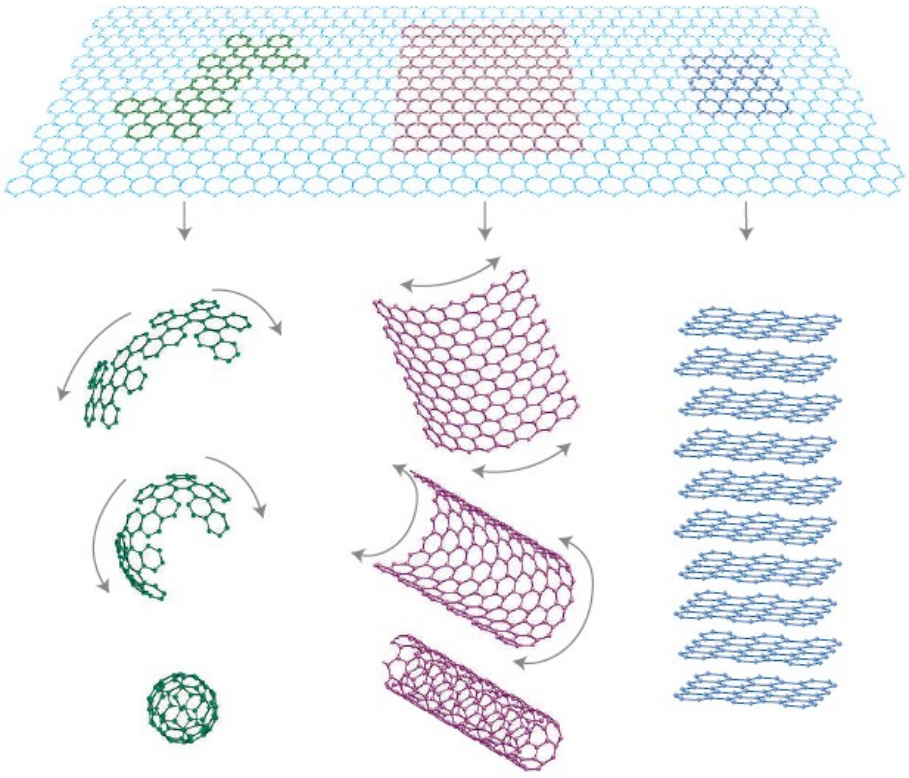

Figure 1. Graphene as the mother of all graphitic forms including 0D fullerene, 1D SWNT and 3D graphite.[2]

As regarded as a thin strip of graphene or unrolled SWNTs, graphene nanoribbon (GNR) has been theoretically introduced by Prof. M. Fujita in 1996,[23] and experimentally obtained by the group of Prof. P. Kim in 2007.[24] Different to graphene which is always a zero-gap semiconductor,[25] the electronic structure of GNR is found largely depended on its width,[24, 26] thereby some GNRs can be semiconductor of finite band gap with less than 5 nm width. This characteristic is very important for the development of graphene electronics. Therefore, it will be interesting to study the electronic properties of GNR wire adsorbed by phosphododecamolybdic acid (PMo_{12}), whose electronic properties are proved dependent to the chirality of SWNT (see detail in Chapter 3).

In this chapter, I focus on the rectification properties of PMo_{12}/semi-metallic GNR which was prepared by unzipping of carbon nanotube. The preliminary experimental data indicates a tunable rectification ratio (RR) and plateau width (PW) controllable by GNR width and PMo_{12} molecular size, respectively.

4.2 Experimental

GNRs were synthesized by unzipping of double-walled carbon nanotube (DWNT, SIGMA-ALDRICH Co.). Detailed procedure can be found in the literature previously reported.[27]

Prepared GNRs were suspended with poly(m-phenylenevinylene -co-2,5-dioctoxy-p-phenylenevinylene) (PmPV) in chloroform. The suspension was cast on a SiO_2 substrate, which was mirror polished and treated by bis(trimethylsilyl)amine in advance. Spin-casting was then performed (1000 rpm, 60 s) so as to disperse GNRs on the substrate homogenously. After that, the substrate was annealed in the furnace under 450 °C for 3 h to remove PmPV molecules via thermal degeneration. PMo_{12} (0.3 mg) was dissolved in 20 mL ethanol and sonicated for 1 h. Subsequently the solution was spin-cast on GNRs dispersed on SiO_2 substrate (5000 rpm, 30 s). After the thermal deposition of gold electrode, electrical properties of the PMo_{12}/GNRs complex were measured by PCI-AFM.

Figure 2 shows a typical AFM image of PMo_{12}/GNRs complex in this work. GNRs of 20 nm width and 1.5 nm height can be observed clearly, on which 2.1 nm-thick PMo_{12} nanoparticles were adsorbed. The particle size of PMo_{12} on GNR is smaller and more homogenous than that on SWNTs (Figure 1 in Chapter 3).

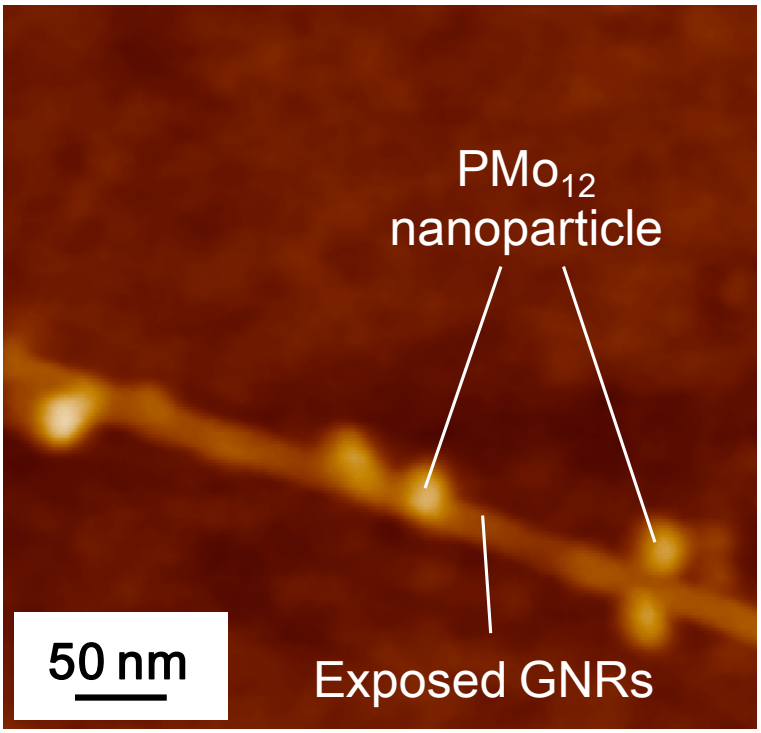

Figure 2. AFM image of PMo_{12}/GNRs complex cast on SiO_2 substrate. Width and height of exposed GNRs were around 20 and 1.5 nm, respectively. PMo_{12} nanoparticle on GNRs was about 2.1 nm high.

4.3 Electrical properties of PMo_{12} on GNRs

As seen in **Figure 3**a, a GNR wire adsorbed by PMo_{12} nanoparticle was connected to gold electrode. Metallic state of exposed GNR was confirmed by the *I-V* curves measured by PCI-AFM (inset in Figure 3b), which was due to a relatively large width (18 nm) of the GNR synthesized in this work. It has been reported that band gap of GNR with a width of 20 nm was very tiny (0.028 eV),[25] and 1-2 nm width GNR is a necessity to obtain a large band gap.[26]

Similar to the case of PMo_{12}/SWNT complex described in Chapter 4, rectification occurred on the interface of smaller PMo_{12} particles (1-2 nm high) with GNR (width 18 nm). As shown in Figure 3b, currents were suppressed at the positive bias, while the rectification ratio (RR) could be as large as 75 and the average RR was around 20. Additionally, it was found that conductivity of PMo_{12} on GNR wire depended on their shape and size. At the large particles (15-20 nm high), as indicated by the dotted circles in the figure, no current could be observed on them. It was speculated that the interaction between bulk PMo_{12} and GNR was not as large as that between smaller PMo_{12} particles and GNR, though detailed mechanism is not clear yet.

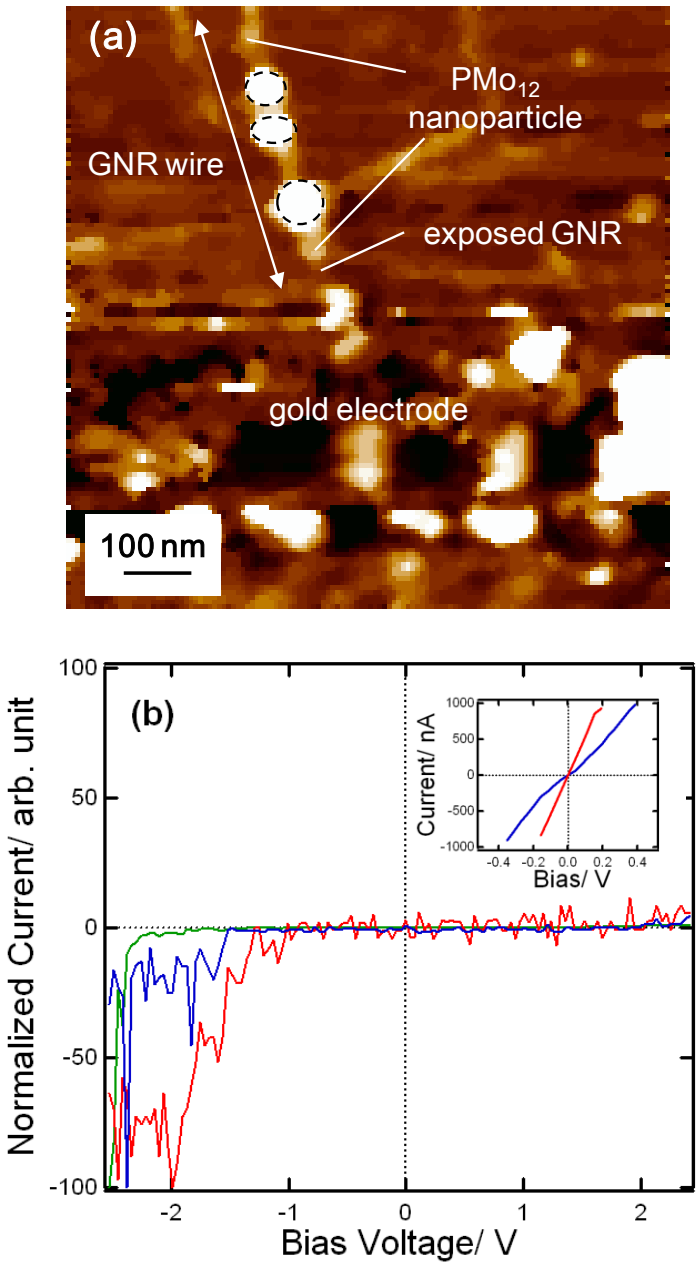

Figure 3. (a) AFM topography and (b) normalized *I-V* curves of PMo_{12}/GNR complex cast on SiO_2 substrate. Inset in (b): *I-V* curves of exposed GNR which indicated metallic state. Large rectification was observed at smaller PMo_{12} nanoparticles (1-2 nm high) on GNR, while no conductivity at larger (15-20 nm) PMo_{12} particles (dotted circles in (a)).

For the purpose of tuning a large rectification in GNR complex, it was essential to find out the factors which control the RR value. As discussed in Chapter 2 and 3, particle size could impose an influence to RR value. Plot of RR value against PMo_{12} particle height on GNR was shown as **Figure 4**. Although RR value increased with the increasing of PMo_{12} particle size, the maximum value of RR could not exceed 3 with GNR of 27.9 nm width. The relatively low RR demonstrated that particle size was not a determining factor for RR of PMo_{12}/GNR complex.

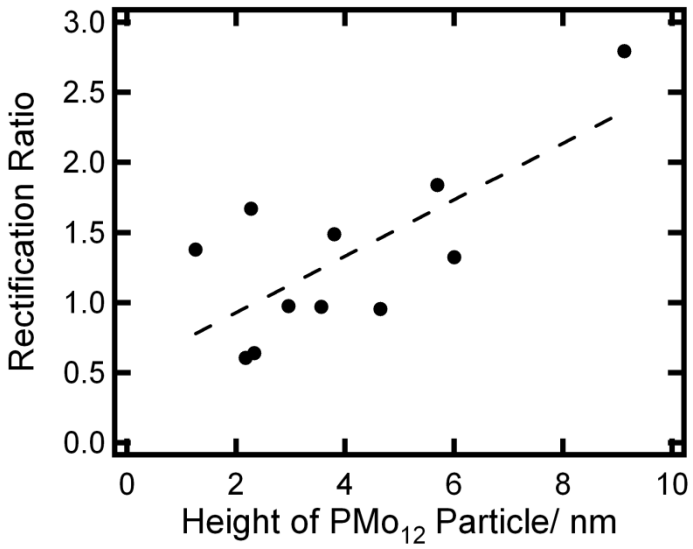

Figure 4. Plot of rectification ratio (RR) vs. PMo_{12} particle height on GNR (width 27.9 nm). RR value increased as the PMo_{12} particle height increased. Dotted line was added for eye guide. Height of PMo_{12} particle is equal to addition of PMo_{12} thickness and GNR height.

Since the electronic structure of GNR was dependent to its width, GNR width might play an important role in the controlling of RR. Electrical properties of PMo_{12} on GNRs of different widths were further measured, and the relationship between average RR calculated by *I-V* data and GNR

width was shown in **Figure 5**. As the GNR width increased from 18 to 28 nm, the average RR sharply decreased from 19.9 to 1.7. This interesting result has been confirmed by the reported calculation, which indicated that rectification ratio could be largely decreased by a slight increase in the width of GNR doped by N atom.[28] Therefore, GNR width was proved as an essential factor in determining RR value rather than particle size. This preliminary result can be quite helpful in enhancing the quality of graphene-based diode in future.

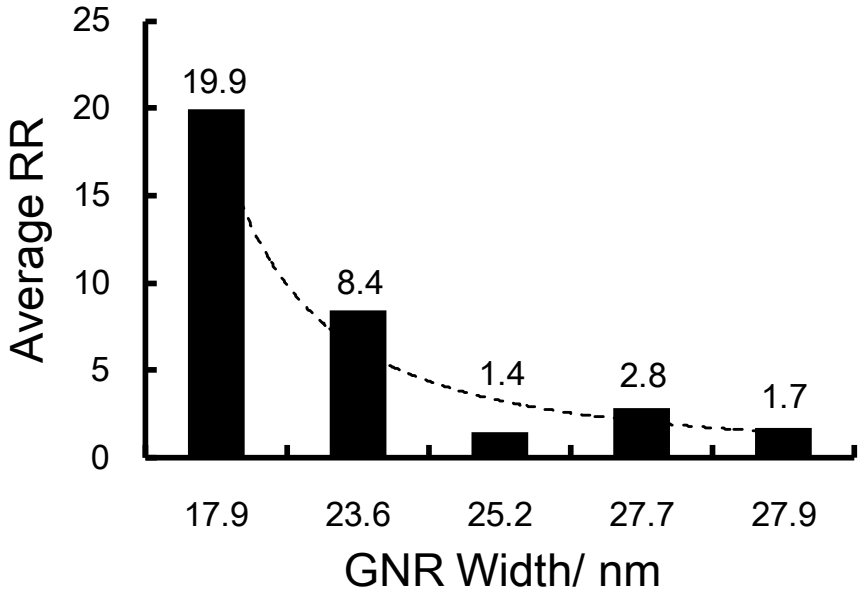

Figure 5. Relationship between GNR width and average RR. *I-V* measurements of PMo_{12} molecules on five GNRs were conducted by PCI-AFM, and the width of GNRs were measured as 17.9, 23.6, 25.2, 27.7 and 27.9 nm, respectively. Average RR of PMo_{12}/GNR complex was calculated based on the *I-V* curves, of which at least 8 data sets were included in each case. As the GNR width increased, average RR decreased sharply.

Plateau width (PW) in *I-V* curve was plotted against PMo_{12} nanoparticle height as shown in **Figure 6**. PW was calculated from plot of d*I*/d*V* against bias voltage. It was apparent that PW decreased as an increase of PMo_{12} particle height, which is similar to the tendency of naphthalene -diimide (NDI)/SWNT case described in Chapter 2.

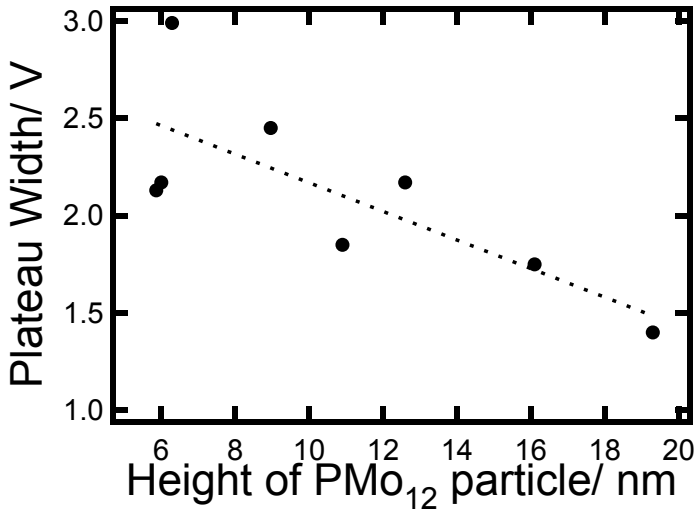

Figure 6. Plot of plateau width (PW) vs. PMo_{12} particle height. PW was obtained by plot of d*I*/d*V* against bias voltage. PW decreased as an increasing of PMo_{12} nanoparticle height.

It is worthy to be noticed that many electron acceptors like NDI derivatives,[29, 30] and tetracyanoquinodimethane (TCNQ),[31] have been proved as good dopants in tuning the electronic structure of graphene. As a molecule with a powerful electron reservoir property,[32, 33] PMo_{12} may be able to change the electronic state of GNR as well. FET device will be introduced in the future work of this study. Via the variation of gate voltage, band structure of GNR adsorbed by PMo_{12} is expected to be changed.

4.4 Summary

In this chapter, PMo_{12} was physically adsorbed on GNR which was synthesized by the unzipping of DWNTs. Large rectification appeared at the interface of PMo_{12} with GNR, and RR was mainly determined by GNR width. Besides, PW decreased with the increase of PMo_{12} particle size. The preliminary result can be helpful in improving the quality of graphene-based electronic device.

References

1. Novoselov, K. S.; Geim, A. K.; Morozov, S. V.; Jiang, D.; Zhang, Y.; Dubonos, S. V.; Grigorieva, I. V.; Firsov, A. A. *Science* **2004,** 306, (5696), 666-669.
2. Geim, A. K.; Novoselov, K. S. *Nat. Mater.* **2007,** 6, (3), 183-191.
3. Avouris, P. *Nano Lett.* **2010,** 10, (11), 4285-4294.
4. Castro Neto, A. H.; Peres, N. M. R.; Novoselov, K. S.; Geim, A. K. *Rev. Mod. Phys.* **2009,** 81, (1), 109-162.
5. Nair, R. R.; Blake, P.; Grigorenko, A. N.; Novoselov, K. S.; Booth, T. J.; Stauber, T.; Peres, N. M. R.; Geim, A. K. *Science* **2008,** 320, (5881), 1308-1308.
6. Wang, F.; Zhang, Y.; Tian, C.; Girit, C.; Zettl, A.; Crommie, M.; Shen, Y. R. *Science* **2008,** 320, (5873), 206-209.
7. Bunch, J. S.; van der Zande, A. M.; Verbridge, S. S.; Frank, I. W.; Tanenbaum, D. M.; Parpia, J. M.; Craighead, H. G.; McEuen, P. L. *Science* **2007,** 315, (5811), 490-493.
8. Bao, W. Z.; Miao, F.; Chen, Z.; Zhang, H.; Jang, W. Y.; Dames, C.; Lau, C. N. *Nat. Nanotechnol.* **2009,** 4, (9), 562-566.
9. Yu, A. P.; Ramesh, P.; Itkis, M. E.; Bekyarova, E.; Haddon, R. C. *J. Phys. Chem. C* **2007,** 111, (21), 7565-7569.
10. Balandin, A. A.; Ghosh, S.; Bao, W. Z.; Calizo, I.; Teweldebrhan, D.; Miao, F.; Lau, C. N. *Nano Lett.* **2008,** 8, (3), 902-907.
11. Stoller, M. D.; Park, S. J.; Zhu, Y. W.; An, J. H.; Ruoff, R. S. *Nano Lett.* **2008,** 8, (10), 3498-3502.
12. Pumera, M. *Chem. Soc. Rev.* **2010,** 39, (11), 4146-4157.
13. Lu, J.; Drzal, L. T.; Worden, R. M.; Lee, I. *Chem. Mater.* **2007,** 19, (25), 6240-6246.
14. Kato, D.; Sekioka, N.; Ueda, A.; Kurita, R.; Hirono, S.; Suzuki, K.; Niwa, O. *J. Am. Chem. Soc.* **2008,** 130, (12), 3716-3717.
15. Yoo, E.; Kim, J.; Hosono, E.; Zhou, H.; Kudo, T.; Honma, I. *Nano Lett.* **2008,** 8, (8), 2277-2282.
16. Takamura, T.; Endo, K.; Fu, L.; Wu, Y.; Lee, K. J.; Matsumoto, T. *Electrochimica Acta* **2007,** 53, (3), 1055-1061.
17. Torrisi, F.; Hasan, T.; Wu, W. P.; Sun, Z. P.; Lombardo, A.; Kulmala, T. S.; Hsieh, G. W.; Jung, S. J.; Bonaccorso, F.; Paul, P. J.; Chu, D. P.;

Ferrari, A. C. *ACS Nano* **2012,** 6, (4), 2992-3006.
18. Sordan, R.; Traversi, F.; Russo, V. *Appl. Phys. Lett.* **2009,** 94, (7), 073305.
19. Matyba, P.; Yamaguchi, H.; Eda, G.; Chhowalla, M.; Edman, L.; Robinson, N. D. *ACS Nano* **2010,** 4, (2), 637-642.
20. Wang, Y.; Chen, X.; Zhong, Y.; Zhu, F.; Loh, K. P. *Appl. Phys. Lett.* **2009,** 95, (6), 063302.
21. Yin, Z.; Wu, S.; Zhou, X.; Huang, X.; Zhang, Q.; Boey, F.; Zhang, H. *Small* **2010,** 6, (2), 307-312.
22. Yang, N. L.; Zhai, J.; Wang, D.; Chen, Y. S.; Jiang, L. *ACS Nano* **2010,** 4, (2), 887-894.
23. Fujita, M.; Wakabayashi, K.; Nakada, K.; Kusakabe, K. *J. Phys. Soc. Jpn.* **1996,** 65, (7), 1920-1923.
24. Han, M.; Özyilmaz, B.; Zhang, Y.; Kim, P. *Phys. Rev. Lett.* **2007,** 98, (20), 206805.
25. Chen, Z.; Lin, Y.-M.; Rooks, M. J.; Avouris, P. *Physica E* **2007,** 40, (2), 228-232.
26. Barone, V.; Hod, O.; Scuseria, G. E. *Nano Lett.* **2006,** 6, (12), 2748-2754.
27. Jiao, L. Y.; Wang, X. R.; Diankov, G.; Wang, H. L.; Dai, H. J. *Nat. Nanotechnol.* **2010,** 5, (5), 321-325.
28. Zeng, J.; Chen, K.-Q.; He, J.; Fan, Z.-Q.; Zhang, X.-J. *J. Appl. Phys.* **2011,** 109, (12), 124502.
29. Kozlov, S. M.; Vines, F.; Gorling, A. *Adv. Mater.* **2011,** 23, (22-23), 2638-2643.
30. Park, J.; Lee, W. H.; Huh, S.; Sim, S. H.; Kim, S. B.; Cho, K.; Hong, B. H.; Kim, K. S. *J. Phys. Chem. Lett.* **2011,** 2, (8), 841-845.
31. Park, J.; Jo, S. B.; Yu, Y.-J.; Kim, Y.; Yang, J. W.; Lee, W. H.; Kim, H. H.; Hong, B. H.; Kim, P.; Cho, K.; Kim, K. S. *Adv. Mater.* **2012,** 24, (3), 407-411.
32. Park, H.; Choi, W. *Catal. Today* **2005,** 101, (3-4), 291-297.
33. Ozer, R. R.; Ferry, J. L. *J. Phys. Chem. B* **2002,** 106, (16), 4336-4342.

Chapter 5

Conclusion

5.1 Conclusion

Since its discovery, single-walled carbon nanotube (SWNT) has attracted a lot of research interests due to its excellent electronic, mechanical, optical and thermal properties. Novel functionalities appear when SWNTs are hybridized with molecules. In this thesis, I aimed to control the various electronic properties of SWNTs complex by the physical adsorption of different molecules, and the experimental results are summarized as below:

In Chapter 1, electronic states of SWNT were briefly introduced. Previous researches demonstrated that electrical performances of SWNT complex could be controlled by the molecular adsorption. The main objective of this thesis and a short description of the nanoscale electronic measurement method used in this study were stated as well.

In Chapter 2, N,N'-bis(n-alkyl)tetracarbonatenaphthalenediimide (NDI) were physically adsorbed on SWNTs wires. *I-V* analysis demonstrated a large variation in the chirality distribution of SWNTs induced by the adsorption of NDI with different alkyl chain length. Rectification occurred at the interface of NDI particle with SWNTs, and the plateau width of *I–V* curve decreased as the particle size increased, while the rectification ratio increased. The conduction mechanism was changed

from tunneling conduction to Schottky-like conduction and their boundary was at about 3 nm size. A large rectification effect induced by a combination of SWNTs junction and NDI/SWNT interface was also discussed.

In Chapter 3, electrical properties of phosphododecamolybdic acid (PMo_{12}) nanoparticles adsorbed on SWNTs were studied. Rectification direction was reversed as PMo_{12} particle size increased, and the relation between rectification direction and particle size was found opposite between semiconducting and metallic SWNTs. Kelvin probe force microscopy (KPFM) results indicated an opposite charge distribution of PMo_{12} on semiconducting SWNT to that of metallic SWNT, which was due to the different charging efficiencies between SWNTs and PMo_{12}. Two mechanisms including usual *p-n* junction and *I-V* curve drift induced by dipole moment at the PMo_{12}/SWNT interface, have been proposed for the inversion of rectification direction. Negative differential resistance (NDR) properties were observed in the *I-V* curves of PMo_{12} complex as well.

In Chapter 4, rectification properties of PMo_{12} adsorbed on graphene nanoribbon (GNR) were preliminarily studied. The experimental results showed that rectification ratio of PMo_{12}/GNR complex was mainly determined by GNR width rather than PMo_{12} particle size, while plateau width decreased as the height of PMo_{12} particle increased.

Chapter 5 gives a final conclusion to this whole thesis.

In conclusion, by the physical adsorption of two different molecules (NDI and PMo_{12}), controlling of the current rectification properties has been successfully performed. In the case of NDI/SWNT, rectification ratio and plateau width of the complex has been tuned by the particle size of NDI. In the case of PMo_{12}/SWNT, rectification direction can be reversed by the variation of PMo_{12} particle size or the "chirality" of the SWNTs. All the experimental results demonstrated in this thesis are expected to be helpful in improving the quality of molecular electronic devices in the near future.

5.2 Work in the future

Two research topics are expected to be continued in the near future. Nanoscale device of PMo_{12}/SWNT network is to be designed and prepared, and large NDR effects, as described in this thesis, are expected to be observed via the four-point probe method. The final objective is to fabricate a noise-active electric circuit based on FitzHugh-Nagumo (F-N) model.[1, 2] Besides, in order to tune the electronic structure of GNR, FET device consisted of PMo_{12}/GNR complex is to be utilized, while temperature and gas atmosphere might be the important parameters to be considered.

References

1. Fitzhugh, R. *Biophys. J.* **1961,** 1, (6), 445-466.
2. Pankratova, E. V.; Polovinkin, A. V.; Spagnolo, B. *Phys. Lett. A* **2005,** 344, (1), 43-50.

Acknowledgement

The work in this thesis has been carried out under the direction of Professor Takuji Ogawa of Department of Chemistry, Graduate School of Science, Osaka University from October, 2009 to September, 2012.

The author wishes to express his sincere gratitude to Professor Takuji Ogawa for his kind guidance, valuable discussion and continuous encouragement throughout the work. The author is deeply grateful to Assistant Professor Hirofumi Tanaka and Daisuke Tanaka, for their helpful suggestion and selfless help in the experimental work.

The author wishes to thank Assistant Professor Hirofumi Yoshikawa of Graduate School of Science, Nagoya University for his selfless help and helpful discussion in the work of PMo_{12}/SWNT complex. The author is grateful to Professor Takuya Matsumoto of Graduate School of Science, Osaka University for his great help in KPFM measurement and help discussion in the mechanism of reversible rectification direction of PMo_{12}/SWNT. The author also expresses his thank to the Research Center for Computational Science, Institute for Molecular Science, Okazaki, Japan for the DFT calculation of PMo_{12} and SWNT.

The author wishes to sincerely thank all the lab members including Mr. Annop Klamchnen, Mr. Minoru Fukumori, Ms. Tomoko Inose, Ms. Masaki Imura, Ms. Murni Handayani, Mr. Takashi Tamaki, Mr. Naoki Akeda, Mr. Shinichi Katayose, Ms. Mayuko Ojima, and Mr. Satsuki Shimono, along with alumni including Dr. Yusuke Miyake, Dr. Takami Hino, Mr. Kotaro

Tajima, Ms. Junri Lee, Mr. Syun Gohda, Mr. Yuji Totoki, Mr. Takenori Nosaka, Ms. Fusa Otaka, Mr. Ryo Arima, Mr. Hirotaka Toyama, Mr. Akifumi Goto, Mr. Yusuke Ohta, Ms. Ayuko Yamana, and Mr. Tomoki Akai, for their hospitality and help to his study and life in Japan. The author is grateful to Ms. Takako Abe for the great support for his research in Osaka University. The author specially thanks Professor Wei Huang of Nanjing University for his guidance, suggestion and encouragement during his short visit in Osaka University.

The author thanks all my friends and anonymous people, who have helped and encourage him once upon a time in Japan.

The author expresses thanks to the Ministry of Education, Culture, Sports, Science and Technology of Japan for the scholarship support during the doctoral course in Osaka University. This work was supported in part by Grants-in-Aid for Scientific Research (No. 18710104 and 19310079) and for Scientific Research on Innovative Areas “Emergence in Chemistry” from the Ministry of Education, Culture, Science, Sports, and Technology of Japan.

Finally, the author sincerely thanks his parents in China for their continuous spiritual support.

List of Publications

1) H. Tanaka, **L. Hong**, M. Fukumori, R. Negishi, Y. Kobayashi, D. Tanaka and T. Ogawa, "Influence of nanoparticle size on the electrical properties of naphthalenediimide on single-walled carbon nanotube wiring", *Nanotechnology* **2012**, *23*, 215701.

2) **L. Hong**, H. Tanaka, and T. Ogawa, "Large rectification effect achieved by a combination of carbon nanotube junction and molecule-carbon nanotube interface", submitted.

3) **L. Hong**, H. Tanaka, and T. Ogawa, "Rectification direction inversion in a phosphododecamolybdic acid nanoparticle/SWNT nanoscale junction due to the particle size and chirality of SWNT**"**, to be submitted.

4) **L. Hong**, H. Tanaka, and T. Ogawa, "Nano-scale diodes composed of single-walled carbon nanotube and physically adsorbed organic molecule nanoparticles", submitted.

5) G. Wang, H. Tanaka, **L. Hong**, Y. Matsuo, K. Niikura, M. Abe, K. Matsumoto, T. Ogawa and K. Ijiro, "Novel charge transports in DNA-templated nanowires", *J. Mater. Chem.* **2012**, *22*, 13691.

List of Presentations

1) “Population variation of single-walled carbon nanotube chirality as naphthalene diimide complex” (poster), AsiaNANO 2010, Tokyo, Japan, November 2, 2010.

2) “Electrical properties of nanoparticles/SWNT complex measured by PCI-AFM” (oral), the 91th Annual Meeting of the Chemical Society of Japan, Yokohama, Japan, March 29, 2011.

3) “Electrical properties of nanoparticles/SWNT complex measured by PCI-AFM” (poster), the 9th Annual Meeting of the Society of Nano Science and Technology, Sapporo, Japan, June 3, 2011.

4) “Electrical properties of nanoparticles/single-walled carbon nanotube complex” (oral), the 72nd Fall Meeting of the Japan Society of Applied Physics, Yamagata, Japan, September 2, 2011.

5) “Rectification nanodevice of 1:12 phosphomolybdic acid adsorbed on single-walled carbon nanotube” (poster), the 3rd Symposium of Emergence in Chemistry, Osaka, Japan, February 3, 2012.

6) “Study on electronical properties of phosphododecamolybdic acid/SWNT nanocomplex” (oral), the 92nd Annual Meeting of the Chemical Society of Japan, Yokohama, Japan, March 25, 2012.

7) “Electrical properties of molecules/single-walled carbon nanotube nanocomplex” (oral), Mini-symposium on Supramolecular Spintronics and Electronics, Toyonaka, Japan, May 15, 2012.

8) “Electrical properties of phosphododecamolybdic acid/single-walled carbon nanotube complex” (poster), the 10th Annual Meeting of the Society of Nano Science and Technology, Toyonaka, Japan, June 14, 2012.

9) “Electronical properties of phosphododecamolybdic acid adsorbed on single-walled carbon nanotube” (oral), IEEE NANO 2012 – 12th International Conference on Nanotechnology, Birmingham, United Kingdom, August 23, 2012.

10) “Controlling rectification direction by nanoparticle size of phosphododecamolybdic acid adsorbed on single-walled carbon nanotube” (poster), AsiaNANO 2012, Lijiang, China, September 9, 2012.

Scholarship and Award

1) Japanese Government (MEXT, Monbukagakusho) Scholarship

2) Young Researcher Award, AsiaNANO 2010, Tokyo, Japan